



Virginia Commonwealth University
VCU Scholars Compass

Theses and Dissertations


Graduate School

2018

Galantamine's Deconstruction in the Quest of a PAM Pharmacophore

Malaika Argade
Virginia Commonwealth University

Follow this and additional works at: <https://scholarscompass.vcu.edu/etd>

 Part of the [Cognitive Neuroscience Commons](#), [Heterocyclic Compounds Commons](#), [Medicinal and Pharmaceutical Chemistry Commons](#), and the [Organic Chemicals Commons](#)

© Malaika D. Argade

Downloaded from

<https://scholarscompass.vcu.edu/etd/5461>

This Dissertation is brought to you for free and open access by the Graduate School at VCU Scholars Compass. It has been accepted for inclusion in Theses and Dissertations by an authorized administrator of VCU Scholars Compass. For more information, please contact libcompass@vcu.edu.

© Malaika D. Argade, 2018

All Rights Reserved

GALANTAMINE'S DECONSTRUCTION IN THE QUEST OF A PAM
PHARMACOPHORE

A dissertation submitted in partial fulfillment of the requirements for the degree of
Doctor of Philosophy at Virginia Commonwealth University.

by

MALAIKA D. ARGADE, M.S.
Bachelor of Pharmacy, University of Mumbai, India, 2010

Director: DR. MAŁGORZATA DUKAT, PHD
ASSOCIATE PROFESSOR, MEDICINAL CHEMISTRY

Virginia Commonwealth University
Richmond, Virginia
May 2018

Acknowledgment

Once upon a time, there was a young graduate student who unintentionally thanked everyone but her advisor after her first research presentation. I don't know who that student was, but I'm sure it was an honest mistake. Not to repeat the same mistake (twice), *dziękuję bardzo* Dr. Dukat! Few years back, I was convinced that I wanted to earn a PhD degree in your laboratory with you as my teacher and I'm very grateful for the opportunity to pursue this goal. Thank you for being supportive by attending all possible presentations and a billion student-related things. Thank you for being kind with all of my ideas and thoughts on the project, however ridiculous they might've been. I was lucky to have a caring advisor to check up on me (from a safe distance), every time I set up a particularly dangerous reaction. You have always believed in me (after saying, "You better know your stuff!"), have always forgiven my mistakes (such as when I glued the acetone drum to the lab floor), and have always been patient (I know you practice your yoga because of me). I can't believe I'm writing this but thank you for the tough love!

I consider myself lucky to have had Dr. Richard A. Glennon's support and insight into my project. Thank you Dr. Glennon, for all the witty banter and especially for answering all the burning questions I've had over the years (such as, "why are manhole covers round?" and "what's up with the rotating barber poles?"). On a serious note, I'm grateful for all that I've learnt from you.

A special thanks to all the lab members: Dr. Renata Kolanos, Atul, Osama, Kavita, Supriya, Farhana, Urjita, Abdelrahman, Rachel, Dr. Umberto Battisti, Alessandro, Ahmed,

Barkha, Pallavi and Preeth for their help and support through the years. I have learnt something from each and every one of you.

I'm grateful to Dr. Marvin K. Schulte for giving me an opportunity to visit his laboratory in the University of Sciences, Philadelphia and to conduct electrophysiological studies. Special thanks to Dr. Schulte's graduate student, Laura DeCristofano for teaching me the TEVC method. I also thank Dr. MaryPeace McRae and Dr. Glen E. Kellogg for being a part of my graduate research committee and for their valuable advice and suggestions. Special thanks to my PhD. Program directors, Dr. William Eggleston for giving me a chance and being incredibly supportive, and also Dr. Brian Verrelli for his patience and support throughout my PhD.

I'm lucky to have a family that not only wants to talk about my research but also pretends to listen intently as I explain it. I thank my parents, Manjiri and Dilip Argade for having unshakeable faith in me. Mamma and papa, thanks for being supportive whenever I needed help and for the reality checks when it was necessary. I am forever grateful to my brother Akshay, for constantly watching out for me and having my back! Life away from home can be difficult at times, but it is so much more bearable when you have the right friends. For that, I thank Kavita and Urjita who are my little family in Richmond. I couldn't have found better people to grow up with and I would be lost (and hungry) without you two. I am also grateful to Nehru and Balaji for being a tremendous support system for me in Richmond. A special thanks to Farahnoz and Francy for being very kind and very, very helpful especially during the last year of my PhD.

Lastly, I thank Satish and Vrushali Rajguru for having never-ending faith in me. Vrushali aunty, I miss your presence and I know how proud you would've been to see me graduate.

Table of Contents

Acknowledgment	ii
List of Tables	xi
List of Figures	xii
List of Schemes	xxi
List of Abbreviations	xxii
Abstract	xxv
I. Introduction.....	1
II. Background	5
1. Alzheimer's Disease (AD).....	5
a. Cholinergic hypothesis	8
b. Amyloid cascade hypothesis	9
c. Tau Hypothesis	11
d. Vascular hypothesis	11
e. Cholesterol hypothesis	12
f. Inflammation hypothesis	12
g. Oxidative stress hypothesis	13
2. Current treatment options	14

3. Galantamine	15
4. Targeting nAChRs as a treatment strategy	24
5. Nicotinic acetylcholine receptors	27
a. Classification	27
b. Structure of nAChRs – emphasis on $\alpha 7$ nAChRs	29
c. States of nAChRs and allosterism	30
d. PAMs and their types	34
e. Negative allosteric modulators (NAMs).....	39
f. Silent allosteric modulators (SAMs)	41
g. Ago-PAMs	42
h. Agonist binding site	43
III. Rationale and specific aims	44
Specific Aim 1: To identify the minimum structural features of galantamine that will retain the PAM action at human $\alpha 7$ nAChRs	45
Specific Aim 2: To study the molecular interactions of galantamine and its deconstructed analogs with the human $\alpha 7$ nAChR by molecular modeling	51
Specific Aim 3: To determine a pharmacological profile of galantamine and its deconstructed analogs at human $\alpha 7$ nAChRs by two-electrode voltage clamp (TEVC) techniques.....	54
IV. Results and Discussion.....	57

Specific Aim 1: To identify the minimum structural features of galantamine that will retain the PAM action at human $\alpha 7$ nAChRs	57
a. Perform a 3D overlap of the structural features of galantamine (3, Figure 1) with codeine (8, Figure 5).....	57
b. Based on Approach 1a, synthesize smaller, structurally-abbreviated analogs of galantamine by employing the deconstruction approach in medicinal chemistry.....	65
Specific Aim 2: To study the molecular interactions of galantamine and its deconstructed analogs with the human $\alpha 7$ nAChR by molecular modeling	77
a. Generate 3-dimensional homology models of the human $\alpha 7$ nAChR.....	77
1. Amino acid sequence alignment.....	77
2. Structure validation.....	79
3. Docking studies.....	83
Specific Aim 3: To determine a pharmacological profile of galantamine and its deconstructed analogs at human $\alpha 7$ nAChRs by two-electrode voltage clamp (TEVC) techniques	93
V. Conclusions.....	97
VI. Experimental	104
A. Synthesis	104

{(4a <i>S</i> ,6 <i>R</i> ,8a <i>S</i>)-4a,5,9,10,11,12-Hexahydro-3-methoxy-11-methyl-6 <i>H</i> -benzofuro[3a3,2- <i>ef</i>][2]-benzazepin-6-ol} (Galantamine; 3)	106
{(4a <i>S</i> ,6 <i>R</i> ,8a <i>S</i>)-4a,5,7,8,9,10,11,12-Octahydro-3-methoxy-11-methyl-6 <i>H</i> -benzofuro[3a3,2- <i>ef</i>][2]-benzazepin-6-ol} Hydrochloride (Lycoramine; 6)	106
7-Methoxy-2-methyl-1,2,3,4,4a,5-hexahydrobenzofuro[4,3- <i>cd</i>]azepine Hydrochloride (34)	108
<i>N,N</i> -Dimethyl-2,3-dihydro-7-methoxy-3-benzofuranethylamine (35).....	109
4-(<i>N,N</i> -Dimethylamino)methyl-7-methoxy-2,3-dihydrobenzofuran (36).....	110
6,7-Dimethoxy-2-methyl-1,3,4,5-tetrahydro-2 <i>H</i> -benzo[<i>c</i>]azepine Hydrochloride) (37).....	111
7-Methoxy-2-methyl-1,3,4,5-tetrahydro-2 <i>H</i> -benzo[<i>c</i>]azepine Hydrochloride) (38).....	112
3-(2,3-Dimethoxyphenyl)- <i>N,N</i> -dimethylpropylamine Hydrochloride (39).....	113
3-(3-Methoxyphenyl)- <i>N,N</i> -dimethylpropylamine Hydrochloride) (40).....	114
3,4-Dimethoxybenzyl- <i>N,N</i> -dimethylamine Hydrochloride) (41).....	115
4-Methoxybenzyl- <i>N,N</i> -dimethylamine Hydrochloride) (42).....	116
3-Deoxy-3-chlorogalantamine (45).....	117

Ethyl-(7-methoxy-1-benzofuran-3-yl)acetate (47).....	118
7-Methoxy-3-(2-hydroxyethyl)benzofuran (48)	118
7-Methoxy-3-(2- <i>p</i> -toluenesulfonylethyl)benzofuran (49)	119
<i>N,N</i> -Dimethyl-7-methoxy-3-benzofuranethylamine (50)	120
<i>N</i> -Methyl-7-methoxy-3-benzofuranethylamine Hydrochloride (51)	121
<i>N</i> -Methyl-2,3-dihydro-7-methoxy-3-benzofuranethylamine Hydrochloride (52)	122
7-Methoxy-benzofuran-3-yl acetic acid (53)	122
7-Methoxy-3-(<i>N</i> -methylacetamide)benzofuran (54)	123
2,3-Dihydro-7-methoxy-3-(<i>N</i> -methylacetamide)benzofuran (55)	125
7-Methoxy-2-methyl-1,2,4a,5-tetrahydrobenzofuro[4,3- <i>cd</i>]azepin-3(<i>4H</i>)- one (56)	126
4-Bromo-2-(2,3-diethoxyethoxy)methoxy benzene (58)	126
4-Bromo-7-methoxybenzofuran (59)	127
4-Cyano-7-methoxybenzofuran (60)	128
4-Aminomethyl-7-methoxybenzofuran Hydrochloride (61)	129
4-Aminomethyl-7-methoxy-2,3-dihydrobenzofuran (62)	130
3-(2,3-Dimethoxyphenyl)- <i>N</i> -methylpropanamide (64)	130
6,7-Dimethoxy-2-methyl-1,3,4,5-tetrahydro-2 <i>H</i> -benzo[<i>c</i>]azepin-3-one (65)	132
3-(3-Methoxyphenyl)- <i>N</i> -methylpropanamide (67)	132

7-Methoxy-2-methyl-1,3,4,5-tetrahydro-2 <i>H</i> -benzo[c]azepin-3-one (<i>p</i> - <i>isomer</i> ; 68)	133
9-Methoxy-2-methyl-1,3,4,5-tetrahydro-2 <i>H</i> -benzo[c]azepin-3-one (<i>o</i> - <i>isomer</i> ; 69)	134
9-Methoxy-2-methyl-1,3,4,5-tetrahydro-2 <i>H</i> -benzo[c]azepine (70)	135
3-(2,3-Dimethoxyphenyl)- <i>N,N</i> -dimethylpropanamide (71)	136
3-(3-Methoxyphenyl)- <i>N,N</i> -dimethylpropanamide (72)	137
Sodium 1-hydroxy-1-(3,4-dimethoxyphenyl)methanesulfonate (75)	138
Sodium 1-hydroxy-1-(4-methoxyphenyl)methanesulfonate (76)	139
B. Electrophysiology-Two-electrode voltage clamp	139
1. Expression and cRNA microinjection	140
2. Two-electrode voltage clamp recording and data collection.....	140
C. Molecular modeling.....	141
1. 3D-overlap of molecules.....	141
2. Generation of homology models	142
3. Docking studies	143
Bibliography.....	145
Appendix	162
Vita	172

List of Tables

Table 1: nAChR subunit classification based on amino acid sequence similarities	29
Table 2: HINT scores of mode-I and mode-II of galantamine and the human $\alpha 7$ nAChR homology model	86
Table 3: Literature reports for galantamine as an agonist, a PAM, and an antagonist. The focus has been on the effect of galantamine on $\alpha 7$ nAChRs or in some cases α -BgTx-sensitive nAChRs.....	102

List of Figures

Figure 1. Drugs used in the treatment of Alzheimer’s disease. Donepezil (1), rivastigmine (2), galantamine (3), and tacrine (5, discontinued) are AChE inhibitors. Memantine (4) is an NMDA-receptor blocker	15
Figure 2. <i>Galanthus woronowii</i>	16
Figure 3. (A) Crystal structure of hrAChE (PDB ID: 4EY6) showing the α -helices (blue), the β -sheets (salmon) and galantamine (yellow sticks) in its binding site. (B) Interactions of galantamine (yellow-colored sticks) with the residues in the active site of hrAChE. Hydrogen bonds are denoted by black dotted lines and water molecules by cyan spheres. Accessed from PDB ID: 4EY6 ²⁴	19
Figure 4. The deconstructed analog dihydrogalantamine (lycoramine; 6)	20
Figure 5. Physostigmine (7) - one of the first "APLs" of nAChRs along with codeine (8), another "APL" or nAChR PAM	20

Figure 6. The 73-amino acid-long, α -bungarotoxin (**9**). Accessed from PDB ID: 4HQP.....21

Figure 7. Structures of the agonists, ACh (**10**), (-)-nicotine (**11**), muscarine (**12**) and epibatidine (**13**).....21

Figure 8. Schematic representation of an nAChR highlighting the ECD, TMD, and ICD traversing the lipid bilayer. (A) Arrangement of an individual subunit from the N-terminus to the C-terminus. The polypeptide is denoted by black-colored lines and the four TM-spanning units are represented as cylinders – orange (TM1), blue (TM2), yellow (TM3) and green (TM4). (B) 2D schematic highlighting the topology of an individual subunit. (C) Rearrangement of 5 subunits (20 TM-spanning units in total) with the central ion pore being formed by TM2 from each subunit. This figure is adapted from Chatzidaki et al.¹²³31

Figure 9. The Monod-Wyman-Changeux model¹³⁷ explaining allosteric transition states in nAChRs with 'R' depicting resting state, 'A' is active state, 'I' is fast-onset while 'D' is slow-onset desensitized state.....33

Figure 10. The type-I and type-II PAMs of nAChRs, ivermectin (**14**), DMPP (**15**), 5HI (**16**), genistein (**17**) and the selective α 7 nAChR antagonist, MLA (**18**)35

Figure 11. Other PAMs of nAChRs, Compound 6 (19), NS-1738 (20), LY-2087101 (21), PNU-120596 (22) and TQS (23)	37
Figure 12. NAMs of nAChRs. KYNA (24), UCI-30002 (25), HDMP (26), PCP (27), MD-354 (28)	40
Figure 13. SAMs of nAChRs – 2,3,5,6MP-TQS (29), 2,4,6MP-TQS (30) and the allosteric agonist 2,4MP-TQS (31)	41
Figure 14. Ago-PAM of nAChRs with the racemate 4BP-TQS (32) and its resolved (+)-enantiomer, GAT-107 (33)	42
Figure 15. Galantamine (center; black) and some probable deconstructed analogs. The structural features that can be deconstructed are colored grey. The scaffolds represented in this figure are the “modified galantamine” (violet), furobenzazepine (blue), benzofuran (green and yellow), benzazepine (magenta), phenylpropylamine (red) and benzylamine (teal)	47
Figure 16. Deconstruction of galantamine to 34	48
Figure 17. Selective deconstruction of the azepine ring of analog 34	49

Figure 18. Deconstruction of dihydrofuran ring of analog 34	50
Figure 19. Deconstruction of the azepine ring of analog 37 to form the phenylpropylamine analogs 39 and 40	50
Figure 20. Deconstruction of the azepine ring of analog 37 to form the benzylamine analogs 41 and 42	51
Figure 21. Schematic representation of the components of a TEVC set-up. The output from the electrode e_v is compared to the potential of the bath electrode and the difference is indicated by V_m . The potential V_m is then compared to the command voltage and the difference is injected to the electrode through the current electrode e_i . The bath electrodes are denoted by blue-colored cylinders. Adapted from Stühmer et al. ¹⁷⁶	55
Figure 22. Division of galantamine's structure into three parts. The "left-side" (red) portion consists of the phenyl ring with the methoxy group. The "central" portion (yellow) is comprised of the tetrahydroazepine ring with the tertiary amine and the dihydrofuran ring. The "right-side" (blue) portion contains the cyclohexene ring with the allylic hydroxyl group.	58
Figure 23. 3D structure of galantamine (yellow-colored sticks) and codeine (salmon-colored sticks). Frame A highlights the "left-hand" side of the overlap consisting of the	

phenyl ring with the methoxy group and the tertiary nitrogen atom. Frame B highlights the overlap of the dihydrofuran oxygen atom in both of these molecules. Frame C displays the dissimilar orientation of the cyclohexene ring and the hydroxyl group in both galantamine and codeine.....59

Figure 24. Deconstruction of the cyclohexenol ring in galantamine (**3**) results in **6** and **44**60

Figure 25. Structural derivative of galantamine (**3**), galanthaminone (narwedine) (**43**).....61

Figure 26. Sequence alignment of the template, *Ls*-AChBP-human $\alpha 7$ nAChR chimera (3SQ6) and the receptor of interest, human $\alpha 7$ nAChR. The conserved amino acids are denoted by asterisks (*), while colons (:) and periods (.) indicate strongly and weakly conserved residues, respectively. Amino acids that were compared to the template as part of alignment are indicated in red boxes..... 78

Figure 27. A. Structure of epibatidine (**13**, yellow-colored sticks) located at the center of the “aromatic cage” in the crystal structure of the chimera *Ls*-AChBP-human $\alpha 7$ nAChR. The amine from the azabicyclo group and the chloropyridine of epibatidine participate in a number of interactions with the surrounding residues of the aromatic cage. Hydrogen bonds (h-bonds) are denoted by black dotted lines while halogen-bonds are denoted by

red, dotted lines. The residues of the receptor are denoted by teal-colored sticks or cartoon. B. Epibatidine (**13**, magenta-colored sticks) docked in the homology model of the human $\alpha 7$ nAChR. The azabicyclo amino group retains the h-bonds with Trp145 and Tyr91. The chlorine atom of the chloropyridine ring of epibatidine is also oriented towards Leu106 and Gln114 as seen in the crystal structure.....81

Figure 28. A Ramachandran plot for the human $\alpha 7$ nAChR homology model. The psi and phi values indicate the dihedral angles of the backbone of the amino acids in the protein. The plot distributes the amino acids according to their dihedral angles into energetically favourable or unfavourable regions.....82

Figure 29. The homology model (dimer) of the human $\alpha 7$ nAChR is displayed on the left as a slate-colored cartoon. The image also highlights two molecules of galantamine, in yellow- (mode-1) and magenta- (mode-2) colored sticks, docked near the residue, Thr221. A close-up image on the right sheds light on the differences between the two different docking poses.....83

Figure 30. Docking modes-I and -II of galantamine at the human $\alpha 7$ nAChR. The amino acids of the protein are denoted by slate-colored sticks. Image A denotes galantamine in mode-I (yellow-colored sticks) while image B denotes galantamine in mode-II (magenta-colored sticks). The surrounding Lys residues, 165,167 and 204 are represented by teal-colored spheres to emphasize their “pincer-like” arrangement around Thr221. A. Structure

of galantamine in docking mode-I wherein the three oxygen atoms of the molecule are oriented towards Thr221 or docking site. Hydrogen bonds are denoted by black-dotted lines. B. Structure of galantamine in docking mode-II wherein the oxygen atoms are oriented away from Thr221 and towards the subunit interface..... 84

Figure 31. Structure of lycoramine (**6**) (green-colored sticks) docked at the site surrounding Thr221. The amino acid residues are displayed as slate-colored sticks or cartoon. Dashed black lines indicate hydrogen bonds..... 87

Figure 32. Structure of deshydroxygalantamine (**44**; cyan-colored sticks) docked at the site surrounding Thr221. The amino acid residues are displayed as slate-colored sticks or cartoon. Dashed black lines indicate hydrogen bonds..... 88

Figure 33. Structures of furobenzazepine (**34**) and benzazepines (**37** and **38**) docked at the site surrounding Thr221. The ligands and the amino acid residues are displayed as purple-, maroon- and mustard-colored and slate-colored sticks, respectively. Dashed black lines indicate hydrogen bonds..... 89

Figure 34. Structures of the benzofuran analogs **35-R** isomer (salmon pink), **35-S** isomer (magenta), **51** (orange), **50** (yellow), **36** (wheat); **52-R** isomer (blue), **52-S** isomer (cyan) docked at the site surrounding Thr221. The amino acid residues are displayed as colored

sticks. Dashed black lines indicate hydrogen bonds. Red dashed lines indicate ionic interactions.....90

Figure 35. Structures of the phenylpropylamines **39** (green) and **40** (purple) docked at the site surrounding Thr221. The propylamine nitrogen atom participates in an ionic interaction with the oxygen atom of Asp219 while the methoxy oxygen atoms of the analogs form hydrogen bonds with Thr223. Dashed black lines indicate hydrogen bonds. Red dashed lines indicate ionic interactions.....91

Figure 36. Structures of the benzylamines **41** (light green) and **42** (teal) docked at the site surrounding Thr221. The benzylamine nitrogen atom participates in an ionic interaction with the oxygen atom of Asp219 while the methoxy oxygen atoms of the analogs form hydrogen bonds with Thr223. Dashed black lines indicate hydrogen bonds. Red dashed lines indicate ionic interactions.....91

Figure 37. Electrophysiological data on galantamine and some of its deconstructed analogs at human $\alpha 7$ nAChRs expressed in *X. laevis* oocytes.....94

Figure 38. The homology model of two ECD subunits of the human $\alpha 7$ nAChR (slate-colored surface) displaying the orthosteric binding site (red-colored surface) and the galantamine binding site (green-colored surface)95

Figure 39. The deconstructed analogs of galantamine. Except for compound **44**, all others were synthesized successfully. Also added are those molecules which were not part of the originally proposed molecules or “true” deconstructions but served as positional isomers (**70**) or eliminated chirality (**50** and **51**).....98

List of Schemes

Scheme 1: Preparation of lycoramine (6).....	62
Scheme 2: Attempted synthesis of compound 44	64
Scheme 3: Preparation of compounds 34 and 35	67
Scheme 4: Preparation of compound 35 via a different route	69
Scheme 5: Preparation of compound 36	71
Scheme 6: Preparation of compound 37	72
Scheme 7: Preparation of compound 38	74
Scheme 8: Preparation of compound 39	75
Scheme 9: Preparation of compound 40	75
Scheme 10: Preparation of compounds, 41 and 42	76

List of Abbreviations

A β ₁₋₄₂	Amyloid beta peptide (1-42)
A β	Amyloid beta peptide
ACh	Acetylcholine
AChE	Acetylcholinesterase
AD	Alzheimer's Disease
Ac-AChBP	<i>Aplysia californica</i> Acetylcholine Binding Protein
APP	Amyloid Precursor Protein
4BP-TQS	4-(4-bromophenyl)-3a,4,5,9b-tetrahydro-3H-cyclopenta[c]quinoline-8-sulfonamide
BSA	Bovine serum albumin
ChAT	Choline acetyltransferase
Compound 6	(N-4-chlorophenyl)- α -[[(4-chlorophenyl)amino]methylene]-3-methyl-5-isoxazole acetamide)
DMPP	1,1-Dimethyl-4-phenylpiperazinium
DS	Down's Syndrome
EDCI	1-Ethyl-3-(3-dimethylaminopropyl)carbodiimide
FAD	Familial Alzheimer's Disease

FDA	Food and Drug Administration
HDMP	1,2,3,3a,4,8b-hexahydro-2-benzyl-6N,N-dimethylamino-1-methylindeno[1,2,-b]pyrrole
hrAChE	Human recombinant acetylcholinesterase
HMG-CoA reductase	3-Hydroxy-3-methylglutarylcoenzyme A reductase
HMPA	(1,2,3,3a,4,8b-hexahydro-2-benzyl-6N,N-dimethylamino-1-methylindeno[1,2,-b]pyrrole)
5HI	5-Hydroxyindole
¹²⁵ I- α Bgtx	¹²⁵ I- α -bungarotoxin
ICD	Intracellular domain
KYNA	Kynurenic acid
<i>Ls</i> -AChBP	<i>Lymnaea stagnalis</i> -AChBP
mAChRs	Muscarinic acetylcholine receptors
MLA	Methyllycaconitine
MS	Mass Spectrometry
nAChRs	Nicotinic acetylcholine receptors
NAMs	Negative allosteric modulators
NMDA	N-methyl-D-aspartate
NMR	Nuclear Magnetic Resonance
PAMs	Positive allosteric modulators
PCP	Phencyclidine
PHY	Physostigmine

PSEN1	Presenilin 1
PSEN2	Presenilin 2
ROS	Reactive oxygen species
SLURP1	Secreted mammalian Ly-6/uPAR related protein
SAD	Sporadic Alzheimer's Disease
SAR	Structure-Activity Relationship
SAMs	Silent allosteric modulators
TLC	Thin-layer chromatography
TMD	Transmembrane domain
TM	Transmembrane
TQS	4-Naphthalene-1-yl-3a,4,5,9b-tetrahydro-3H-cyclopenta[c]quinoline-8-sulfonic acid amide
2,4MP-TQS	<i>cis-cis</i> -4-(2,4-Dimethylphenyl)-3a,4,5,9b-tetrahydro-3H-cyclopenta[c]quinoline-8-sulfonamide
2,3,5,6MP-TQS	<i>cis-trans</i> -4-(2,3,5,6-Tetramethylphenyl)-3a,4,5,9b-tetrahydro-3H-cyclopenta[c]quinoline-8-sulfonamide

Abstract

GALANTAMINE'S DECONSTRUCTION IN THE QUEST OF A PAM PHARMACOPHORE

By Malaika D. Argade, Ph. D.

A dissertation submitted in partial fulfillment of the requirements for the degree of
Doctor of Philosophy at Virginia Commonwealth University.

Virginia Commonwealth University, 2018

Major Director: Dr. Małgorzata Dukat, Ph. D.
Associate Professor, Department of Medicinal Chemistry

Alzheimer's disease is a progressive neurodegenerative disorder generally affecting people above the age of 65 years. Even though the pathophysiological hallmarks of AD were established more than a hundred years ago, there is yet to be a drug that can stop its characteristic neuronal damage. Of the five currently FDA-approved drugs, galantamine has a unique mechanism of action. Apart from being an AChE inhibitor, galantamine can effectively potentiate (positive allosteric modulator) the

effect of agonists at nAChRs at concentrations lower than those required for its action as an AChE inhibitor. Perhaps the clinical benefits observed with galantamine are associated mainly with its nAChRs-PAM action and not its AChE inhibitory effect. Inhibiting AChE causes a delay in the degradation of ACh and a prolonged presence of ACh might act at either nAChRs or mAChRs. By indirectly targeting mAChRs as well, AChE inhibitors may lead to potential side effects. Hence there is a need for specific nAChR agents.

The aim of this study was to identify the structural features of galantamine that contribute solely towards its $\alpha 7$ nAChR-PAM effect. In doing so, we wish to divorce the structural features that might be important for interacting with AChE. Using the deconstruction approach, we have synthesized structurally abbreviated analogs of galantamine. To study the probable interactions, we docked these molecules in human $\alpha 7$ nAChR homology models. Ultimately, it is of interest to determine which analogs retain the PAM activity of galantamine and to address that, a preliminary screening was performed with a select few analogs using the two-electrode voltage clamp technique

I. INTRODUCTION

Although the behavioral and pathological characteristics of Alzheimer's Disease (AD) were first described more than a hundred years ago, there is yet to be a therapeutic option that can stop, let alone reverse or cure the neurodegeneration caused by AD.^{1,2} AD generally affects people above 65 years of age and individuals with Down Syndrome (DS) in the 4th decade of their lives.^{3,4} In the U.S. alone, an alarming 14 million people are estimated to be affected by AD by 2050, a time when the youngest of the baby boomers will be 85 years of age.³ Additionally, by 2050 the total annual payments in terms of health care, hospice and long-term care for AD patients will reach 1 trillion dollars, which is ~4 times the annual payments in 2017.^{3,5}

Currently, there are five FDA-approved treatment options in the U.S. that can provide symptomatic relief and delay neurodegeneration.⁶ The drugs are donepezil, rivastigmine, galantamine, memantine and a combination formulation of memantine and donepezil.⁶ Galantamine, in particular, is used in the treatment of mild-to-moderate forms of AD.⁶

Based on various pathological observations, over the years, a number of hypotheses have attempted to explain the occurrence of AD. Disruption of cholinergic function in the brain areas essential for memory and learning (hippocampus and neocortex) led to the formulation of the cholinergic hypothesis in the 1970s and 1980s.^{7,8} The amyloid cascade hypothesis⁹ and the tau hypothesis,¹⁰ shift the blame towards the deposition of amyloid plaques and neurofibrillary tangles, respectively, which are considered to be the pathognomonic features of AD. Other hypotheses focus on the damage done to the vascular system in the brain,¹¹ occurrence of inflammation,¹² oxidative stress caused by presence of reactive oxygen species,¹³ and even the role of cholesterol¹⁴ in AD. However, it is only the cholinergic hypothesis that has resulted in a majority of FDA-approved drugs for treating AD.¹⁵ Of the previously mentioned drugs, galantamine, rivastigmine, and donepezil are acetylcholinesterase (AChE) inhibitors, while memantine is an N-Methyl D-Aspartate (NMDA) receptor blocker.¹⁵ Tacrine, a drug that was discontinued in 2013 over hepatotoxicity concerns, is also an AChE inhibitor.¹⁶

The cholinergic deficit observed in AD, also takes into account the reduced number of nicotinic acetylcholine receptors (nAChRs) in AD brains, especially in areas considered to be important for learning and memory.^{17,18} The second most populous neuronal nAChRs, $\alpha 7$, are considered to have a central role in AD pathophysiology.¹⁹ Apart from their reduced numbers, $\alpha 7$ nAChRs are also capable of interacting with the amyloid beta peptide (1-42) ($A\beta_{1-42}$), a hallmark feature of AD.²⁰

Of the previously described AChE inhibitors, galantamine has a dual mode of action and in this sense, is unique.²¹ Apart from being an AChE inhibitor, galantamine is a PAM of $\alpha 7$ nAChRs.²¹ Galantamine can act as a PAM at $\alpha 7$ nAChRs at much lower concentrations than the concentrations required for it to act as an AChE inhibitor.^{22,23} Thus, we hypothesize that galantamine's $\alpha 7$ nAChR-PAM action might underlie its clinical benefit. Additionally, by inhibiting AChE, the degradation of ACh is delayed and this accumulated ACh can affect not only various subtypes of nAChRs but also muscarinic acetylcholine receptors (mAChRs). Therefore, there is a need to identify the structural features of galantamine that are essential for $\alpha 7$ nAChR specifically and separating these from the features that contribute towards AChE inhibition.

The interaction of galantamine with AChE has been well studied. The crystal structure of human recombinant AChE co-crystallized with galantamine, provides clues to how it interacts with AChE.²⁴ There are also studies that have explored the structure-activity relationship (SAR) of galantamine for AChE inhibition.²⁵ However, the SAR of galantamine for $\alpha 7$ nAChR action is unknown. Since we hypothesized that galantamine's $\alpha 7$ nAChR-PAM activity contributes significantly to its clinical benefit, it is of importance to study the structural features that might contribute towards this effect. The overall aim of this project is to identify the minimal structural features (pharmacophore) of galantamine required for its PAM action at $\alpha 7$ nAChRs. In doing so, we wish to divorce the features that play a role in inhibiting AChE. To achieve this, we have employed the deconstruction approach to study the influence of specific structural features on $\alpha 7$

nAChRs. At the same time, it was of essence to study the possible interactions of galantamine and its deconstructed analogs with the human $\alpha 7$ nAChR. For this, we generated homology models of the human $\alpha 7$ nAChR and docked the molecules to identify potential docking poses. Additionally, we have attempted at screening galantamine and some of its deconstructed analogs for activity at the human $\alpha 7$ nAChRs expressed in *Xenopus laevis* oocytes using the two-electrode voltage clamp technique. In the future, we wish to separate galantamine's structural features that contribute towards AChE inhibition and to tease out a pharmacophore for human $\alpha 7$ nAChRs.

II. BACKGROUND

1. Alzheimer's Disease (AD)

Alzheimer's Disease is a progressive neurodegenerative disorder, and the most common form of dementia, generally affecting populations older than 65 years of age.²⁶ Another subset of the population affected by AD are individuals with DS.^{3,27} Almost all individuals with DS above the age of 40 years develop the characteristic plaques and tangles in the brain.^{3,4,28} With age, around 50% of the DS individuals will suffer from Alzheimer's dementia.²⁹ The symptoms of AD were first described by Alois Alzheimer in 1907.¹ However, the disease was identified as one of the leading causes of death in the U.S. only in the 1970s when Katzman described it as a "major killer".³⁰

In terms of pathophysiology, depositions of a protein, amyloid beta peptide (amyloid plaques), outside the neurons and in cerebral blood vessels, and accumulation of hyperphosphorylated tau protein inside the neurons (neurofibrillary tangles) are the characteristic structural abnormalities in an AD brain.³ The plaques disrupt neuronal communication while the tangles prevent nutrient flow inside the neurons thereby

contributing to neuronal damage and death. Other changes such as disruption of cholinergic function in the basal forebrain, inflammation, brain shrinkage due to drastic cell loss, and the presence of cell debris also occur.³ The most common form of dementia, AD neurodegeneration lasting for ~8.5 years from diagnosis, starting from mild cognitive impairment to very severe AD, results in death.^{31,32} Severe forms of AD tend to last longer than mild forms of cognitive impairment.³³ The cognitive and non-cognitive symptoms of AD can be generally classified into three groups. The first group comprises cognitive and executive dysfunctions, such as loss of memory, language impairment, and inability to carry out higher-level planning and tasks requiring intellectual coordination.³⁴ The second group consists of non-cognitive symptoms such as hallucinations, agitation, delusions, depression, and other behavioral disturbances.³⁴ The third group is composed of problems with performing day-to-day activities such as eating, dressing unaided, bathing, and the ability to communicate.³⁴ Difficulty to swallow, which occurs in severe forms of AD leads to Alzheimer's-related dehydration and malnutrition. Additionally, as the patient becomes bed-bound, requiring constant caregiving, the propensity to contract infections increases.^{3,35} As a result, Alzheimer's pneumonia is observed frequently in the most severe cases, often contributing to death.^{3,36}

Apart from age, two other risk factors for AD are family history and genetic predisposition (sporadic) to possess the $\epsilon 4$ allele of the ApoE gene.³ Individuals whose first-degree relatives (parent or siblings) have AD have an increased tendency to develop AD as opposed to those whose family members do not have AD. AD cases can generally be

classified as being either familial (≥ 1 family members) or sporadic (without influence of familial aggregation).³⁷ Familial AD (FAD) accounts for about 25% of the total cases while the remainder fall under sporadic AD (SAD). FAD is further classified into early-onset AD (5% of cases, < 65 years) while late-onset AD (> 65 years) accounts for the majority of the cases ($\sim 95\%$).^{35,38} FAD is associated with genetic mutations in genes encoding the amyloid precursor protein (APP) on chromosome 21, presenilin 1 (PSEN1) on chromosome 14, and presenilin 2 (PSEN2) on chromosome 1.^{38,39} Most presenilin mutations result in elevated production of amyloid beta peptide ($A\beta_{1-42}$) that makes up amyloid plaques in the brain.⁴⁰ For SAD, the most common risk factor is the presence of the genetic variant $\epsilon 4$ allele of the ApoE gene (chromosome 19) which encodes the apolipoprotein ApoE. ApoE is a 299-residue-long lipoprotein that plays a role in cholesterol homeostasis.⁴⁰ The presence of one copy of the ApoE $\epsilon 4$ allele results in a 3-fold, whereas two copies results in a 12-fold risk of developing AD.⁴⁰ Apart from playing a role in cholesterol modulation, ApoE is also involved in interactions with $A\beta$ peptides.⁴⁰

Several hypotheses propose explanations for AD occurrence. Although each hypothesis has its own reasoning, most of these proposed pathological events are interconnected and, perhaps, might even occur simultaneously. Some of these hypotheses are the:

- a. Cholinergic hypothesis
- b. Amyloid hypothesis
- c. Tau hypothesis
- d. Vascular hypothesis

- e. Inflammation hypothesis
- f. Cholesterol hypothesis
- g. Oxidative stress hypothesis

While the cholinergic hypothesis will be a focus here, the other hypotheses will be discussed briefly.

a. Cholinergic Hypothesis

Between 1970-1980 several findings emerged that associated AD with a pronounced cholinergic deficit in the brain that led to the formulation of the cholinergic hypothesis.⁷ Particularly in post-mortem studies, the level of the enzyme choline acetyltransferase (ChAT), which is responsible for the synthesis of the neurotransmitter acetylcholine (ACh), was drastically reduced.⁴¹⁻⁴⁴ The levels of another enzyme, acetylcholinesterase (AChE), that breaks down ACh, were also reduced, although to a lower extent.⁴¹⁻⁴⁴ The levels of ACh are also reported to be reduced, perhaps, because the enzyme pyruvate dehydrogenase complex that synthesizes it is affected.⁸ Severe neuronal degeneration was observed in brain locations essential for learning and memory, such as the hippocampus and the neocortex.^{8,45} The cholinergic blocker scopolamine was capable of inducing cognitive-like deficits in healthy individuals similar to those observed in older (non-AD) patients.⁴⁶ Also, in the human frontal cortex, the number of [³H]-nicotine and [³H]-ACh binding sites were lower in AD patients as compared to age-matched controls, reflecting a reduction in the nicotinic cholinergic receptors in AD brains.^{17,18,47} This reduction is attributed to a reduction in the number of sites as opposed to the affinity of

the ligand for the site.^{18,48} These observations form an association of the cholinergic system to memory and cognition. Studies also reported significant losses in cholinergic neurons in the basal forebrain, and affected pre-synaptic ACh release as well as disruption in the high-affinity synaptic reuptake of choline in AD patients.⁴⁹ The observed reductions of cholinergic markers and enzymes in AD brains lead to decreased synthesis and release of ACh into the synapse. This cluster of observations forms the basis of the cholinergic hypothesis.

Considering the different number of hypotheses that propose alternate theories, it is surprising that only the cholinergic hypothesis has led to marketed drugs (discussed below). However, AChE inhibitors can only delay cognitive impairment but cannot prevent it from progressing and are incapable of reversing neurodegeneration.⁵⁰ This indicates that perhaps there is more to the pathophysiology of AD than can be explained by the cholinergic hypothesis.

The FDA-approved agents currently used in the treatment of AD are rivastigmine, donepezil, memantine and galantamine (see Figure 1, later). Apart from memantine, all others are AChE inhibitors.

b. Amyloid Cascade Hypothesis

The amyloid cascade hypothesis^{9,51} was proposed when the amino acid sequence of the major protein component of plaques was determined. Plaques from meningeal blood

vessels from AD patients revealed a protein, the amyloid beta ($A\beta$) peptide.^{52,53} The protein that gives rise to $A\beta$ peptides upon cleavage by enzymes was later identified as the APP⁵⁴ The sequential cleavage of a protein, APP, by enzymes β - and γ -secretases, produces $A\beta$ peptides (39-42 residues). $A\beta_{42}$, a peptide of 42 residues, in particular, is said to be harmful and tends to aggregate to form plaques.⁵⁵ The $A\beta$ peptide isolated from AD patients was found to be similar to the one isolated from brain samples of DS patients.^{56,57} Individuals with DS have an extra copy of chromosome 21 that involves a genetic region that encodes for APP.³⁹ This strengthens the connection between abnormal amyloid processing and the tendency to develop AD.

Additionally, plaques are suggested to cause a cascade of events such as formation of neurofibrillary tangles, vascular damage, and neuronal death, which are observed in AD patients.⁵⁸ However, a strong correlation does not exist between the extent of $A\beta$ P deposition and the progression of AD.⁵⁹ Individuals who are not diagnosed with dementia or AD can also exhibit $A\beta$ plaques, indicating that this observation is not AD-specific. Also, drugs that reduce $A\beta$ peptide levels in the brain do not seem to reverse or stop the progression of AD, thereby questioning the validity of this hypothesis.^{60,61} Hence, even after ~40 years since its inception, the amyloid hypothesis has yet to result in a promising drug.

c. Tau hypothesis

The tau hypothesis identifies the presence of tau tangles as the major cause of AD. Described by Alzheimer as a “tangle of fibrils”,¹ the identity of the major component of AD lesions was established only in the 1980s.^{62,63} A hyperphosphorylated form of the microtubule-associated protein tau was determined to be the main element of the AD lesions made up of neurofibrillary tangles, neuritic (senile) plaques, and neuropil threads.⁶² Studies suggested that the occurrence and distribution of tangles, and not plaques, serve as a good indicator of the pathological stage of AD.^{10,64} The inability of the amyloid hypothesis to come up with promising therapy directs attention to another neurological hallmark: hyperphosphorylated tau as a potential target or combined therapy.^{65,66}

d. Vascular hypothesis

The vascular hypothesis, proposed in 1993, suggests that the development of AD is due to abnormal vasculature and blood flow in the brain.⁶⁷ The brain depends on blood circulation to transport extra-cerebral resources such as glucose, electrolytes, oxygen, and amino acids.⁶⁷ Nutrients are generally supplied by capillaries through the blood-brain barrier and, to a smaller extent, via cerebrospinal fluid.⁶⁷ A decrease in the supply of essential nutrients such as oxygen and glucose results in impaired production of required energy, thereby disrupting neuronal homeostasis.⁶⁷ A weakening of the cerebral blood vessels is also anticipated with ageing as it is accompanied with thickening of the basement membranes, cerebral atrophy, decreased elasticity of cerebral vessels, and

even due to a genetic predisposition.⁶⁷ Apart from ageing, cardiovascular disease, atherosclerosis, and brain injury are also associated with occurrence of AD as these conditions might reduce blood flow to the brain.¹¹ AD brains exhibit a reduced rate of oxygen consumption and glucose metabolism, pointing towards abnormal energy-producing processes such as oxidative phosphorylation.

e. Cholesterol Hypothesis

Atherosclerosis, a condition caused by high levels of cholesterol, is considered to be one of the risk factors for developing AD.⁶⁸ Patients who were prescribed cholesterol-lowering drugs, statins, were at a lower risk for developing dementia.⁶⁹ Statins, capable of crossing the blood brain barrier, decrease the *de novo* synthesis of cholesterol. They do so by inhibiting an enzyme 3-hydroxy-3-methylglutarylcoenzyme A reductase (HMG-CoA reductase).^{68,69} One of the major cholesterol carrier proteins in the brain is apolipoprotein, ApoE. Of the three alleles ($\epsilon 2$, $\epsilon 3$ and $\epsilon 4$) for the gene that encodes ApoE, the presence of the $\epsilon 4$ allele poses as a major risk factor for AD. The ApoE $\epsilon 4$ allele tends to increase cholesterol concentrations in the brain along with increasing the β -secretase-mediated cleavage of APP to give A β P.¹⁴ Although the mere presence of this allele alone is not enough to initiate AD, it certainly increases the risk of developing AD.

f. Inflammation Hypothesis

Amyloid plaques and neurofibrillary tangles are accompanied by the presence of immune-related antigens and inflammatory mediators in AD brains.¹² Amyloid plaques are also

found to contain factors of the complement pathway such as C_{1q}, C_{3b}, C_{3c}, C_{3d} and C₄ and cytokines such as interleukin 1.^{70,71} Additionally, the A β peptide can bind the first component, C_{1q} of the classical complement pathway, perhaps leading to its activation.⁷² A number of retrospective studies have indicated that patients who were on anti-inflammatory drugs have a delayed onset of AD as compared to those who were not.¹² Interestingly, patients who displayed plaques and tangles upon autopsy, but did not have a history of dementia, did not exhibit significant inflammation as opposed to AD patients.⁷³ This indicates that, perhaps, neuroinflammation is a downstream process that occurs when severe neurodegeneration has occurred. Therefore, neuroinflammation is an important aspect of AD pathology but, perhaps, not its root cause.^{74,75} An immune response is most likely a secondary reaction in AD pathology because it is, after all, a response to a primary injury or insult to the body.⁷⁵

g. Oxidative Stress Hypothesis

This hypothesis suggests that the accumulation of free radicals and reactive oxygen species (ROS) over the years results in neuronal damage resulting in neurodegenerative diseases such as AD.^{13,76} Other factors such as head injury and the presence of certain metals in the brain also contribute towards formation of free radicals.^{77,78} The free radicals suspected to cause neurodegeneration are the free hydroxyl radical, hydrogen peroxide, and peroxynitrite.⁷⁷ In particular, the concentrations of iron and aluminium are elevated in an AD brain.⁷⁷ Iron, ferritin, and transferrin are located at the same site as amyloid plaques in the brain, indicating involvement of these species.⁷⁷ These metals also interact directly

with APP.⁷⁷ The APP has specific binding sites for copper, which catalyzes reactions that might further produce ROS, and also for Zinc (II).⁷⁷ These ROS play a role in converting non-aggregated forms of A β into aggregated forms. A β peptide, in turn, is capable of reacting with vascular endothelial cells and generating free superoxide radicals.⁷⁷

AD can be considered as a multifactorial disorder. Most events such as cholinergic deficit, accumulation of reactive oxygen species, free radicals, rise in cholesterol, abnormal cerebral vasculature, high metal content, and inflammation converge to give rise to AD. Among these happenings is also the hyperphosphorylation and subsequent deposit of tau protein and the abnormal production and deposition of A β peptide.

2. Current treatment options

Even though it has been 100 years since the pathophysiology and behavioral observations of AD were first described, there is still no drug that can stop or reverse AD's characteristic degeneration. Currently, five drugs/formulations for treating AD are available (Figure 1): donepezil (**1**) and rivastigmine (**2**, used for all stages of AD), galantamine (**3**, mild-to-moderate form) and memantine (**4**) and memantine + donepezil (severe form).⁶ With the exception of memantine, all the other drugs (donepezil, rivastigmine and galantamine) are inhibitors of the AChE. In 2013, tacrine (**5**), another AChE inhibitor, was discontinued in the U.S. due to issues of hepatotoxicity.¹⁶

AChE rapidly degrades ACh into acetate and choline at the rate of 25,000 molecules per second.⁷⁹ By inhibiting AChE, galantamine, rivastigmine, and donepezil reduce the degradation of ACh thereby possibly improving the cholinergic deficit in AD brains.⁷⁹

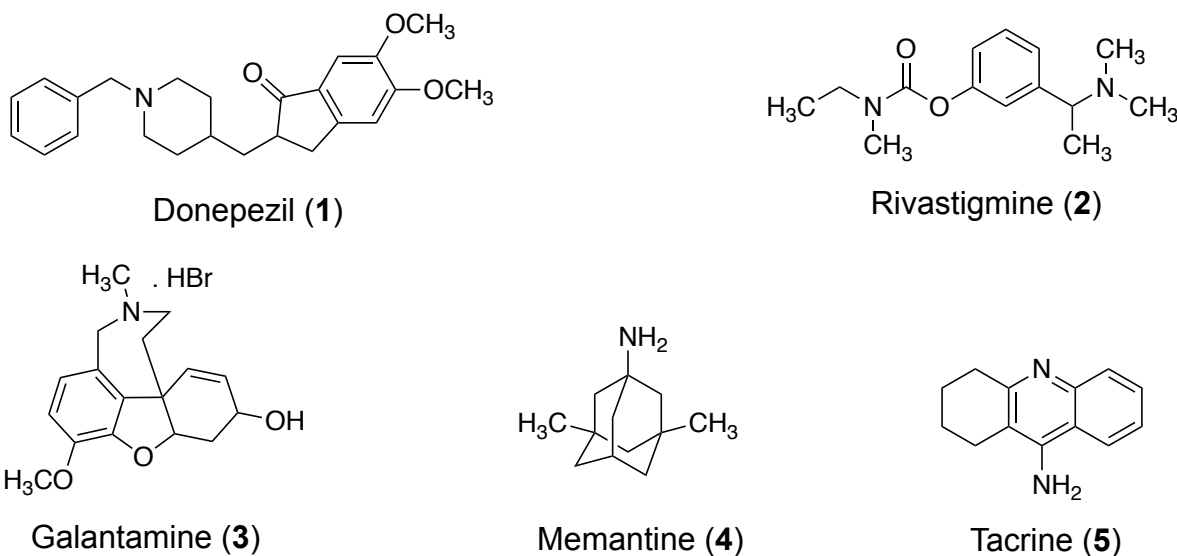


Figure 1. Drugs used in the treatment of Alzheimer's disease. Donepezil (1), rivastigmine (2), galantamine (3) and tacrine (5, discontinued) are AChE inhibitors. Memantine (4) is an NMDA receptor blocker.

Unlike the currently available AChE inhibitors for AD, galantamine has a dual role of action. In addition to inhibiting AChE, galantamine (3) demonstrates positive modulation of nicotinic acetylcholine receptors (nAChRs).²¹

3. Galantamine

Galantamine is an alkaloid originally isolated from *Galanthus woronowii* (Figure 2), but has also been extracted nowadays from *Leujocum aestivum* and *Amaryllidaceae* plants.⁶⁶ Additionally, it has been successfully prepared in a laboratory setting.⁸¹ Interestingly, the

oldest literature that mentions galantamine might be by Homer in his epic poem, *Odyssey*.⁸¹ The poem narrates the King Odysseus' adventures as he returned to Ithaca



Figure 2. *Galanthus woronowii*

after the Trojan war.⁸² One of the stories involves Odysseus saving his men from the curse of Circe, the sorceress.⁸² The men were given a poison by Circe that induced amnesia, delusions and hallucinations.⁸² The antidote to this poison, mentioned as moly was provided by Odysseus with the help of the god Hermes.⁸² Based on the descriptions in the poem, Circe's poison is suspected to be *Datura stramonium*,

containing the anticholinergic agents atropine and scopolamine.^{81,83} Based on the description of the milk-like flowers in the *Odyssey* that Hermes gave to Odysseus, the antidote is believed to be the plant *Galanthus nivalis*, which contains the anti-cholinesterase galantamine.⁸³ Reports of galantamine being isolated from *G. woronowii* and subsequently its capability to inhibit AChE in *ex vivo* studies were first reported in the early 1950s.⁸⁰ The chemical structure of galantamine as isolated from *G. woronowii* was revealed in 1952.⁸⁴

Galantamine was approved as an anti-Alzheimer's agent in the U.S. in 2001.¹⁵ It is a specific, reversible, and competitive inhibitor of AChE with approximately 53-fold specificity for AChE in erythrocytes ($IC_{50} = 0.35 \mu\text{mol/L}$) over butyrylcholinesterase in plasma ($IC_{50} = 18.6 \mu\text{mol/L}$).^{85,86} However, the molecule displays 10-fold less potency for

brain AChE (~2.7-3.2 μM) than for erythrocytic AChE (~0.36-0.37 μM).²² In post-mortem studies, the IC_{50} of galantamine for hippocampal tissue was 2.8 $\mu\text{mol/L}$, whereas for the frontal cortex it was 3.2 $\mu\text{mol/L}$.²² When tested against human recombinant AChE (hrAChE), the inhibition constant, K_i , of galantamine was 520 nM.⁸⁷

The target, AChE, is a serine hydrolase that is located in neuromuscular junctions and synapses of cholinergic neurons.⁷⁹ The enzyme is ellipsoidal in shape and is an α/β protein composed of 12 mixed β -sheets which are surrounded by 14 α -helices (Figure 3).⁷⁹ The ACh-binding site or the active site is located at the base of a narrow gorge that runs 20 Å deep into the enzyme.^{79,88} The gorge is lined by 14 conserved aromatic amino acids of which Trp84 is crucial.^{79,88} The active site can be divided into two regions – the esteratic and anionic sites. The esteratic site consists of the catalytic triad that is composed of Ser200, His440 and Glu327 whereas the anionic site, composed of aromatic residues, interacts with the quaternary amines of ligands.^{79,88} The crystal structure of galantamine with human recombinant AChE is available (PDB ID: 4EY6).²⁴ Galantamine interacts with residues at the base of the active site. Particularly, the oxygen of the hydroxyl group forms a hydrogen bond with the oxygen of Glu202. Additionally, this oxygen also interacts with a water molecule (W860) which sits between the NH groups of Gly121 (2.6 Å), Gly122 (2.9 Å) and Ala204 (3.1 Å) forming the oxyanion hole. This water molecule is also located 3.5 Å from the dihydrofuran oxygen atom. Another water molecule (W707) is located 3.3 Å from the hydroxyl oxygen of galantamine. The methylene groups of the tetrahydroazepine ring are oriented towards the indole ring of

Trp86. Also, the double bond of the cyclohexenol ring is stacked against the indole ring of Trp86 and the oxygen of the methoxy group forms a hydrogen bond with the hydroxyl group oxygen of Ser203 (2.9 Å).

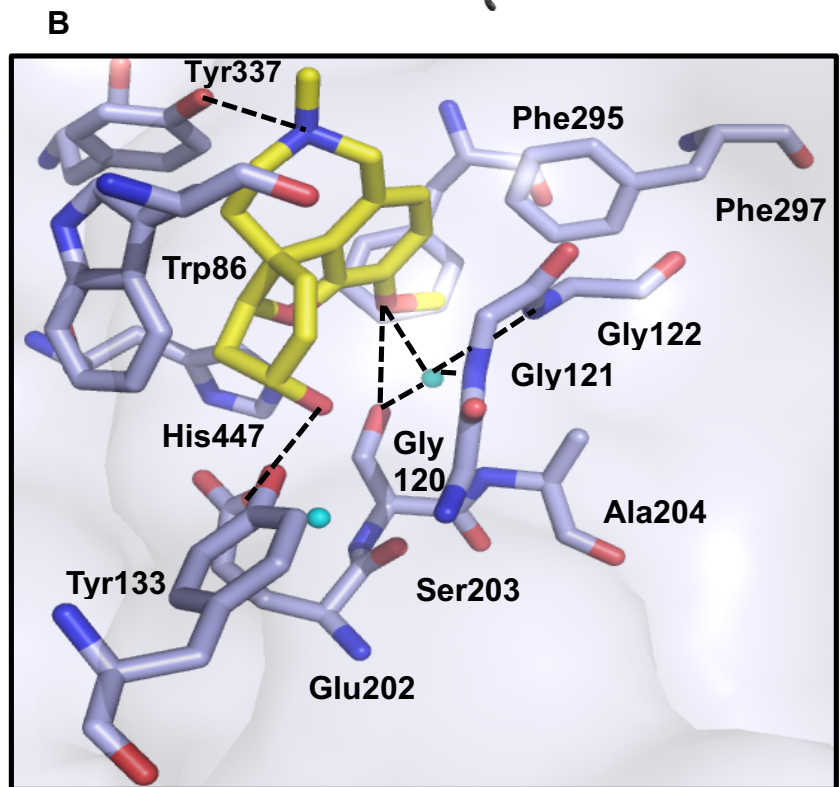
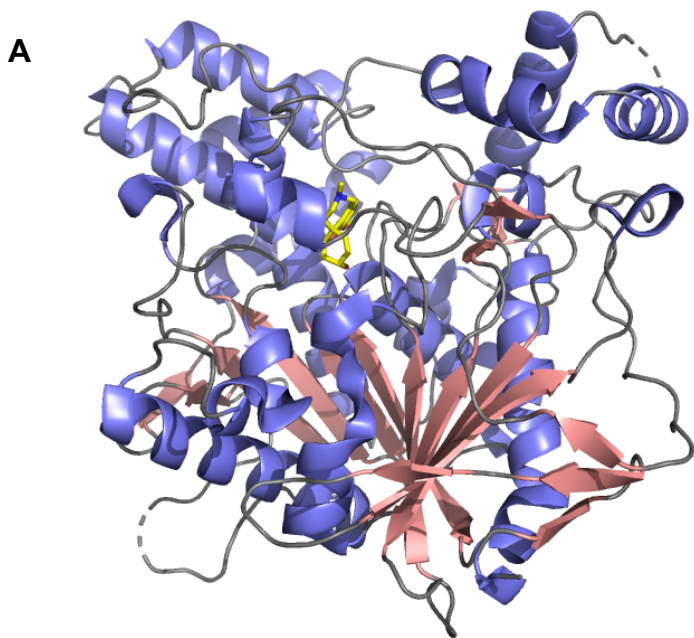


Figure 3. (A) Crystal structure of hrAChE (PDB ID: 4EY6) showing the α -helices (blue), the β -sheets (salmon) and galantamine (yellow sticks) in its binding site. (B) Interactions of galantamine (yellow-colored sticks) with the residues in the active site of hrAChE. Hydrogen bonds are denoted by black dotted lines and water molecules by cyan spheres. Accessed from PDB ID: 4EY6.²⁴

Reduction of the double bond of the cyclohexenol ring of galantamine (**3**) results in a molecule called lycoramine (**6**, Figure 4), which is not as potent as galantamine in inhibiting AChE.²⁵ The cost of reducing this double bond is a loss of the π - π interaction with Trp86 which might explain why lycoramine has lower inhibitory activity than galantamine.^{25,89} The interactions of galantamine with rhAChE mentioned above are similar to those seen in the crystal structures of galantamine with *Torpedo californica* AChE (PDB IDs: 1DX6 and 1QTI).^{89,90} In addition to these shared similarities, the hrAChE-galantamine crystal structure exhibits a hydrogen bond between the nitrogen atom of the azepine ring with the hydroxyl oxygen atom (2.9 Å) of Tyr337.²⁴

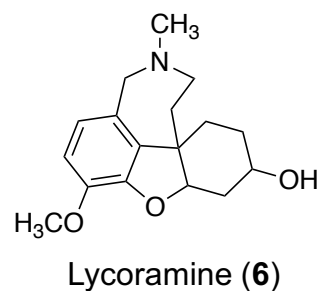


Figure 4. The deconstructed analog dihydrogalantamine (lycoramine; **6**).

Reports of galantamine as a potential allosteric agonist were initially published in the 1990s.⁹¹⁻⁹⁵ Galantamine was considered a member of a novel class of allosteric agonists of which physostigmine (PHY, **7**, Figure 5) was a forerunner. PHY, a drug used to treat myasthenia gravis, was accepted to exert its therapeutic effect by inhibiting AChE.⁹⁶

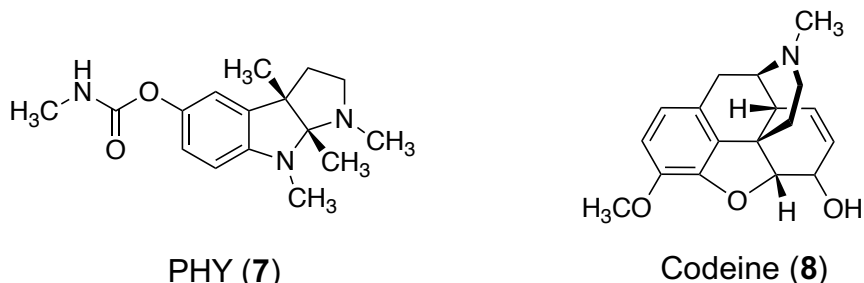
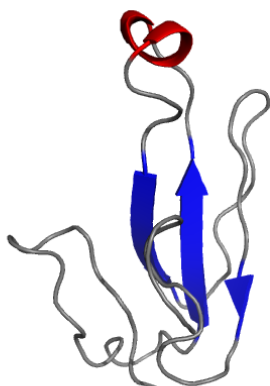


Figure 5. Physostigmine (**7**) - one of the first "APLs" of nAChRs along with codeine (**8**), another "APL" or nAChR PAM.

However, its direct effect on nAChRs was considered a more compelling reason for its



α -Bungarotoxin (9)

Figure 6. The 73-amino acid-long α -bungarotoxin (9) Accessed from PDB ID: 4HQP.

therapeutic benefit.⁹⁶ PHY activated single-channels of nAChRs from *Torpedo marmorata* electric tissue and cultured rat hippocampal neurons.^{97,98} It was also capable of activating nAChRs that were desensitized by pre-incubation with ACh.⁹⁸ Interestingly, the single-channel currents induced by PHY were not inhibited by ACh receptor antagonists such as α -bungarotoxin (9, Figure 6) and D-tubocurarine.⁹⁷ Screening with potential antagonists for the PHY-binding site resulted in an antibody, FK1, which could block the PHY-induced nAChR currents.⁹⁷ PHY was the first AChE inhibitors to be considered as a treatment option for AD.¹⁶

However, a narrow therapeutic index and a short half-life along with side effects such as nausea, vomiting, diarrhea, dizziness, and headaches made PHY an unsuitable drug for

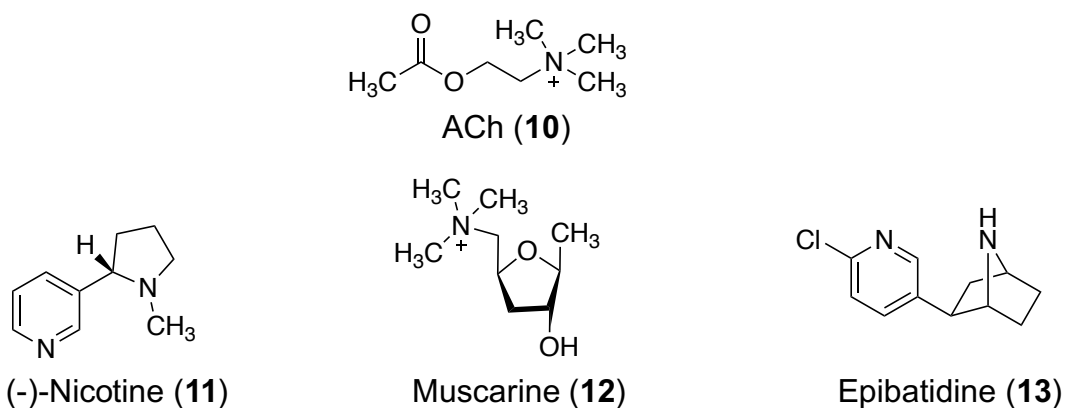


Figure 7. Structures of the agonists, ACh (10), (-)-nicotine (11), muscarine (12) and epibatidine (13).

AD therapy.^{99,100} This novel class of “non-competitive agonists” or “allosteric potentiating ligands (APLs)” of which PHY was a prototype, included two other molecules, galantamine and codeine (**8**, Figure 5).^{92,93,95,101} Like PHY, galantamine also activated single channel currents in nAChRs expressed in fibroblast and rat clonal pheochromocytoma cells.^{94,95} Prolonged exposure of nAChRs to galantamine caused receptor desensitization, unlike PHY which caused channel blockade. However, like PHY, galantamine was unable to induce a response in whole cells.^{94,95} Galantamine (**3**) could, however, potentiate the currents evoked by agonists such as acetylcholine (**10**, Figure 7), (-)-nicotine (**11**, Figure 7), and epibatidine (**13**, Figure 7). The potentiating effect of galantamine worked over a narrow range of concentrations (0.1- 1 μ M) and, beyond 10 μ M, resulted in inhibition of the response.¹⁰²

The location of the galantamine-binding site was deduced with the observation that although conventional antagonists could not block the activity of galantamine, FK1 could.^{91,103} Photoaffinity labeling studies with PHY indicated that the APL-binding site was located on the α -subunit of nAChRs.¹⁰⁴ Further, an enzyme-linked immunosorbent assay employing FK1 and WF6 (orthosteric antagonists) revealed that the APL-site was distinct but quite close to the orthosteric site.¹⁰⁵ The orthosteric and PHY binding sites, in fact, even had an overlapping region.¹⁰⁵ Based on these studies, Lys125 was proposed to be an important residue for the binding of positive allosteric modulators (PAMs) or APLs at the time.^{104,105} A blind docking study was carried out with galantamine, physostigmine, codeine and 5HT at the homology models of human α 7 nAChrs among other subunits.¹⁰⁶

The amino-acid sequence used as a template in this study was the crystal structure of *Ls*-AChBP.¹⁰⁶ The docking results suggested five potential binding sites, of which three were located on the outer surface while the other two were located at the inner surface of the ECD.¹⁰⁶ The importance of these sites for binding of allosteric modulators like galantamine were tested by mutagenesis studies.¹⁰⁷ In conjunction with photo-affinity and epitope-mapping studies,^{104,105} two of the potential sites on the outer surface were excluded from consideration.¹⁰⁷ One being, the ACh-binding site where APLs were found to have no interaction and the other being a site whose sequence was not flagged down by epitope-mapping studies.¹⁰⁷ Additionally, the site with Lys125 was located in the inner surface of the ECD, in a pocket too large for FK1 to interact with.¹⁰⁷ It was nevertheless included in the mutagenesis study to ascertain the importance of this residue, as stressed by previous studies.^{104,107} Mutagenesis data in chicken $\alpha 7$ nAChR/mouse 5HT₃ chimera revealed that replacing Thr197 by Ala had the most drastic effect on galantamine-mediated potentiation and completely abolished it.¹⁰⁷ Although to a lesser extent, replacement of Phe196 and Ile198 also affected potentiation by galantamine.¹⁰⁷ The potential binding site of galantamine was also explored by Iorga et al.¹⁰⁸ in a blind docking approach at the *Ls*-AChBP crystal structure.

Galantamine (**3**, Figure 1) can act as a positive allosteric modulator at nAChRs in rat hippocampal and human cerebral cortical slices when expressed in human embryonic kidney-293 cells and *Xenopus laevis* oocytes, in the range of 0.1-1 μ M.^{23,102,109} A study conducted in rats, rabbits and mice revealed that this optimum range for galantamine's

PAM activity can be achieved in a dose range of 1.5-5 mg/kg in these animals.¹¹⁰ However, at 3 mg/kg the calculated inhibition of brain AChE by galantamine was estimated to be only 1-12% in the animals.¹¹⁰ These numbers are in agreement with other in vivo studies conducted for determining AChE by various galantamine doses in mouse brains.^{111,112} However, at these concentrations, the AChE inhibition by donepezil (1, Figure 1) is much higher (30-40%) than galantamine (1-12%).¹¹⁰ This suggests that at low concentrations galantamine is capable of positively modulating nAChRs even when it is only poorly inhibiting brain AChE. Perhaps galantamine improves the cholinergic deficit in AD primarily through its nAChR activity and not by inhibiting AChE.

4. Targeting nAChRs as a treatment strategy

Histochemical observations and autoradiography studies in post-mortem brain tissues highlight a distinct loss of cholinergic neurons and nAChRs but not muscarinic acetylcholine receptors (mAChRs) in AD patients.^{17,18,41,48,113,114} In particular, the $\alpha 7$, $\alpha 4$, and $\beta 2$ -subunit-containing nAChRs constitute a majority of the nAChR population in mammalian brain.¹¹⁵ Of these, the homopentameric $\alpha 7$ and the heteropentameric $\alpha 4\beta 2$ nAChRs constitute about 90% of neuronal nAChRs, and are highly expressed in brain regions implicated in AD.^{116,117} The other neuronal nAChRs such as $\alpha 3\beta 4$ are predominantly present in the autonomic ganglia and adrenal medulla.¹¹⁸ Hence, activating these receptors to improve the cholinergic deficit is considered as a possible strategy for treating AD.¹¹³ Of these two receptors, the $\alpha 7$ nAChR is unique as a biological target for treating AD. One of the properties of $\alpha 7$ nAChR that sets it apart from other

nAChR subtypes is its high permeability and selectivity for Ca^{+2} amongst other cations.¹¹⁹ This indicates the receptor's possible role in cognition as neuronal Ca^{+2} signaling is involved in synaptic plasticity.¹¹⁹ Apart from being located on neuronal cells, $\alpha 7$ nAChRs are present on non-neuronal cells, especially those belonging to the immune system, indicating additional roles of this subtype.¹²⁰ Unlike the $\alpha 4\beta 2$ nAChRs which have a high affinity (nM) for ACh, $\alpha 7$ nAChRs have a low affinity (μM) for ACh and are, in fact, activated by choline, a precursor of ACh.^{119,120} Another feature of $\alpha 7$ nAChRs is that they undergo a reversible and rapid desensitization in a concentration-dependent manner when exposed to agonists.¹¹⁹ Unlike the other heteromeric nAChR subtypes that are desensitized by prolonged exposure to a low agonist concentration, the $\alpha 7$ nAChRs remains sensitive to fluctuating agonist levels.¹²⁰ The desensitized state of $\alpha 7$ nAChRs does not have high affinity for the agonist as compared to its resting state. But this desensitized state is responsive to PAMs which can destabilize it and increase the probability of the channel opening.¹²⁰

From the cholinergic hypothesis perspective, three means of improving the cholinergic deficit involve – administering ACh precursors, reducing ACh degradation, or by administering nAChR agonists.¹¹³ Agents meant to be a replacement for ACh precursors such as choline and lecithin did not yield encouraging results for treating AD.⁴⁵ Also, a major disadvantage of nAChR agonists is the receptor desensitization caused by their prolonged exposure, thus making them unsuitable as treatment options.¹¹³ In terms of reducing ACh degradation, a majority of the drugs currently on the market are AChE

inhibitors, which can delay but not stop the progression of AD. The end result of the action of these drugs is an increase in ACh, which can act at both types of acetylcholine receptors, nicotinic and muscarinic, which can have varied effects. Non-selective agonists of nAChRs can lead to autonomic side effects such as constipation associated with activating the ganglionic $\alpha3\beta4$ nAChRs.¹²¹ In light of these issues, selective PAMs of nAChRs seem to be a viable therapeutic strategy for treating AD. These allosterically acting molecules targeting nAChRs specifically, offer certain advantages over orthosteric nAChR agonists. By definition, PAMs are incapable of activating the receptors by themselves and only improve the potency or efficacy of endogenous agonists such as acetylcholine or choline. In doing so, PAMs maintain the natural spatiotemporal sequence of neurotransmitter-mediated nAChR activation in the brain and also circumvent the problem of receptor desensitization.¹²² Also, due to a non-existent or very low intrinsic activity, a PAM may have a low possibility of causing off-target effects and associated toxicity.¹²³ Furthermore, residues involved in an allosteric site are less conserved as compared to those involved in an orthosteric site among proteins of the same family.¹²² By targeting a protein's unique allosteric region, synthetic agents can achieve selectivity for a particular receptor over other subtypes.^{122,123}

The $A\beta_{1-42}$ peptide which is the crux of the amyloid hypothesis is also found to interact with nAChRs. Particularly, immunohistochemical studies in postmortem cortex and hippocampus brain tissues of patients with SAD displayed colocalization of $\alpha7$ nAChR (but not $\alpha4$ -subunit-containing nAChRs) in the neuritic plaques and neurons that were

abundant with the A β_{1-42} peptide.¹²⁴ A cell proliferation assay with wild-type SK-N-MC and $\alpha 7$ SK-N-MC, exposed to 100 nM of A β_{1-42} indicated that only ~5% of the wild-type cells compared to 85% of the $\alpha 7$ SK-N-MC cells survived after 24 h indicating a role of these nAChRs in protection against A β_{1-42} -induced cytotoxicity.¹²⁴ *Ex vivo* studies with rat hippocampal slices suggested that A β_{1-42} could inhibit nicotine-evoked currents and probability of channel-opening by interacting with post-synaptic nAChRs.¹²⁵ Binding studies indicate that the $\alpha 7$ nAChRs bind A β_{1-42} with a picomolar affinity while the $\alpha 4\beta 2$ nAChRs bind in the nanomolar range.^{20,124} Specifically, the sequence of amino acids 12-28 in A β_{1-42} is important for binding $\alpha 7$ nAChRs.¹²⁴ Agonists such as nicotine (**11**, Figure 7) and epibatidine (**13**, Figure 7), and the antagonist α -bungarotoxin (**9**, Figure 6) affect and inhibit the binding of $\alpha 7$ nAChR to A β_{1-42} thus suggesting that perhaps A β_{1-42} interacts with the orthosteric site of the receptor.¹²⁶

5. Nicotinic acetylcholine receptors

a. Classification

ACh, one of the first neurotransmitters to be identified, exerts its effects by interacting with acetylcholine receptors (AChRs).^{8,127} The AChRs are divided into two subtypes – the ionotropic nAChRs (activated by nicotine) and the metabotropic mAChRs (activated by muscarine - **12**, Figure 7).¹²⁸ The mAChRs are G-protein couple receptors (GPCRs) that are further subdivided into 5 types –M1, M2, M3, M4 and M5.¹²⁹ These receptors are coupled to secondary messenger pathways and are activated in the milliseconds to seconds range.¹²⁸ In contrast, activation of the cationic nAChRs is relatively faster and

occurs within the micro- to sub-microsecond range.¹²⁸ The nAChRs are ligand-gated ion channel receptors (LGICRs) that belong to the Cys-loop receptor family characterized by a disulfide bond between two Cys residues separated by 13 amino acids in the mammalian subunits.¹²⁸ The LGICs are structures made of 5 subunits surrounding a central aqueous ion pore which gates the flow of ions. Other members of the Cys-loop superfamily include the cation-sensitive 5-HT₃ receptor and zinc-activated channels and anion-sensitive GABA_A and glycine receptors.¹³⁰ Initially, the different neuronal nAChRs were classified by radioligand binding assays employing ¹²⁵I- α -bungarotoxin (¹²⁵I- α Bgtx) and ³H-nicotine.¹³¹ Those that displayed nM affinity for α Bgtx and μ M affinity for nicotine were classified as α Bgtx-sensitive nAChRs.^{131,132} Those that showed greater affinity for nicotine as compared to bungarotoxin were classified as α Bgtx-insensitive nAChRs.¹¹⁵ The α Bgtx-sensitive nAChRs can exist as either homopentamers (α 7-9) or heteropentamers (α 7 α 8, α 9 α 10) while the α Bgtx-insensitive nAChRs exist as heteropentamers composed of a combination of α (α 2- α 6) and β (β 2- β 4) subunits.¹¹⁵ The diversity of these receptors was further explored by the cloning of 17 subunits of nAChRs - α 1- α 10, β 1- β 4, γ , δ and ϵ .¹²⁹ Of these, the α 1, β 1, γ , δ and ϵ comprise two kinds of muscle nAChRs – one combining the α 1, β 1, δ and γ subunits while the other combining the α 1, β 1, δ and ϵ subunits in a 2:1:1:1 stoichiometry.¹²⁹ The neuronal nAChRs are pentamers that are combinations of the α 2- α 10 and β 2- β 4 subunits.¹²⁹ Based on the similarities in the amino acid sequences, these subunits can be classified into Types I-IV (shown in Table 1).¹²⁹

Table 1. nAChR subunit classification based on amino acid sequence similarities.

nAChR subunit classification			
Type I	Type II	Type III	Type IV
$\alpha 9, \alpha 10$	$\alpha 7, \alpha 8$	a. $\alpha 2-4, \alpha 6$ b. $\beta 2, \beta 4$ c. $\beta 3, \beta 5$	$\alpha 1, \beta 1, \gamma, \delta, \epsilon$

b. Structure of nAChRs – emphasis on $\alpha 7$ nAChRs

The nAChRs (~290 kDa) are composed of 5 identical (homopentamer as in $\alpha 7$ nAChRs) or different (heteropentamer) subunits arranged symmetrically around a central pore.^{127,133} Although established as being homopentamers, $\alpha 7$ nAChRs are also reported to form heteropentamers with $\beta 2$ -subunits in rat and human brains.^{134,135} The general structure of the neuronal nAChRs, composed of 500-600 amino acid residues, can be divided into an extracellular domain (ECD), a transmembrane domain (TMD), and an intracellular domain (ICD) (Figure 8).^{129,133} For each subunit, the long extracellular N-terminus is composed of approximately 200 amino acids and contains the agonist and antagonist binding regions (i.e., orthosteric binding site).¹³³

The TMD is composed of 4 transmembrane-spanning units (TM1-4) with an intracellular loop connecting TM3 and TM4, ending ultimately in a short C-terminus on the extracellular side (Figure 8).¹³⁶ TM2 from all five subunits contributes towards formation of the central ion pore.¹³³ The TM3 and TM4 units are exposed to the lipid bilayer while TM1 plays an important role in structural formation of the ion pore (Figure 7).¹³³ In the case of $\alpha 7$ nAChRs, the identical subunits provide five agonist-binding sites at the subunit interface.

c. States of nAChRs and allosterism

According to the Monod-Wyman-Changeux model for nAChRs, allosteric proteins can exist in at least three different states – resting state (R), active state (A), and desensitized state which is further divided into fast-onset (I) or slow-onset (D) states (Figure 9).^{129,137}

The rate at which the receptor will switch from one state to another is dependent upon the energy barriers between the states.¹²⁹

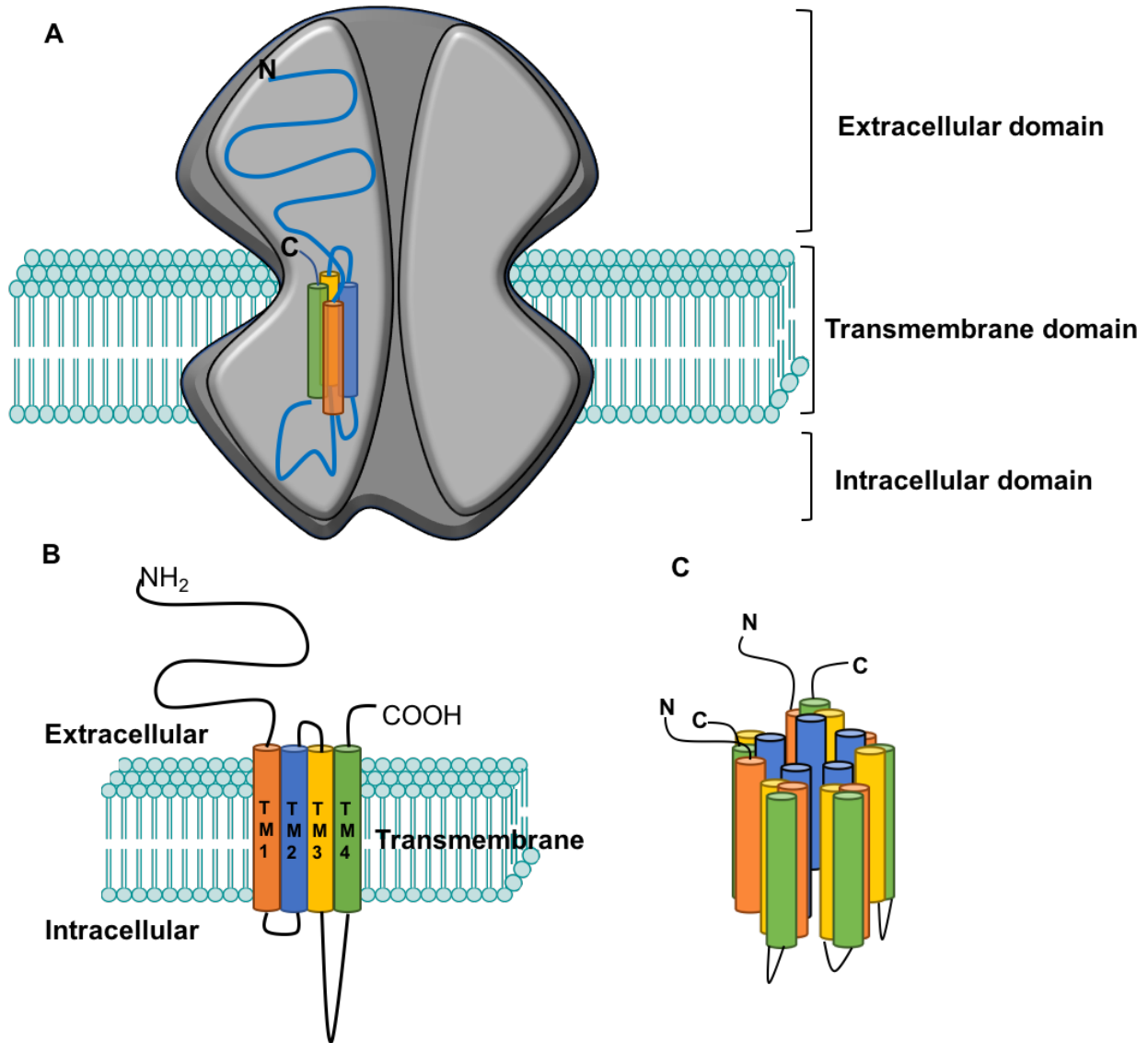


Figure 8. Schematic representation of an nAChR highlighting the ECD, TMD, and ICD traversing the lipid bilayer. (A) Arrangement of an individual subunit from the N-terminus to the C-terminus. The polypeptide is denoted by black-colored lines and the four TM-spanning units are represented as cylinders – orange (TM1), blue (TM2), yellow (TM3) and green (TM4). (B) 2D schematic highlighting the topology of an individual subunit. (C) Rearrangement of 5 subunits (20 TM-spanning units in total) with the central ion pore being formed by TM2 from each subunit. This figure is adapted from Chatzidaki et al.¹²³

While the rate of receptor action is rapid and a short process (microsecond-to-millisecond), desensitization takes place slowly, over a millisecond to second time range.¹²⁹ Orthosteric agonists have a high affinity for the active state (A) and tend to stabilize it. On the other hand, orthosteric (competitive) antagonists stabilize and have a high affinity for the resting or inactive state (R).¹²⁹

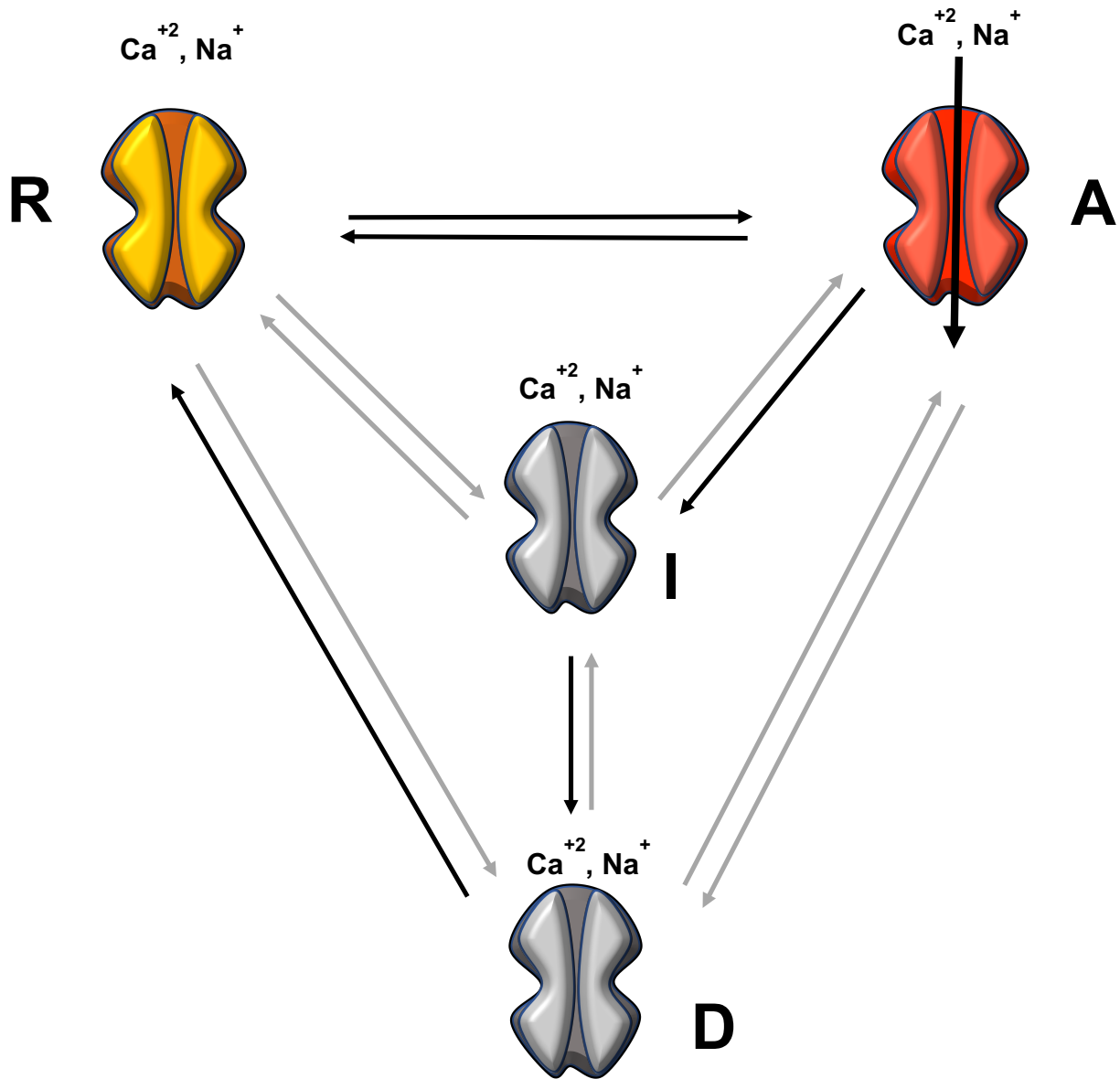


Figure 9. The Monod-Wyman-Changeux model¹³⁷ explaining allosteric transition states in nAChRs with 'R' depicting resting state, 'A' is active state, 'I' is fast-onset while 'D' is slow-onset desensitized state.

d. PAMs and their types

PAMs improve the activity of the endogenous, orthosteric agonists without eliciting a response on their own.¹²³ One of the earliest nAChR-PAMs to be identified is the divalent cation, Ca^{+2} .¹³⁸ This was based on several reports indicating that high levels of Ca^{+2} are released from the presynaptic neuron along with neurotransmitters and that Ca^{+2} levels in brain regions varied according to synaptic activity.^{138,139} Moreover, the observation that the chick $\alpha 7$ -5HT₃ chimera with the N-terminal of the chick $\alpha 7$ and C-terminal of 5HT₃ receptor, could be potentiated by Ca^{+2} .¹³⁸ Ca^{+2} could also potentiate $\alpha 7$ nAChRs like the chimera, but not 5HT₃ receptors, thus indicating the role of the N-terminal domain of $\alpha 7$ nAChRs in Ca^{+2} binding.¹³⁸ Mutagenesis studies in the $\alpha 7$ -V201-5HT₃ chimera suggested that mutations in Asp163 (human $\alpha 7$ -Asp186) and Glu172 (human $\alpha 7$ -Glu195) on the complementary subunit affected ACh and Ca^{+2} apparent affinity.¹³⁸ Ivermectin (**14**, Figure 10), an anthelmintic agent is an allosteric modulator of worm (*Caenorhabditis elegans*) glutamate receptors.¹⁴⁰ Application of ivermectin potentiated the ACh-evoked currents in chick and human neuronal $\alpha 7$ nAChRs but itself had no activity.¹⁴⁰ Furthermore, pre-application of ivermectin to chick $\alpha 7$ nAChRs could potentiate the current evoked by the partial agonist, DMPP (1,1-dimethyl-4-phenylpiperazinium) (**15**, Figure 10) such that it emulated currents elicited by a full agonist such as ACh.^{140,141} Another molecule that can potentiate the potency along with the efficacy of ACh at $\alpha 7$ nAChRs is 5-hydroxyindole (5-HI) (**16**, Figure 10), a modulator of 5-HT₃ receptors.¹⁴² Like ivermectin, 5-HI does not elicit a response on its own at nAChRs and, hence, does not act as an $\alpha 7$ nAChR agonist

but potentiates ACh-evoked responses with maximum potentiation (12-fold) observed at 20 mM.^{141,142}

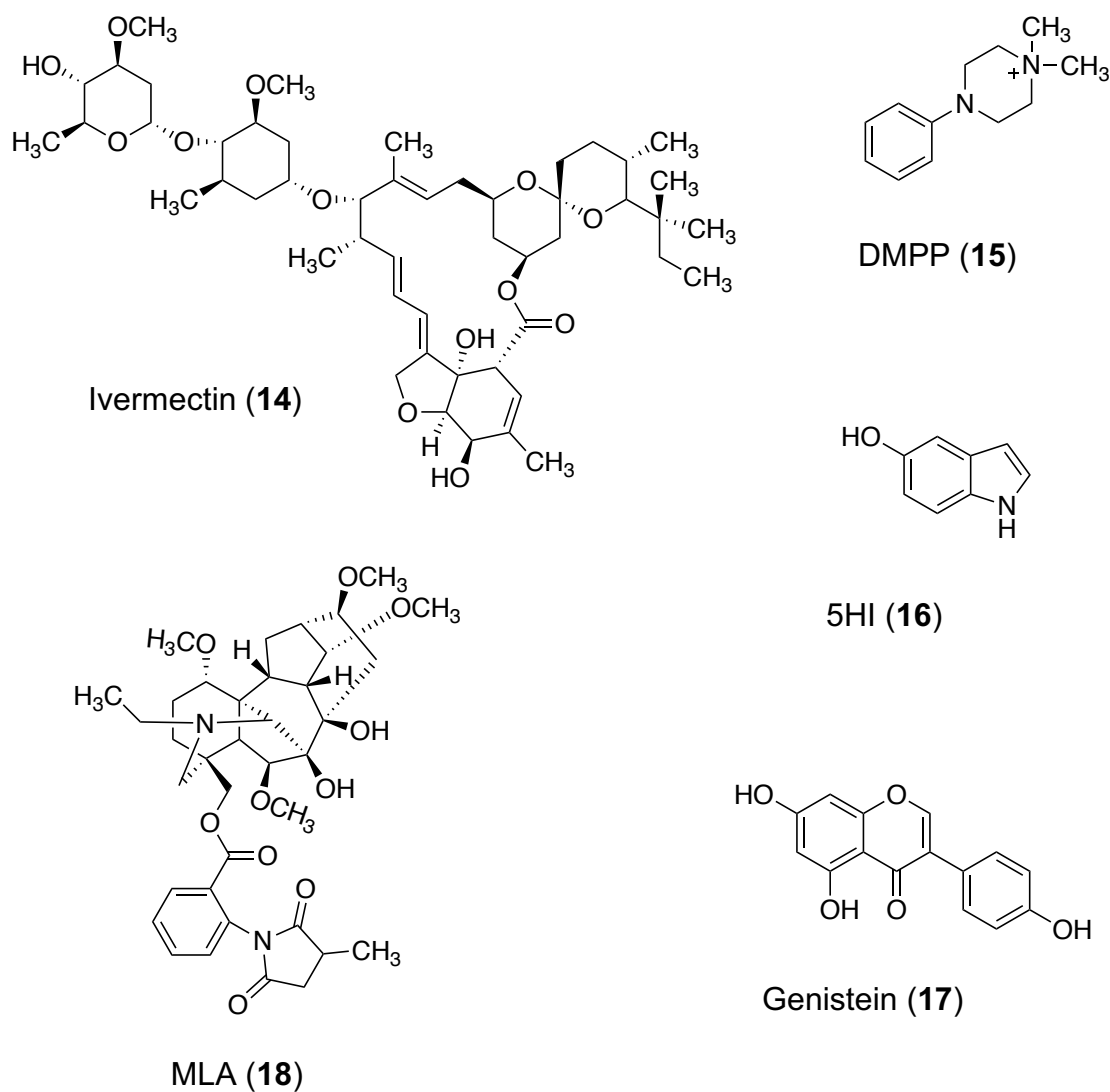


Figure 10. The type-I and type-II PAMs of nAChRs, ivermectin (14), DMPP (15), 5HI (16), genistein (17) and the selective $\alpha 7$ nAChR antagonist, MLA (18).

However, the presence of 5-HI with ACh shifts the inhibition curve of the antagonist methyllycaconitine (MLA) towards higher concentrations, indicating that perhaps 5-HI interacts competitively with $\alpha 7$ nAChRs.¹⁴² Genistein (17, Figure 10), a tyrosine kinase

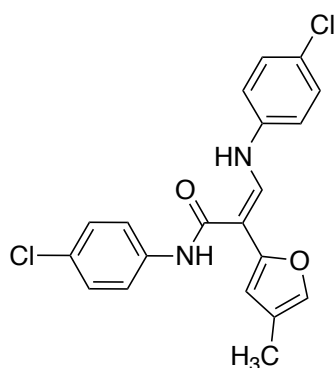
inhibitor, is another molecule like 5-HI that only affected apparent agonist-evoked currents without modulating desensitization states.¹⁴³ The protein, secreted mammalian Ly-6/uPAR related protein (SLURP-1), can also effectively act as an $\alpha 7$ nAChR PAM by increasing ACh-evoked currents and shifting the EC₅₀ curve.¹⁴¹ Specific peptide sequences in bovine serum albumin (BSA) are also capable of potentiating agonist-evoked currents in $\alpha 7$ nAChRs.¹⁴¹

All of the above-mentioned molecules and proteins can be considered as the first generation of $\alpha 7$ nAChR PAMs.^{123,141} The second generation of PAMs are molecules that are classified based on the type of modulation they bring about in the receptor.^{123,141} Generally, PAMs might potentiate the agonist-evoked responses by decreasing the energy barrier between resting and active states or by increasing the energy barrier between the active and desensitized states.¹²³ Additionally, they may also cause destabilization of the desensitized state of the receptor.¹²³ Depending on how they modulate receptor activity, PAMs can be divided into Type-I and Type-II PAMs.¹²³ Type-I PAMs only potentiate agonist-evoked currents and therefore possibly act by modulating the energy barriers between the resting and active states.¹²³ On the other hand, type-II PAMs affect desensitization in addition to potentiating agonist-evoked responses.¹²³

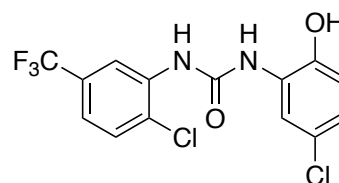
Of the molecules mentioned above, ivermectin (**14**, Figure 10), 5-HI (**16**, Figure 10) and genistein (**17**, Figure 10) are classified as type-I PAMs.^{123,141,144} Other molecules which reportedly belong to this class are compound-6 (**19**, Figure 11) (N-4-chlorophenyl)- α -[[(4-

chloro-phenyl)amino]methylene]-3-methyl-5-isoxazole acetamide), the biarylurea analog NS-1738 (**20**, Figure 11), LY-2087101 (**21**, Figure 11), and galantamine (**3**).^{141,144}

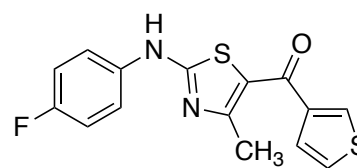
One of the most well characterized molecules that behaves as a type-II PAM is the urea analog PNU-120596 (**22**, Figure 11), which increases ACh-evoked currents in $\alpha 7$ nAChR by 4-fold and also suppresses the desensitization rate.¹⁴⁵ Another molecule that can increase peak currents and slow desensitization in these receptors is the molecule, 4-



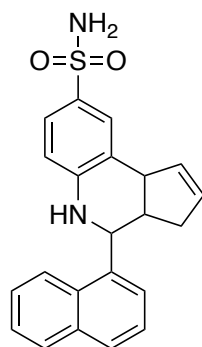
Compound 6 (**19**)



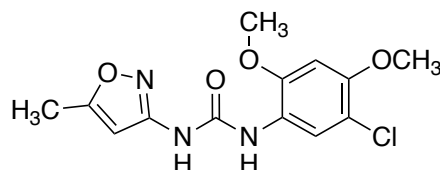
NS-1738 (**20**)



LY-2087101 (**21**)



TQS (**23**)



PNU-120596 (**22**)

Figure 11. Other PAMs of nAChRs, Compound 6 (**19**), NS-1738 (**20**), LY-2087101 (**21**), PNU-120596 (**22**) and TQS (**23**).

naphthalene-1-yl-3a,4,5,9b-tetrahydro-3-H-cyclopenta[c]quinoline-8-sulfonic acid amide (TQS, **23**).¹⁴⁴

Mutagenesis studies with $\alpha 7$ nAChRs indicates that the binding site of PNU-120596 and LY-2087101 is located in an intrasubunit cavity within the TMD.¹⁴⁶ Particularly, mutations in the residues Ser222 and Ala225 of TM1, Met253 of TM2, and Phe455 and Cys459 of TM4 affected potentiation of agonist-evoked currents by PNU-120596.¹⁴⁶ Of these, mutations in the residues Ala225 and Met253 had the most profound effect on PNU-120596's potentiation of agonist-evoked responses in $\alpha 7$ nAChRs.¹⁴⁶ These two residues also significantly decreased the potentiation of agonist-evoked currents by the type-1 PAM, LY-2087101.¹⁴⁶ The type-1 PAM ivermectin is also said to bind in an intrasubunit cavity in the transmembrane region of $\alpha 7$ nAChRs and is affected by mutations in 7 residues: Ser222, Ala225, Met253, Cys459, Glu272, Thr456, Ser276, of which the first four residues are also important for potentiation by PNU-120596.^{146,147} Interestingly, of these residues, mutations S222M, M253L, and S276V converted ivermectin from a positive allosteric modulator to a negative allosteric modulator.¹⁴⁷ The binding site of the type-1 PAM NS1738 was initially proposed to be in the 10-amino acid extracellular segment joining TM2 and TM3. However, mutagenesis data suggested that NS1738's potentiating effect is affected by the same residues that were deemed important for PNU-120596.¹⁴⁸

e. Negative allosteric modulators (NAMs)

Like PAMs, NAMs do not evoke a response on their own, but unlike PAMs, NAMs inhibit agonist-evoked responses by binding to sites (allosteric) that are distinct from the orthosteric sites.¹²³ Kynurenic acid (KYNA, **24**, Figure 12), a major metabolite from the kynurenine pathway of tryptophan degradation in the brain, is a reported NAM of $\alpha 7$ nAChRs.¹⁴⁹ The activity of KYNA as a neuroprotective and anticonvulsant agent is attributed to its action as a competitive antagonist of the glycine-binding site on the NMDA receptor.¹⁴⁹ The concentration of KYNA required to inhibit NMDA receptors in the absence and presence of glycine is 15 and 250 μM , respectively.¹⁵⁰ The KYNA concentration in the brain fluctuates between the low nanomolar to low micromolar range and hence, raises the question whether KYNA is present in sufficient quantities to interact and inhibit NMDA receptors.¹⁵⁰ However, even at a nanomolar concentration, KYNA can antagonize $\alpha 7$ nAChRs but not NMDA receptors, indicating that perhaps $\alpha 7$ nAChRs are a high-affinity target of KYNA.¹⁵¹ Another NAM is the molecule UCI-30002 (**25**, Figure 12), that displays selectivity for neuronal nAChRs over muscle-type nAChRs.¹⁵² HDMP (1,2,3,3a,4,8b-hexahydro-2-benzyl-6-*N,N*-dimethylamino-1-methylindeno[1,2,-b]pyrrole) (**26**, Figure 12) is a molecule that is approximately 360- and 414-fold more selective for $\alpha 7$ nAChRs than $\alpha 4\beta 2$ and $\alpha 3\beta 4$ nAChRs, respectively.¹⁵³ The same study also reported, for the first time, the functional activity of phencyclidine (PCP) (**27**, Figure 12) at $\alpha 7$ nAChR.¹⁵³ PCP is 23- and 5-fold more selective for $\alpha 7$ nAChR than $\alpha 4\beta 2$ and $\alpha 3\beta 4$ nAChRs, respectively.¹⁵³ Previously, from our laboratory we reported the molecule, MD-

354 (**28**, Figure 12) to decrease the (-)-nicotine evoked antinociceptive effect in the mouse tail-flick assay by behaving as a NAM specifically at the $\alpha 7$ nAChRs.¹⁵⁴

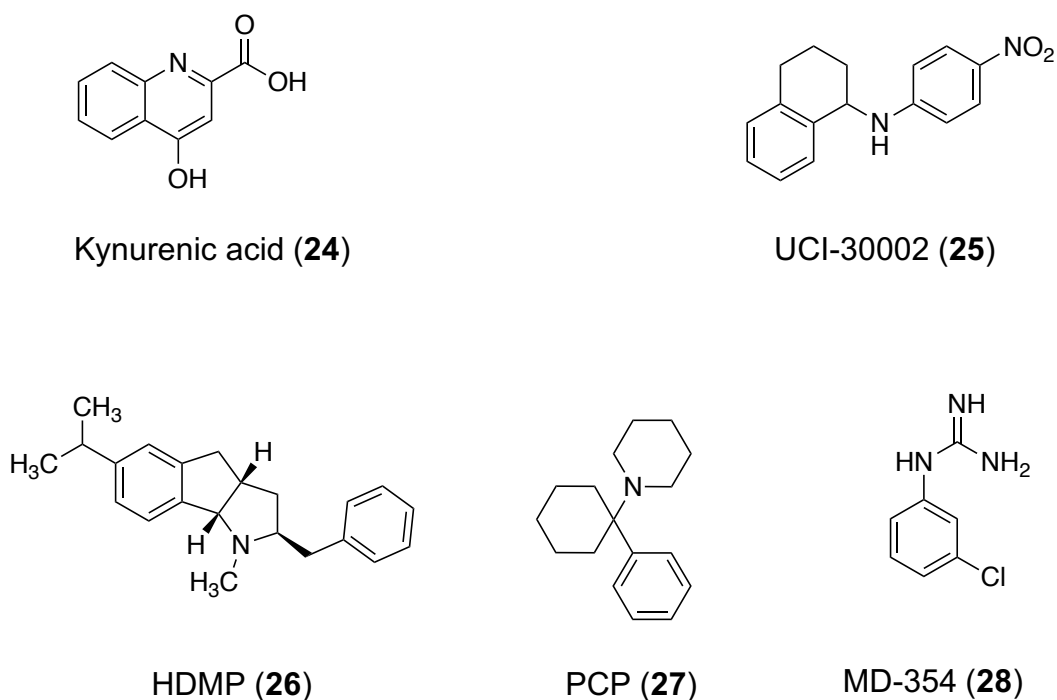


Figure 12. NAMs of nAChRs. KYNA (**24**), UCI-30002 (**25**), HDMP (**26**), PCP (**27**), MD-354 (**28**).

Spurny et al.¹⁵⁵ conducted a study to identify potential allosteric sites on the human $\alpha 7$ nAChR-snail AChBP chimera ECD by employing fragment-based screening, surface plasmon resonance (SPR) studies, and X-ray crystallography. The screening and SPR studies identified five fragments, and electrophysiological studies indicated that these fragments were NAMs of $\alpha 7$ nAChR.¹⁵⁵ The crystal structure of these fragments with the

human $\alpha 7$ nAChR-snail AChBP chimera led to the identification of three allosteric binding sites – one near the N-terminal ECD, another in the intrasubunit pocket in the vestibule of the receptor and the last one in the pocket below the agonist binding site (agonist subpocket).¹⁵⁵

f. Silent allosteric modulators (SAMs)

SAMs are allosteric modulators that do not alter the activity of orthosteric ligands but inhibit the effect of other allosteric modulators.¹²³ Gill-Thind et al.¹⁵⁶ reported two compounds, 2,3,5,6MP-TQS (**29**, Figure 13) (*cis-trans*-4-(2,3,5,6-tetramethylphenyl)-3a,4,5,9b-tetrahydro-3H-cyclopenta[c]quinoline-8-sulfonamide) and 2,4,6MP-TQS (**30**, Figure 13) (*cis-trans*-4-mesityl-3a,4,5,9b-tetrahydro-3H-cyclopenta[c]quinoline-8-

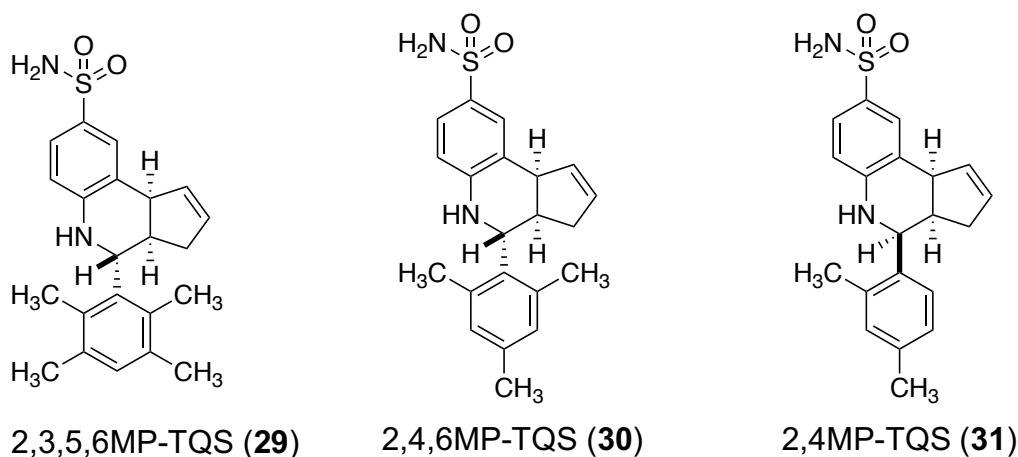


Figure 13. SAMs of nAChRs – 2,3,5,6MP-TQS (**29**), 2,4,6MP-TQS (**30**) and the allosteric agonist 2,4MP-TQS (**31**).

sulfonamide) which, by themselves, did not elicit a response in $\alpha 7$ nAChRs and neither did they potentiate agonist-evoked currents. However, they inhibited the currents evoked by an allosteric agonist 2,4MP-TQS (**31**, Figure 13) (*cis-cis*-4-(2,4-dimethylphenyl)-3a,4,5,9b-tetrahydro-3*H*-cyclopenta[*c*]quinoline-8-sulfonamide) (reported by the same group), hence acting as SAMs of $\alpha 7$ nAChRs.¹⁵⁶

g. Ago-PAMs

Ago-PAMs, are PAMs that are capable of inducing an agonist-like response in the receptor, in the absence of the orthosteric agonist.¹²³

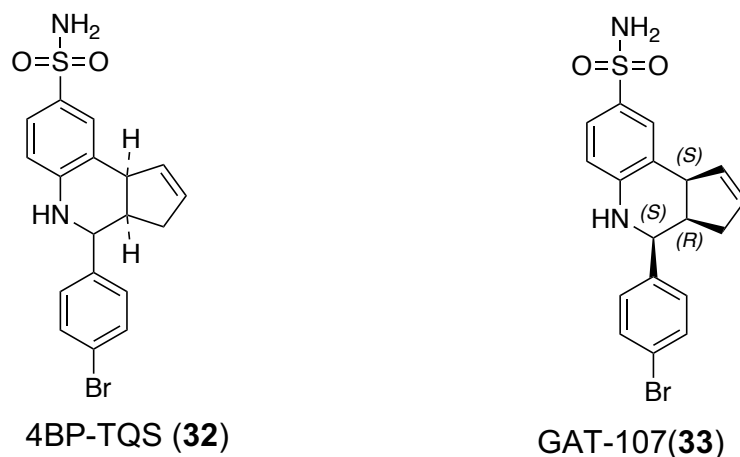


Figure 14. Ago-PAM of nAChRs with the racemate 4BP-TQS (**32**) and its resolved (+)-enantiomer, GAT-107 (**33**).

A structural analog of the previously mentioned SAMs, 2,3,5,6MP-TQS and 2,4,6MP-TQS, 4BP-TQS (**32**, Figure 14) (4-(4-bromophenyl)-3a,4,5,9b-tetrahydro-3*H*-

cyclopenta[c]quinoline-8-sulfonamide), is not only an allosteric agonist but also a type-II PAM.^{157,158} Although initially studied as the racemate, the enantiomers of the compound were separated by chiral HPLC to reveal, GAT-107 (**33**, Figure 14), the (+)-enantiomer (stereochemistry-3aR,4S,9bS) of 4BP-TQS to be the most potent.¹⁵⁹

h. Agonist binding site

Agonists (e.g. ACh) bind at the interface of two subunits – designated as the principal and complementary subunits.¹³³ The α subunits in all cases form the principal component while the complementary component is usually provided by a non- α subunit, except in the case of homopentameric $\alpha 7$ nAChRs, wherein all subunits are $\alpha 7$.¹²⁹ Therefore, based on the composition of nAChRs (heteromeric vs homomeric), the number of binding sites range from 2-5. The amino acids that are involved in the ligand-binding domain of $\alpha 7$ nAChRs are Tyr115, Trp171 and Tyr217. Additionally, the residues Cys212 and Cys213 are involved in a disulfide bond within the C-loop of the ECD. Two other cysteine residues, Cys 150 and Cys164, separated by 13 amino-acid residues form the characteristic disulfide bond that gives the receptor family the name, “Cys-loop” receptors.

III. Rationale and Specific Aims

Although a vast number of hypotheses (as described previously) offer pathophysiological explanations for AD, only the cholinergic hypothesis is supported by 4 out of 5 FDA-approved drugs for treating AD.⁶ One of these drugs is the natural alkaloid galantamine (**3**, Figure 1), that is used to treat mild-to-moderate forms of AD and exerts its effect by a poor, reversible inhibition of AChE.⁸⁵ Unlike the other, currently FDA-approved drugs, galantamine is also a PAM at neuronal nAChRs.⁹¹⁻⁹⁵ Perhaps the cholinergic deficiency in AD is ameliorated by galantamine by its combined AChE inhibition and nAChR PAM activity. However, galantamine can act as a nAChR-PAM at concentrations lower than those required for it to act as an AChE inhibitor.^{78,102,103} Therefore, galantamine's clinical benefits might be primarily associated with its nAChR-PAM effect and, at a secondary level, by its AChE inhibitory action. To explore this possibility, it is essential to separate the nAChR-PAM component from the AChE inhibitory portion, in terms of chemical structures. The overall, long-term goals of this project are: 1) To identify and separate the structural features of galantamine that are required for nAChR-PAM activity from those required for AChE inhibition; 2) To study the ligand-receptor interactions using molecular

modeling studies; 3) To determine the pharmacological profile of galantamine and its deconstructed analogs for $\alpha 7$ nAChR.

The specific aims of this project are;

Specific Aim 1: To identify the minimum structural features of galantamine that will retain the PAM action at human $\alpha 7$ nAChRs.

Approach

- a. Perform a 3D overlap of the structural features of galantamine (**3**, Figure 1) with codeine (**8**, Figure 5).

Codeine (**8**, Figure 5), another $\alpha 7$ nAChR PAM bearing structural resemblance to galantamine (**3**, Figure 1), lacks inhibitory action at AChE.⁹⁴ A 3D overlap between the two molecules will be performed to ascertain common, shared structural features. Hence, given the similarities between the two molecules, the differences might afford some clues to what is required for the PAM action that is common to both agents.

Hypothesis

If the dissimilarities in the 3D overlap of codeine and galantamine account for their contrasting action at AChE, then deconstructed analogs of galantamine lacking these moieties should retain the nAChR-PAM action of their parent, galantamine (Figure 17).

- b. Based on Approach **1a**, synthesize smaller, structurally-abbreviated analogs of galantamine by employing the deconstruction approach.

To unravel the minimum structural features (pharmacophore) of galantamine that are required to exert its PAM effect at $\alpha 7$ nAChRs, the deconstruction approach will be employed. “Deconstructing” a parent molecule involves removal of particular structural features one at a time, resulting in smaller, structurally abbreviated analogs. In such a way, the influence of these features on the biological target of interest can be studied.¹⁶⁰ In terms of structure, galantamine houses a furobenzazepine, benzofuran, benzazepine, phenylpropylamine and benzylamine scaffold (Figure 15). The analogs that will retain most of the structural features will be those that are a product of deconstructing the substituents on the phenyl (methoxy group), cyclohexyl (hydroxyl group or double bond) and/or the azepine ring (*N*-methyl group). The most deconstructed analogs will be those belonging to the benzylamine scaffold, bearing only the phenyl ring and the alkyl amine portion of galantamine (Figure 15).

Deconstructing the molecule to any of these scaffolds will determine the influence of the trimmed portions on the PAM effect of galantamine at $\alpha 7$ nAChRs. Ultimately it is of interest to tease out the structural components that are essential for PAM activity at $\alpha 7$ nAChRs from those that participate in AChE inhibition.

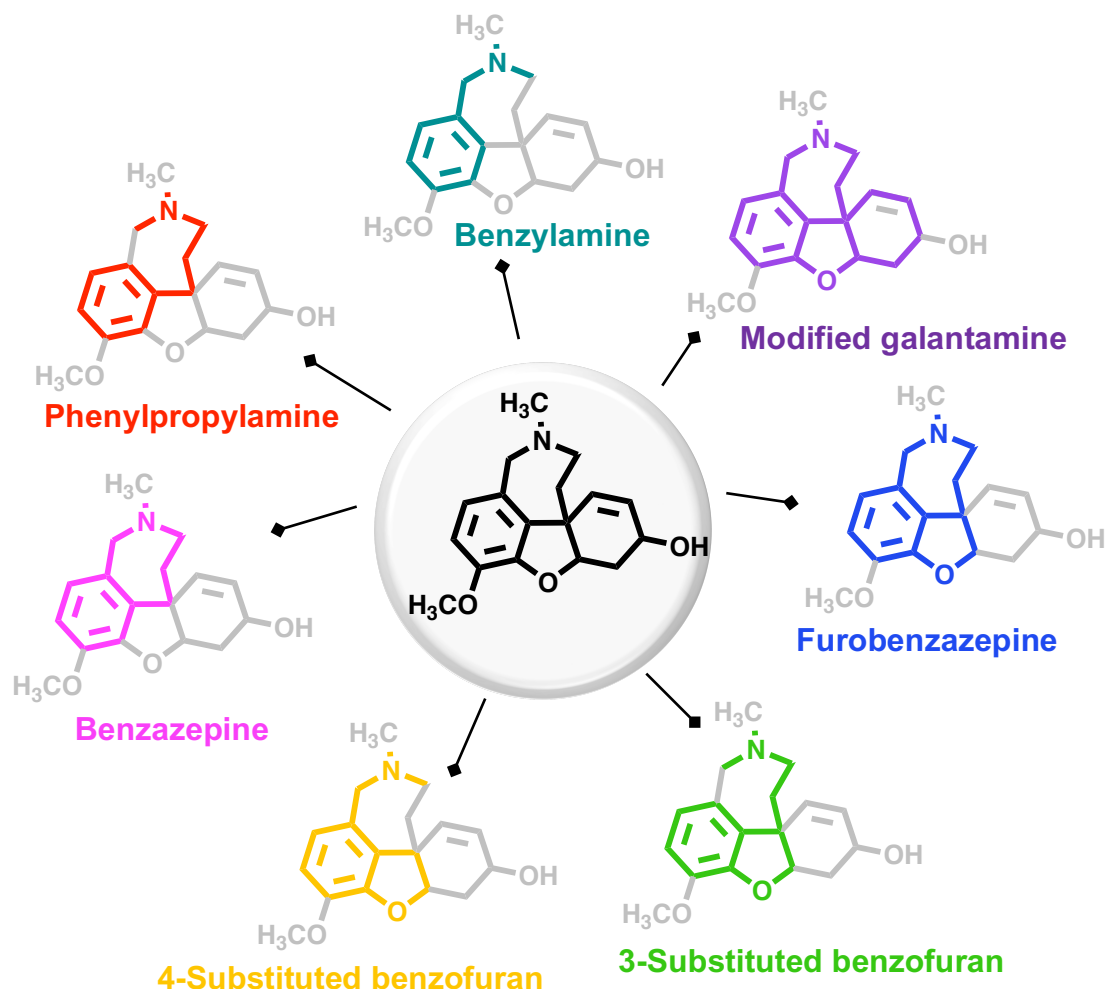


Figure 15. Galantamine (center; black) and some probable deconstructed analogs. The structural features that can be deconstructed are colored grey. The scaffolds represented in this figure are the “modified galantamine” (violet), furobenzazepine (blue), benzofuran (green and yellow), benzazepine (magenta), phenylpropylamine (red) and benzylamine (teal).

The deconstructed analogs with minimal modifications will be dictated by the 3D structural overlap of galantamine and codeine and will be specified in the results and discussion. In order to identify the PAM pharmacophore for $\alpha 7$ nAChRs, galantamine can be systematically deconstructed to its smallest analog belonging to the benzylamine scaffold

(Figure 15). The benzylamine scaffold is a deconstructed form of the benzazepine scaffold, which in turn is borne out of the furobenzazepine scaffold (Figure 15). Cleaving the cyclohexenol ring of galantamine will result in 7-methoxy-2-methyl-1,2,3,4,4a,5-hexahydrobenzofuro[4,3-cd]azepine (**34**; 'furobenzazepine' scaffold; Figure 16).

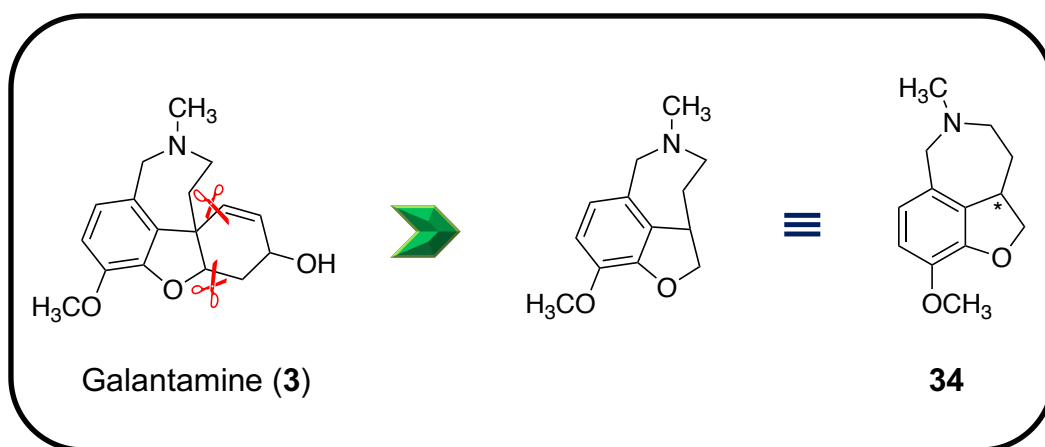


Figure 16. Deconstruction of galantamine to **34**.

Trimming the 2,3,4,7-tetrahydroazepine ring of **34** will give rise to two types of benzofuran analogs depending on which side of the ring is deconstructed. Deconstructing the azepine ring from the phenyl side (**A**, Figure 17) will result in *N,N*-dimethyl-2,3-dihydro-7-methoxy-3-benzofuranethylamine (**35**). For the purpose of this initial study, the deconstructed analogs with a chiral center (such as **35**) will be synthesized as racemic mixtures.

Abbreviating **34** from the dihydrofuran side of the azepine ring (**B**, Figure 17) will result in 4-(*N,N*-dimethylamine)methyl-7-methoxy-2,3-dihydrobenzofuran (**36**).

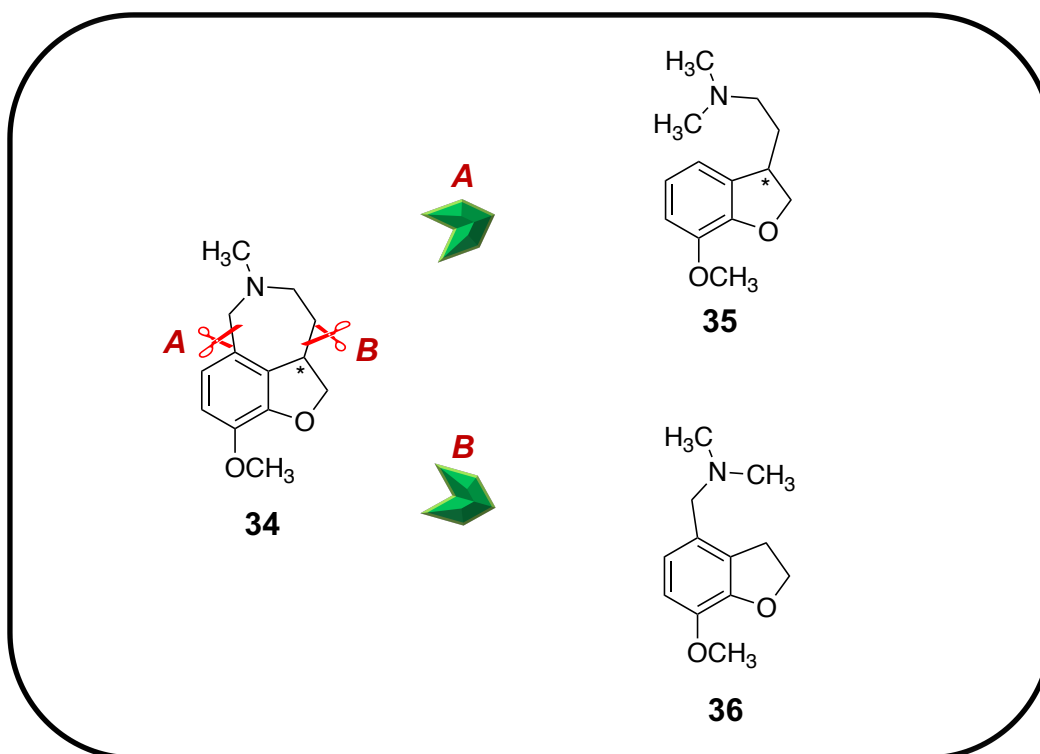


Figure 17. Selective deconstruction of the azepine ring of analog **34**.

A tertiary degree of alkylation of the amine in both, **35** and **36** will be retained by having methyl groups to match the tertiary amine of not only **34** but also the parent, galantamine.

Another way of abbreviating **34** will be to deconstruct the dihydrofuran ring to 6,7-dimethoxy-2-methyl-1,3,4,5-tetrahydro-2*H*-benzo[*c*]azepine (**37**) (Figure 18). Removal of the 6-methoxy group from **37** will result in 7-methoxy-2-methyl-1,3,4,5-tetrahydro-2*H*-benzo[*c*]azepine (**38**) (Figure 18).

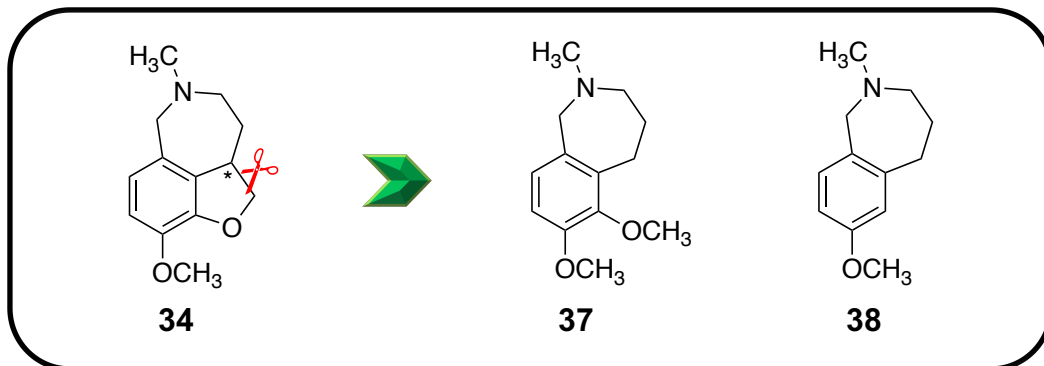


Figure 18. Deconstruction of dihydrofuran ring of analog **34**.

Dissecting the azepine ring from either side of the amine results in analogs belonging to the benzylamine and phenylpropylamine scaffold (Figure 19). Compound **37** can be deconstructed at the 1-9a bond (Figure 19) to give 3-(2,3-dimethoxyphenyl)-*N,N*-dimethylpropylamine (**39**). Further removal of the 2-methoxy substituent in **39** results in 3-(3-dimethoxyphenyl)-*N,N*-dimethylpropylamine (**40**) (Figure 19).

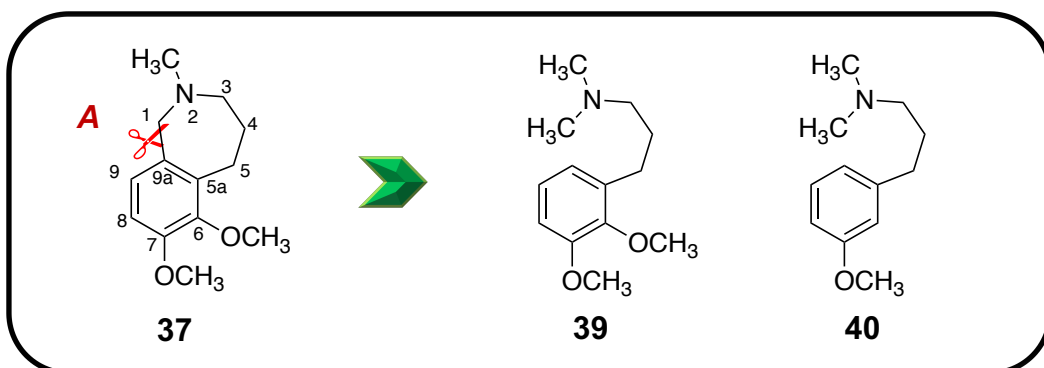


Figure 19. Deconstruction of the azepine ring of analog **37** to form the phenylpropylamine analogs **39** and **40**.

Finally, deconstruction of compound **37** will result in the benzylamines **41** and **42** (Figure 20). Selectively cleaving the 5-5a bond in **37** gives rise to 3,4-dimethoxybenzyl-*N,N*-dimethylamine (**41**, Figure 20). Analog **42** (3-methoxybenzyl-*N,N*-dimethylamine) is a des-methoxy analog of **41** (Figure 20).

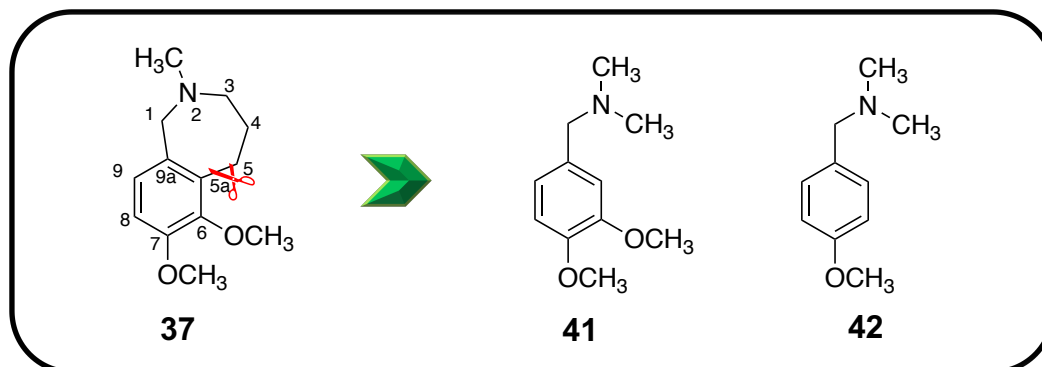


Figure 20. Deconstruction of the azepine ring of analog **37** to form the benzylamine analogs **41** and **42**.

The phenylpropylamines **39** and **40**, and the benzylamines **41** and **42** will determine whether the presence of the complete azepine ring contributes towards PAM activity at $\alpha 7$ nAChRs.

Specific Aim 2: To study the molecular interactions of galantamine and its deconstructed analogs with the human $\alpha 7$ nAChR by molecular modeling.

Approach:

- a. Generate 3-dimensional homology models of the human $\alpha 7$ nAChR.

As of early 2018, there are no crystal structures of the human $\alpha 7$ nAChRs. Therefore, in order to study the interactions of galantamine and its proposed deconstructed analogs, homology models of human $\alpha 7$ nAChRs will be generated from a suitable template. Most of the structural information about nAChRs comes from the crystal structures of the ACh-binding protein (AChBP) from *Lymnaea stagnalis* (*Ls*-AChBP; PDB ID: 1I9B),¹⁶¹ whole crystalline array of nAChRs from *Torpedo maromorata* (PDB ID: 2BG9),^{162,163} and the ECD of the mouse $\alpha 1$ subunit of the nAChR (PDB ID: 2QC1).¹⁶⁴ AChBP is a soluble molluscan protein that is found in glial cells and is capable of modulating cholinergic transmission.^{165,166} It is a protein 210 amino-acids long, which resembles and aligns with the ECD of nAChRs (especially the α subunit) but, unlike nAChRs, the AChBP lacks a TMD and an ICD.¹⁶¹ AChBP shares a 23.9% sequence identity in its 210 amino-acid residues with $\alpha 7$ nAChRs while the mouse $\alpha 1$ nAChR subunit shares a 38% identity.^{165,167} AChBP is also isolated from other species of snails such as *Aplysia californica* (*Ac*-AChBP), which is most widely used for crystallization.¹⁶⁸ However, the ligand-binding site in nAChRs is most comparable to *Ls*-AChBP as it retains all of the five aromatic amino acids that are conserved in nAChRs as opposed to *Ac*-AChBP.¹⁶⁸ To date, more than 50 crystal structures of AChBP with agonists and antagonists have been deposited in the protein data bank.¹⁶⁸ However, the crystal structure that provides 64% sequence identity to the human $\alpha 7$ nAChR is the chimera of *Ls*-AChBP and human $\alpha 7$ nAChR.¹⁶⁹

Prior to this, a number of homology models of $\alpha 7$ nAChRs have been generated.^{148,158,170,171} Schapira et al.¹⁷⁰ based their homology modeling (of various

nAChR subtypes, including $\alpha 7$) on the *Ls*-AChBP crystal structure to dock ACh and nicotine. Cheng et al.¹⁷¹ generated homology models of human $\alpha 7$ nAChRs based on the *T. marmorata* (TMD) and *Ls*-AChBP (ECD) crystal structures to study gating motion. Using these homology models, another group performed molecular docking studies to identify potential binding sites for the PAMs PNU-120596 and LY-2087101 in the TMD of $\alpha 7$ nAChRs.¹⁴⁶ Brannigan et al.¹⁷² conducted molecular dynamic simulations on the *T. marmorata* nAChR crystal structure to identify potential binding sites of the general anesthetic isoflurane. Another group employed a blind docking approach using the homology model of the $\alpha 7$ nAChR TMD to establish the binding site of the PAMs, NS1738 and PNU-120596.¹⁴⁸ In our laboratory, in the past we had based and generated homology models of human $\alpha 7$ nAChRs on the chimera of *Lymnaea stagnalis* acetylcholine-binding protein (AChBP)-human $\alpha 7$ nAChR crystal structure. This work was initially carried out by a graduate student (at the time) in our laboratory, Osama I. Alwassil.¹⁷³

The template that will be used for building the homology models is the crystal structure of the snail acetylcholine-binding protein (AChBP)-human $\alpha 7$ nAChR chimera (PDB ID: 3SQ6) bound to epibatidine.

- b. Dock and analyze the interactions and possible binding modes of galantamine and its deconstructed analogs at homology models of the $\alpha 7$ nAChR.

Specific Aim 3: To determine a pharmacological profile of galantamine and its deconstructed analogs at human $\alpha 7$ nAChRs by two-electrode voltage clamp (TEVC) techniques.

The *Xenopus laevis* oocyte is a widely employed heterologous expression system for ion channels, transporters, and receptors.¹⁷⁴ The main advantage is the large size (1-1.2 mm diameter) of an oocyte, which makes operations such as mRNA microinjections and impaling with electrodes possible.^{175,176} Another advantage of using oocytes for ion channel expression is that the oocytes themselves do not express a significant number of receptors or ion-channels.¹⁷⁴ This allows for an uninterrupted study of the protein (in our case, human $\alpha 7$ nAChRs) of choice.¹⁷⁴ Even if there are endogenous channels being expressed, the currents from these are generally much smaller than those generated by the expressed receptor of interest.¹⁷⁴ Following the microinjection of complementary RNA or complementary DNA (into the nucleus), the subsequently expressed protein can be studied via electrophysiological methods in a semi-automated manner.^{174,175} For recording whole-cell currents of oocytes, the two-electrode voltage clamp (TEVC) technique is considered to be an established approach.¹⁷⁷

In the TEVC, the voltage across the oocyte membrane is “clamped” or controlled and the currents flowing through the expressed channels are measured.¹⁷⁶ One electrode is the voltage recording electrode (e_v) that monitors the membrane potential in the oocyte (Figure 21). The electrode e_v compares this potential to the command voltage which is set at a particular number (Figure 21). Exposure of the expressed ion-channels to agents

such as agonists, will cause the channels to open and allow ions to flow through the membrane. This causes a change in the overall membrane potential which is detected by e_v and compared to the bath potential to give the difference V_m (Figure 21). The V_m is then compared to the command voltage and the difference between the two is supplied as current through the second (current-injection) electrode, e_i , to the oocyte (Figure 21).

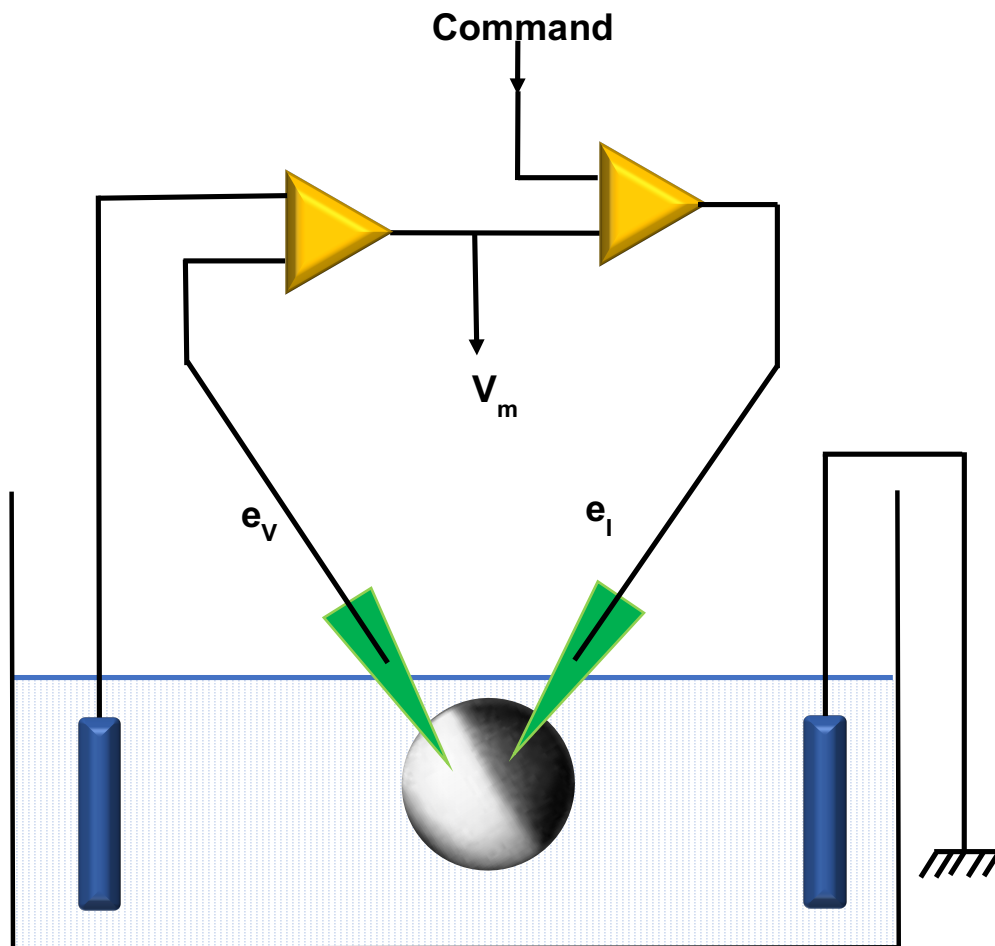


Figure 21. Schematic representation of the components of a TEVC set-up. The output from the electrode e_v is compared to the potential of the bath electrode and the difference is indicated by V_m . The potential V_m is then compared to the command voltage and the difference is injected to the electrode through the current electrode e_i . The bath electrodes are denoted by blue-colored cylinders. Adapted from Stühmer et al.¹⁷⁶

The current supplied to maintain the membrane potential is the parameter that is measured in these experiments. For nAChRs, the current generally presents an inward rectification, meaning that the ion channel allows more current to flow towards the cytoplasm.^{178,179}

The overall aim of this project is to unravel the pharmacophore of galantamine for its PAM action at human $\alpha 7$ nAChRs. Thus, it will be essential to determine the activity of the deconstructed analogs in an AChE inhibitory assay with galantamine as a positive control.

IV. RESULTS AND DISCUSSION

Specific Aim 1: To identify the minimum structural features of galantamine that will retain the PAM action at human $\alpha 7$ nAChRs

- a. Perform a 3D overlap of the structural features of galantamine (3, Figure 1) with codeine (8, Figure 5).**

A 3D overlap of galantamine with codeine was carried out while focusing on three different regions of the structure of galantamine – left-side, central and the right-side portions (Figure 22).

The overlap (Figure 23) revealed a superimposition of the left-side portion bearing the phenyl ring and the methoxy group. The structural features that also overlapped well were the tertiary amines and the dihydrofuran rings between the two molecules. In contrast to this, the right-side portion of these molecules were oriented differently in 3D space (Figure 23). Therefore, the structural features that displayed a good overlap, such as the phenyl ring, the methoxy group, the dihydrofuran ring and the tertiary amine in both of these molecules might participate in the nAChR-PAM action (Figure 23). Similarly, the region

of poor overlap consisting of the differently oriented cyclohexene double bond and the hydroxyl group (Figure 23), might explain why galantamine (**3**) is an AChE inhibitor whereas codeine (**8**) is not.

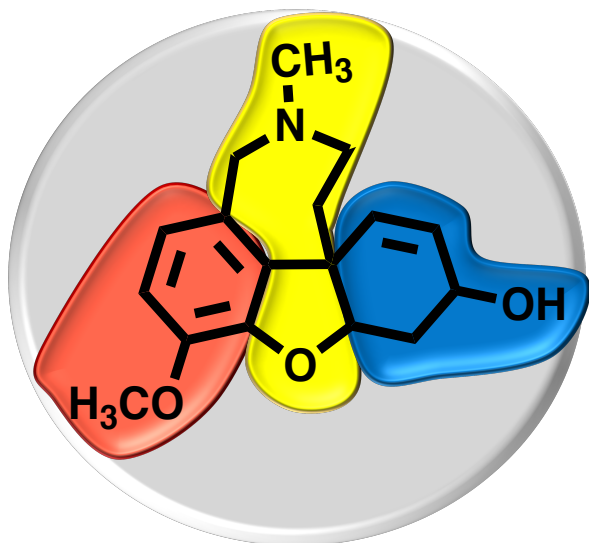
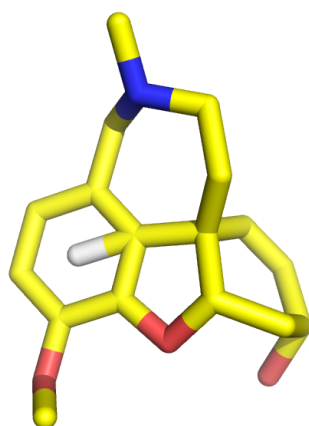
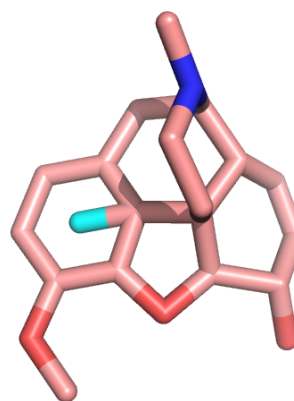


Figure 22. Division of galantamine's structure into three parts. The "left-side" (red) portion consists of the phenyl ring with the methoxy group. The "central" portion (yellow) is comprised of the tetrahydroazepine ring with the tertiary amine and the dihydrofuran ring. The "right-side" (blue) portion contains the cyclohexene ring with the allylic hydroxyl group.

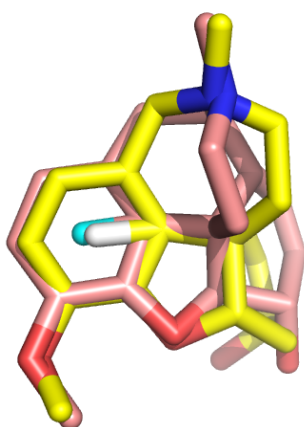
On the basis of this observation, the position of the double bond and the hydroxyl group in galantamine (**3**), perhaps, is not important for its nAChR-PAM activity. However, modifications to these two features has a drastic effect on AChE inhibition. Reduction of the cyclohexene double bond (right-side portion, Figure 22) of galantamine results in lycoramine (**6**) (Figure 24). An *in vitro* study reported that at 10 μM galantamine (**3**) inhibited 93% of cortical AChE activity obtained from mouse brain samples.²⁵ At the same concentration, lycoramine (**6**) inhibited only 30% of AChE activity.²⁵ In an electric eel AChE inhibitory assay, the IC_{50} of galantamine (**3**) was 1.07 μM while no inhibitory activity could be detected for lycoramine (**6**).¹⁸⁰



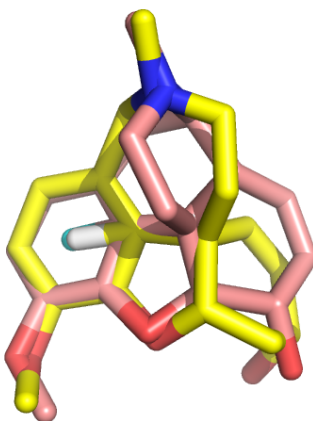
Galantamine (3)



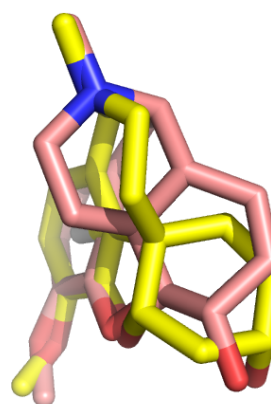
Codeine (8)



A



B



C

Figure 23. 3D structure of galantamine (yellow-colored sticks) and codeine (salmon-colored sticks). Frame A highlights the “left-hand” side of the overlap consisting of the phenyl ring with the methoxy group and the tertiary nitrogen atom. Frame B highlights the overlap of the dihydrofuran oxygen atom in both of these molecules. Frame C displays the dissimilar orientation of the cyclohexene ring and the hydroxyl group in both galantamine and codeine.

Conversion of the hydroxyl group in galantamine (**3**) to a carbonyl group results in galanthaminone (**43**, Figure 25), also known as narwedine. In the previously mentioned mouse cortical AChE inhibitory assay, **43** (Figure 25) could inhibit only 10% of the enzyme activity at 10 μM .²⁵ The IC_{50} s of galantamine (**3**), lycoramine (**6**), and galanthaminone (**43**) against human erythrocyte AChE were 1.7, 456, and 281 μM , respectively.¹⁸¹

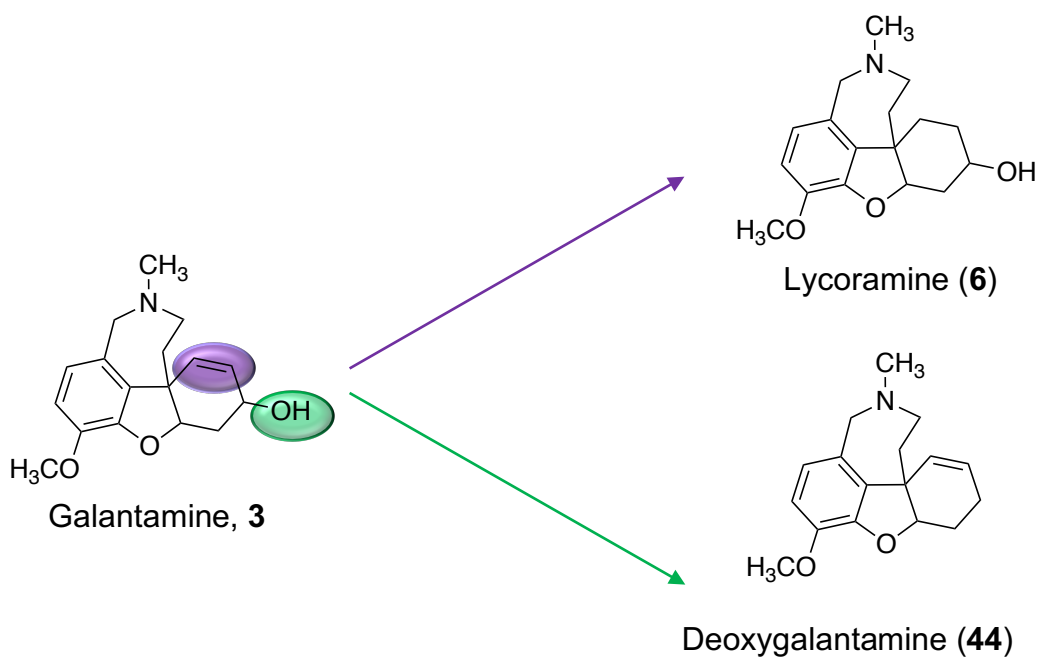


Figure 24. Deconstruction of the cyclohexenol ring in galantamine (**3**) results in **6** and **44**.

As previously discussed, the crystal structure of hrAChE co-crystallized with galantamine

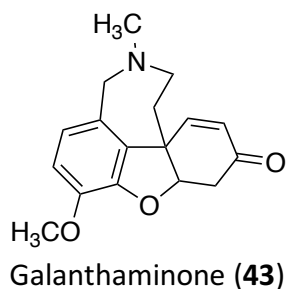


Figure 25. Structural derivative of galantamine (**3**), galanthaminone (narwedine) (**43**).

revealed that the hydroxyl group acts as a hydrogen bond donor in an interaction with the negatively-charged oxygen atom of Glu199. Oxidation of the hydroxyl group of galantamine **3** to **43** results in a loss of activity, perhaps due to the loss of a hydrogen bonding interaction. Since modifications of the hydroxyl group of galantamine (**3**) result in reduction

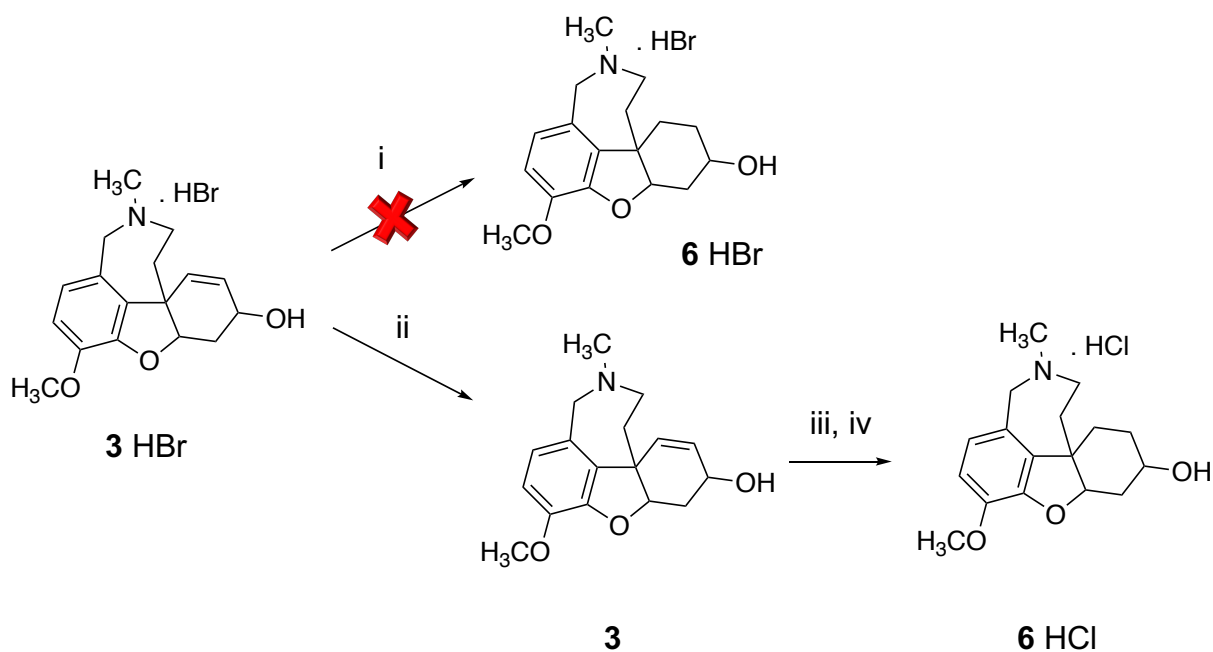
in AChE inhibition, perhaps complete removal of the group might drastically affect inhibitory activity.

Replacement of the hydroxyl group of galantamine (**3**) with a hydrogen atom will result in the deconstructed analog deoxygalantamine (**44**) (Figure 24), whereas the reduction of the double bond will result in lycoramine (**6**), another deconstructed analog (Figure 24). Synthesis of lycoramine (**6**) was attempted in two ways (Scheme 1). The first route involved the hydrogenation of the commercially available hydrobromide salt of **3** under pressure using Pd/C (10%). However, the reaction resulted in the formation of multiple products and isolation of the desired hydrobromide salt of **6** proved to be difficult. The second route of synthesis involved a two-step process starting from the hydrobromide salt of **3**. The salt was converted to its free base, **3**, using ammonium hydroxide according

to a procedure reported in literature.²⁵ The reaction resulted in a poor yield of a sticky solid that required a period of days to dry in a dessicator or under vacuum.

To avoid this, caution had to be taken to ensure that the ammonium hydroxide and solvents used for extraction were added in specific proportions, to **3** HBr, as reported in the literature.²⁵

Scheme 1. Preparation of lycoramine (**6**).^a



^aReagents and conditions: (i) H₂, 10% Pd/C, MeOH, 10 psi, 22 h; (ii) NH₄OH, 0°C for 30 min, rt for 2 h; (iii) H₂, 10% Pd/C, MeOH, 40 psi, 22 h; (iv) HCl/EtOH.

The hydrochloride salt of lycoramine (**6**) was eventually synthesized by hydrogenating the free base of galantamine (**3**) using Pd/C (10%) as catalyst. In the literature, the reaction was carried out for 10 h;²⁵ however, at this time-point the reaction indicated the presence

of starting material, so the reaction was allowed to continue until it was consumed, for a total of 22 h, with constant monitoring.

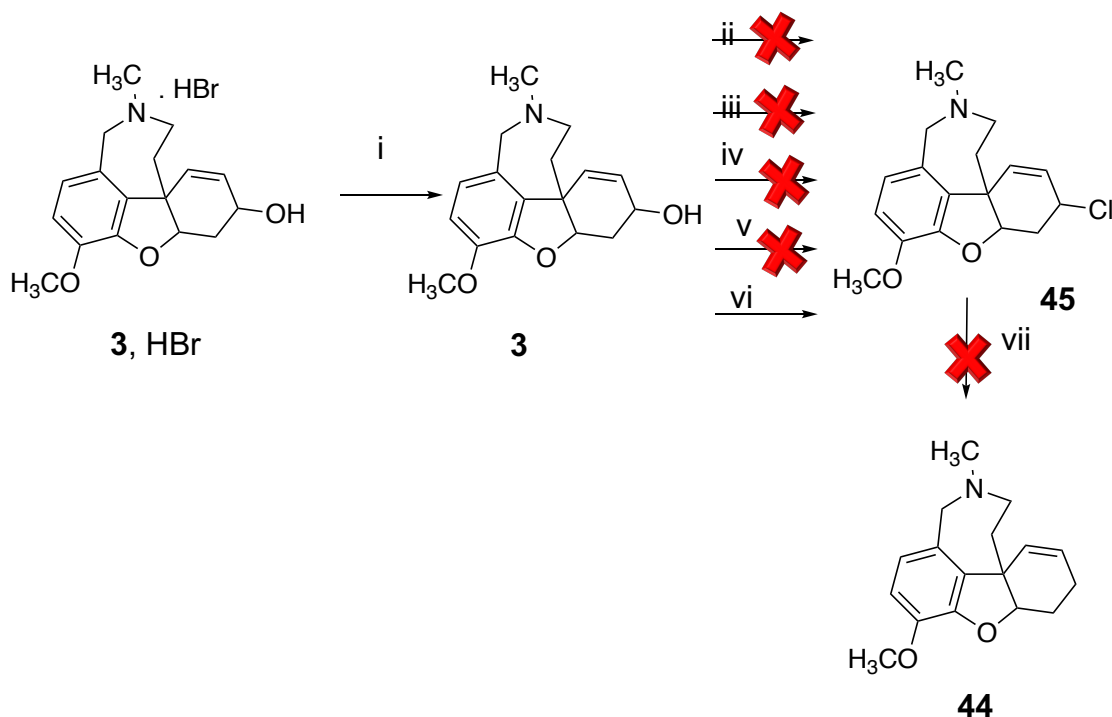
Synthesis of compound **44** was attempted in three steps, with the synthesis of intermediate **45** being attempted by five different methods, as highlighted in Scheme 2. The procedure to synthesize compound **45** from compound **3** was reported in the literature.²⁵ However, in our hands, the reaction never went to completion and isolation of the different products proved to be difficult. A variation of the conditions using Et₃N instead of pyridine as base¹⁸² resulted, again, in multiple products which were difficult to isolate.

Another procedure by Perissutti et al.¹⁸³ reported the synthesis of compound **45** by treating compound **3** with thionyl chloride in toluene as solvent. The reaction did not go to completion but indicated the presence of fewer products by TLC. However, isolation was troublesome and the work-up reported in the literature indicated formation of compound **45** as a free base. The reaction possibly resulted in the formation of a mixture of the hydrochloride salt (from thionyl chloride reaction) of **3** and **45**.

Failed attempts at purifying and isolating compound **45** often resulted in mixtures of compound **45** contaminated with starting material. An attempt was made to reduce this impure mixture, with the hope that perhaps the isolation of the compound **44** might become possible. The reduction reaction of compound **45** was attempted using

LiEt_3BH_3 ,¹⁸² however, the reaction gave additional products, which only made it more difficult to isolate and characterize **44**.

Scheme 2. Attempted synthesis of compound **44**.^a



^aReagents and conditions: (i) NH_4OH , 0°C for 30 min, rt for 2 h; (ii) TsCl , pyridine, CH_2Cl_2 , rt, 24 h; (iii) TsCl , Et_3N , CH_2Cl_2 , rt, 24 h; (iv) SOCl_2 , Et_3N , toluene, 55°C , 2 h; (v) SOCl_2 , toluene, 55°C , 2 h; (vi) SOCl_2 , reflux, 2 h; (vii) 1M solution SuperHydride® (LiEt_3BH_3) in THF, reflux, 2 h.

A variation of the chlorination reaction was reported in an article by Wildman et al.¹⁸⁴ and in a dissertation by Brown¹⁸⁵ for a compound, habranthine, that has a similar structure to **3**. Although this reaction did not go to completion, it resulted in the least number of additional products and finally, compound **45** was isolated, albeit in poor yield (6%). Both

of these reactions and their various conditions proved to be very low-yielding and the additional high cost of the starting material, **3**, made it difficult to set up reactions on a large scale. The synthesis of **44** was abandoned.

b. Based on Approach 1a, synthesize smaller, structurally-abbreviated analogs of galantamine by employing the deconstruction approach.

The synthesis of compound **35** and attempted synthesis of **34** is outlined in Scheme 3. The advantage of following this route was that compounds **34** and **35** shared a common precursor, **49**. The synthesis of compound **49** from **46** has been reported in the literature.^{186–188} The reaction conditions for these four reactions were followed according to those reported for a similar analog.^{189–191}

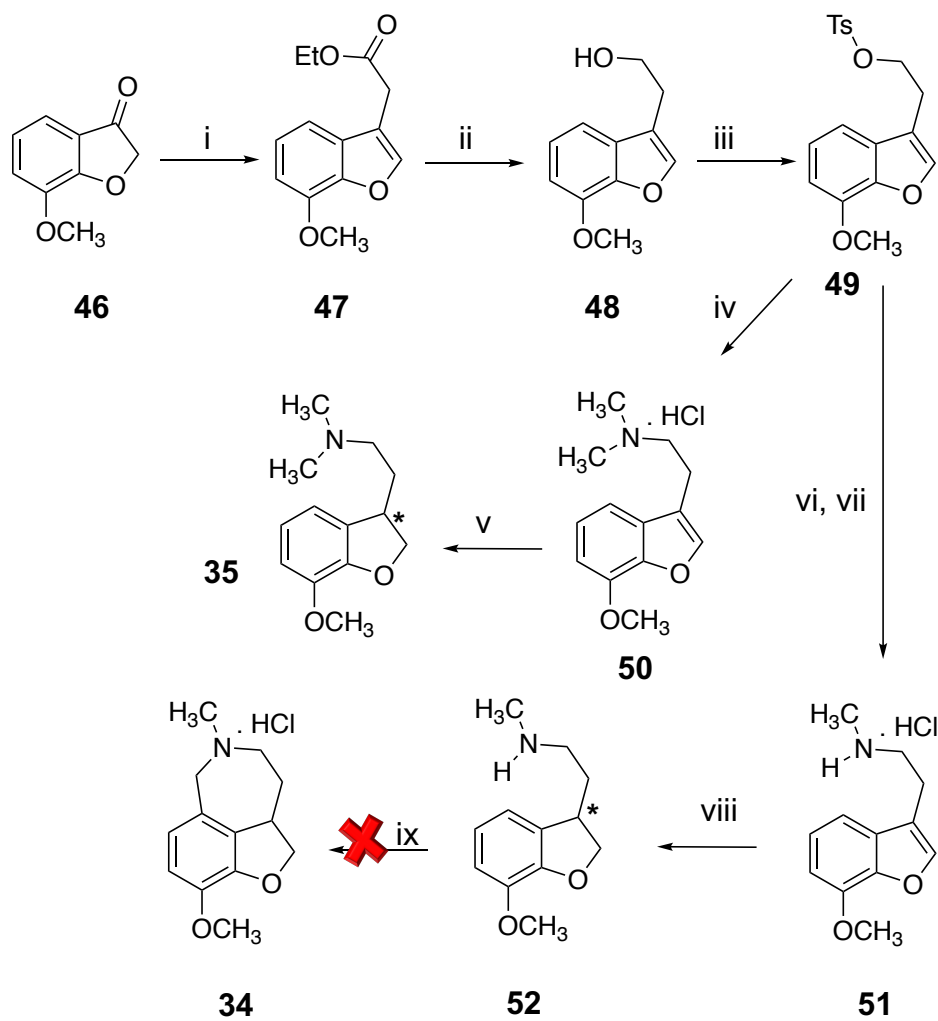
A Wittig reaction of the commercially available compound **46**, using the phosphonium ylide, carbethoxymethylene triphenylphosphorane, gave **47**. The ester group of **47** was reduced to an alcohol using LiAlH₄ to give **48**. The hydroxyl group of **48** was converted to its tosylate **49** (a better leaving group) by a reaction with tosyl chloride. Compound **49** was subsequently reacted in a sealed tube with dimethylamine via a nucleophilic substitution reaction to give **50**. The free base of amines can inhibit or poison catalysts such as palladium during hydrogenation reactions.¹⁹² To avoid this, compound **50** was converted into its HCl salt and then reduced by catalytic hydrogenation using Pd/C (10%)

to give **35**. The reduction is reported in the literature for a similar compound.¹⁹³ Compound **35** contains a chiral center and it was synthesized as a racemate. A molecule similar to **35** but devoid of a chiral center is **50**. Although not a true deconstructed analog of galantamine (**3**), compound **50** was also submitted for biological testing.

A way to synthesize compound **34** was to prepare the *N*-monomethyl analog of **50**, which could then be cyclized to an azepine ring by a Pictet-Spengler reaction. To achieve this, tosylate **49** was reacted with methylamine to form **51** which was reduced successfully by catalytic hydrogenation using Pd/C (10%) to give **52**. To cyclize the amine, a Pictet-Spengler type reaction using paraformaldehyde and trifluoroacetic acid was attempted on compound **52**. Youn¹⁹⁴ reported a Pictet-Spengler cyclization on a benzofuran scaffold. To ensure that the cyclization would occur preferably on the 4-position and not 2-position of the benzofuran ring, the aromaticity of the furan ring of **51** was eliminated by reducing it to a dihydrofuran ring (i.e., **52**). However, this reaction, tried at two different scales resulted in multiple products (as visualized on TLC), which were difficult to separate and isolate.

For reasons similar to compound **50**, compound **51** was also submitted for biological evaluation. No additional reactions were carried out to synthesize these analogs as they were intermediates in Scheme 3, hence it was feasible to submit these for evaluation. Additionally, compound **52**, another intermediate, was also submitted as a deconstructed analog.

Scheme 3. Preparation of compounds **34 and **35**.^a**



^aReagents and conditions: (i) $\text{Ph}_3\text{CHCOOEt}$, toluene, reflux, 22 h; (ii) LiAlH_4 , THF, rt, 1 h; (iii) TsCl , CH_2Cl_2 , rt, 20 h; (iv) $(\text{CH}_3)_2\text{NH}$, K_2CO_3 , 120 °C, 4 h, sealed tube; (v) H_2 , 10%Pd/C, glacial CH_3COOH , 30 psi, 18 h; (vi) CH_3NH_2 , K_2CO_3 , 120 °C, 4 h, sealed tube; (vii) HCl/EtOAc , EtOAc ; (viii) 10% Pd/C, H_2 , glacial CH_3COOH , 30 psi, 18 h; (ix) $(-\text{CH}_2-)_n$, CF_3COOH , $\text{ClCH}_2\text{CH}_2\text{Cl}$, rt, 24 h.

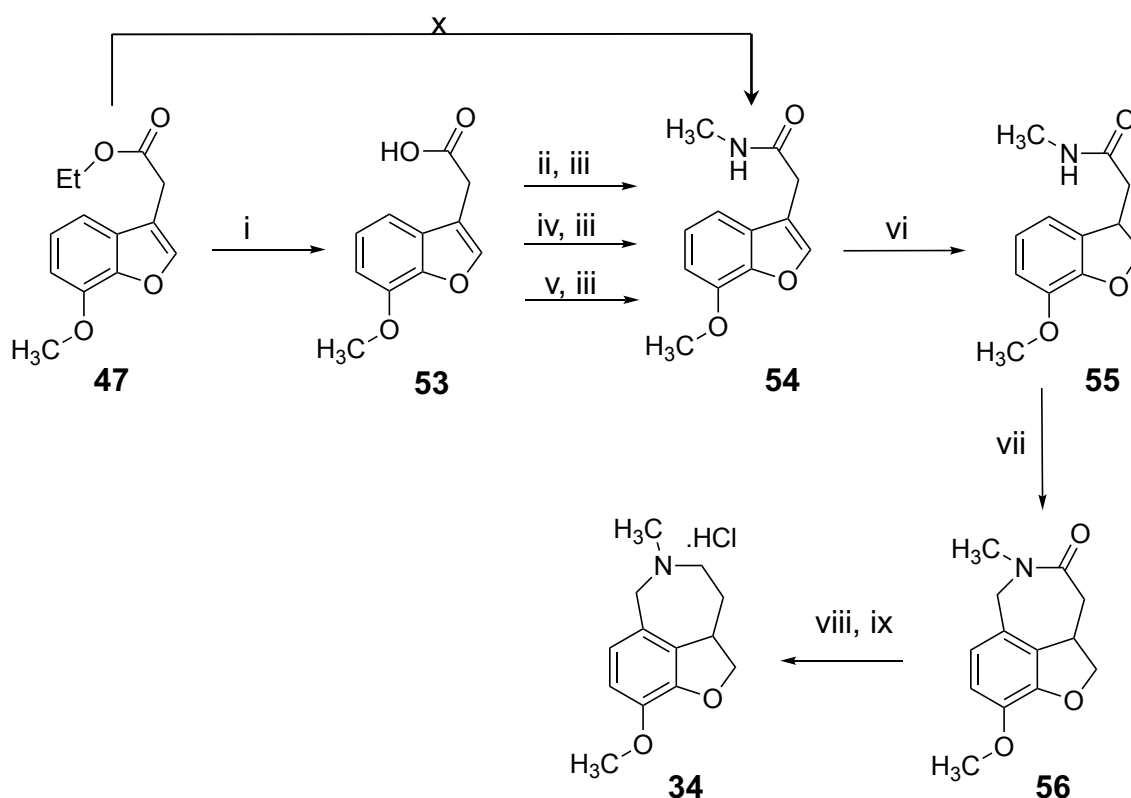
After the failure to synthesize compound **34**, a variation of Scheme 3 was employed. The design of Scheme 4 was based on the literature procedure¹⁹⁵ that reported the successful Pictet-Spengler-type cyclization of the azepinone ring in galantamine.

The ester **47**, synthesized according to the procedure described in Scheme 3, was hydrolyzed by the base NaOH to the acid **53** (Scheme 4). For the formation of amide **54**, the acid **53** was first converted to an acid chloride followed by a nucleophilic substitution reaction with methylamine. The synthesis of the acid chloride was attempted in three different ways. Initially, the acid chloride was obtained by reacting **53** with oxalyl chloride with a catalytic amount of DMF to give the product **54** in 94% yield (Scheme 4). However, the reaction was not reproducible probably due to trace amounts of moisture/humidity. To avoid this, another reaction was attempted using oxalyl chloride as a solvent (neat reaction, 81% yield). For the sake of comparison, a third reaction with thionyl chloride (71% yield) as a solvent was attempted. All three reaction conditions were capable of forming the acid chloride and also the product **54** upon reaction with a freshly prepared solution of methylamine in THF. Additional scale-up reactions were performed using thionyl chloride as it was readily available in the laboratory.

The conversion of the ester **47** directly into the amide **54** was also attempted by treating **47** with methylamine and heating (66 °C) in a sealed tube for 6 days. The yield from this reaction was poor (18%) as compared to the yield via formation of **53** (91%) and hence, this route was not pursued any further.

The furan ring in **54** (Scheme 4) was reduced to the dihydrofuran ring in **55**, similar to Scheme 3, by catalytic hydrogenation using Pd/C (10%). A Pictet-Spengler reaction of **55**, resulted in the furobenzazepinone **56**. The final product, **34** was obtained upon reduction of the amide carbonyl group in **56** using $\text{BH}_3\cdot\text{THF}$.

Scheme 4. Preparation of compound **35** via a different route.^a

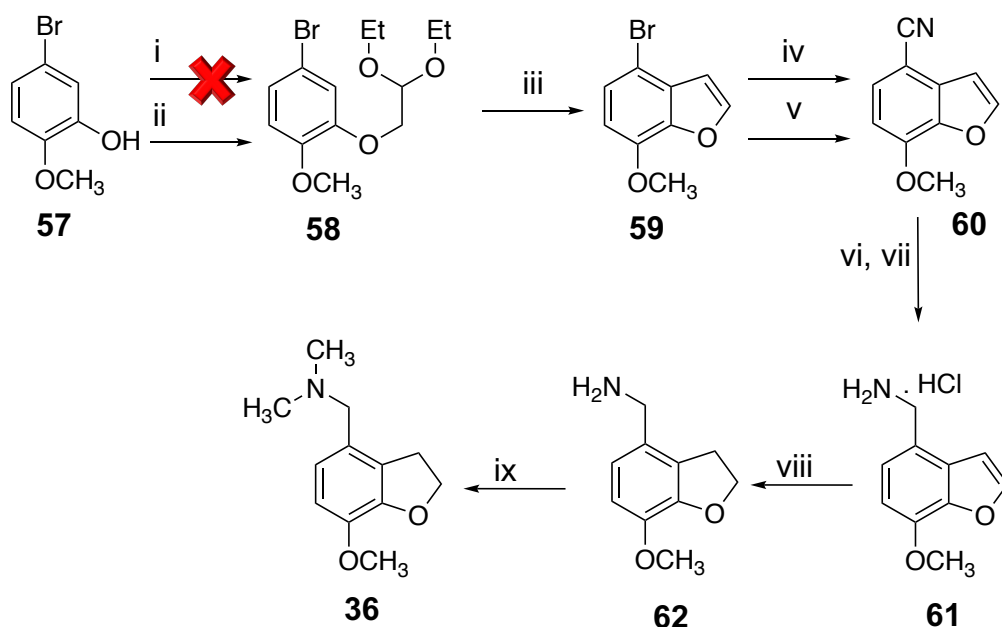


^a Reagents and conditions: (i) 1N NaOH, rt, overnight; (ii) $(\text{COCl})_2$, DMF, CH_2Cl_2 , rt, overnight; (iii) NH_2CH_3 in THF, rt, overnight; (iv) SOCl_2 , rt, 4 h (v) $(\text{COCl})_2$, rt, 4 h (vi) 10% Pd/C, H_2 , MeOH, 30 psi, 36 h; (vii) $(-\text{CH}_2)_n$, CF_3COOH , $\text{ClCH}_2\text{CH}_2\text{Cl}$, rt, 24 h; (viii) $\text{BH}_3\cdot\text{THF}$, THF, reflux, overnight; (ix) HCl/EtOAc; (x) CH_3NH_2 in THF, sealed tube, 66 °C, 6 days.

The synthesis of compound **36** was carried out in 6 steps as outlined in Scheme 5 with commercially available 5-bromo-2-methoxyphenol (**57**) as the starting material. Synthesis of compound **58** was attempted by treating compound **57** with 1-bromo-2,2-diethoxyethane in the presence of NaH (60% dispersion in mineral oil) in DMF. The reaction did not seem to progress even after 6 h and work-up resulted in the recovery of a majority of the starting material. Another alternative was to treat **57** with 1-bromo-2,2-diethoxyethane in DMF with K_2CO_3 as a base, which resulted successfully in **58**. Reaction of compound **58** with polyphosphoric acid resulted in the cyclized benzofuran **59**. The first step towards introducing the *N,N*-dimethylamine portion in the 4-position involved substituting the bromo group in **59** with a nitrile **60**.

This cyanation reaction was initially carried out successfully with zinc cyanide and a Pd catalyst, $Pd(PPh_3)_4$ in DMF. However, isolation of the product was tedious, requiring extensive extractions, filtrations, and separation by column chromatography. Also, the product yield was sensitive to the reaction scale, giving better yields (~40%) at scales <200 mg than at >800 mg (~18% yield). Another potential issue was the “freshness” of the palladium catalyst used. The catalyst was sensitive to moisture and it was possibly less active upon being stored for long periods of time.

Scheme 5. Preparation of compound **36**.^a



^aReagents and conditions: (i) 1-Bromo-2,2-diethoxyethane, NaH 60% dispersion in mineral oil, DMF, reflux, 6 h; (ii) 1-Bromo-2,2-diethoxyethane, K₂CO₃, DMF, reflux, 2 h; (iii) Polyphosphoric acid, chlorobenzene, 120 °C, 1 h; (iv) CuCN, DMF, reflux, 24 h; (v) Zn(CN)₂, Pd(PPh₃)₄, DMF, 100 °C, 22 h; (vi) LiAlH₄ in THF, rt, 1 h; (vii) HCl/EtOAc; (viii) 10% Pd/C, MeOH, 35 psi, 24 h; (ix) HCHO, NaCNBH₃, ZnCl₂, CH₂Cl₂, rt, 24 h.

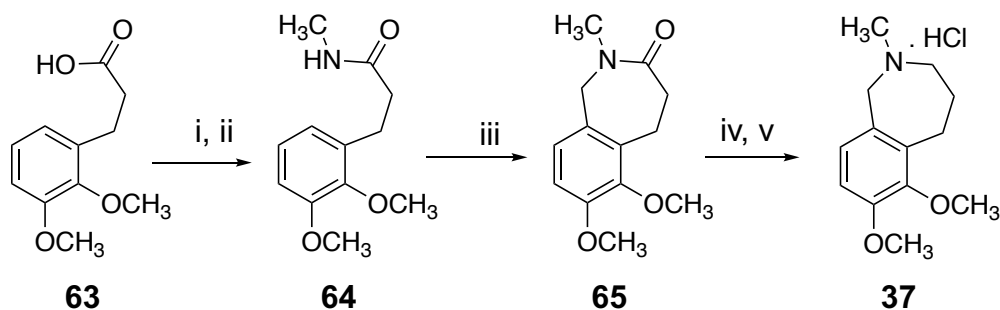
A solution that could circumvent the above-mentioned issues was to carry out a Rosenmund von Braunn reaction¹⁹⁶ which uses CuCN and DMF as solvent. The yields obtained from this reaction were consistently ~40% irrespective of the reaction scale, and isolation of product was also less tedious.

Following the Rosenmund von Braunn reaction, the nitrile group of **60** was reduced to the amine **61** using LiAlH₄. Prior to the Eschweiler-Clarke reaction, the furan ring in **61**

was reduced to a 2,3-dihydrofuran, **62**, by catalytic hydrogenation using Pd/C (10%). Methylation of **62** was carried out by an altered form of the Eschweiler-Clarke reaction using formaldehyde, sodium cyanoborohydride (instead of formic acid), and zinc chloride to give the final product, **36**.

The azepine ring of **37** was constructed in a 5-step process (Scheme 6) from substituted phenylpropionic acid **63**. The acid chloride of compound **63** was reacted with aqueous methylamine under Schotten-Baumann conditions, to give the amide **64**. A Pictet-Spengler-type cyclization reaction of **64** resulted in the benzazepinone **65**. The final product, **37**, was obtained upon reduction of amide **65** with $\text{BH}_3 \cdot \text{THF}$.

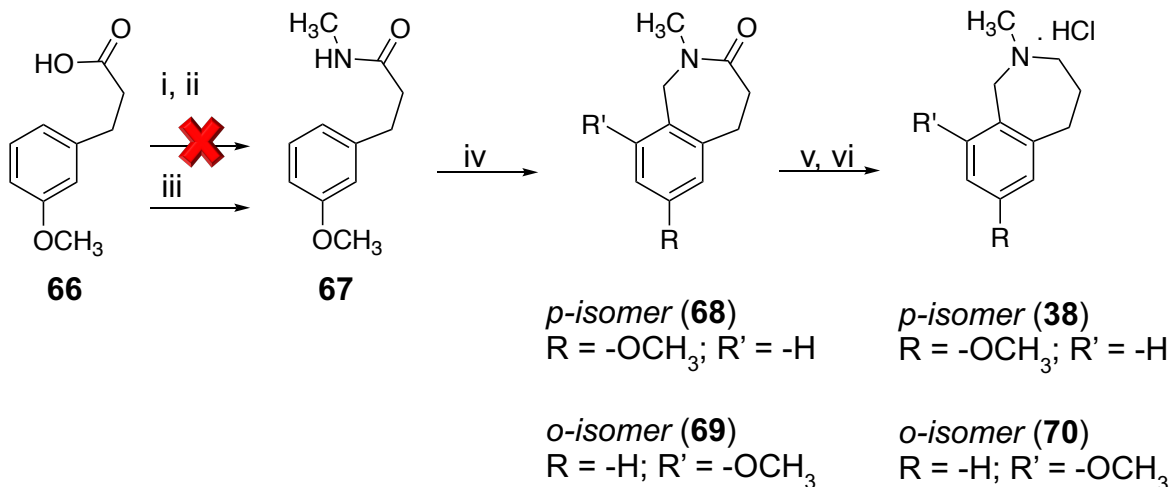
Scheme 6. Preparation of compound **37**.^a



^a Reagents and conditions: (i) SOCl_2 , reflux, 2 h; (ii) 40% aq. CH_3NH_2 , NaHCO_3 , 0-4 °C, 1 h; (iii) $(-\text{CH}_2-)_n$, CF_3COOH , $\text{ClCH}_2\text{CH}_2\text{Cl}$, rt, 24 h; (iv) $\text{BH}_3 \cdot \text{THF}$, THF, reflux, overnight; (v) HCl/EtOAc, EtOAc.

Similar to its 2,3-dimethoxy counterpart, **64**, the synthesis of the amide **67** was attempted by reacting the acid chloride of **66** with aqueous methylamine. Even though TLC indicated the consumption of **64**, an IR spectrum of the reaction did not display the characteristic peak of an acid chloride carbonyl group ($1780\text{-}1820\text{ cm}^{-1}$). Subsequent reaction of the species with aqueous methylamine or methylamine gas resulted in multiple products which were difficult to separate and characterize. So et al.¹⁹⁷ reported the formation of **67** using the coupling agent, 1-ethyl-3-(3-dimethylaminopropyl)carbodiimide (EDCI). Interestingly, the authors reported the use of EDCI for the formation of mono methoxy-substituted phenylpropanamides, while thionyl chloride was used for certain dimethoxy-substituted phenylpropanamides.¹⁹⁷ This indicated that perhaps the mono-methoxy substituted analogs (such as **67**) do not react well with thionyl chloride whereas dimethoxy-substituted analogs (such as **64**) can. Cyclization of compound **67** gave two benzazepinone analogs, the *p-isomer* (**68**) and the *o-isomer* (**69**) from the Pictet-Spengler-type cyclization from **67**.

Scheme 7. Preparation of compound **38**.^a



^a Reagents and conditions: (i) SOCl_2 , reflux, 2 h; (ii) 40% aq. CH_3NH_2 , NaHCO_3 , 0-4 °C, 1 h; (iii) EDCI , Et_3N , $\text{CH}_3\text{NH}_2 \cdot \text{HCl}$, CH_2Cl_2 , rt, 6 h; (iv) $(-\text{CH}_2-)_n$, CF_3COOH , $\text{ClCH}_2\text{CH}_2\text{Cl}$, rt, 24 h; (v) $\text{BH}_3 \cdot \text{THF}$, THF , reflux, overnight; (vi) HCl/EtOAc , EtOAc .

So et al.¹⁹⁷ reported separation of both of these positional isomers by a preparative-HPLC system. In our laboratory, separation of the two was achieved by column chromatography and both were isolated in the ratio of 3:1 (**68:69**). Reduction of compounds **68** and **69** with $\text{BH}_3 \cdot \text{THF}$ resulted in the final compounds **38** and **70**, respectively. Although not a deconstructed analog of galantamine, **70** is a positional isomer of **38**.

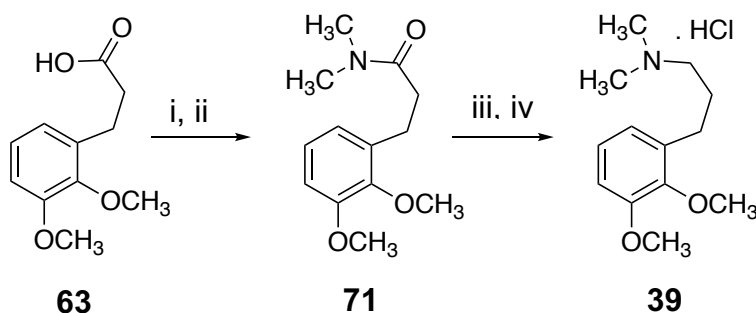
The syntheses of compounds **39** and **40** are outlined in Schemes 8 and 9.

The compounds **63** and **66** were also used as starting materials for the synthesis of the compounds **39** and **40**, respectively. The amides **71** and **72** were synthesized as outlined

in Schemes 8 and 9, respectively, with the exception that the acid chlorides were reacted with an aqueous dimethylamine solution.

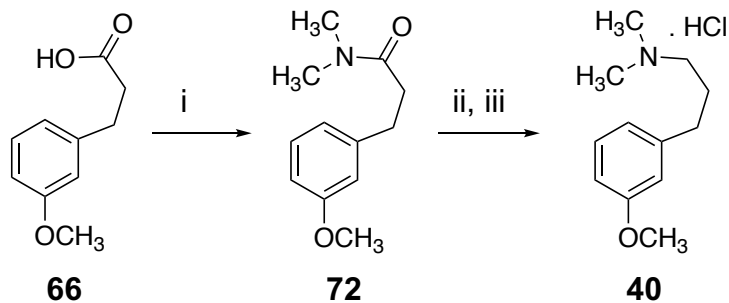
The final products, **39** and **40** were obtained by reducing the amides **71** and **72** with $\text{BH}_3 \cdot \text{THF}$.

Scheme 8. Preparation of compound **39**.^a



^a Reagents and conditions: (i) SOCl_2 , reflux, 2 h; (ii) 40% aq. $(\text{CH}_3)_2\text{NH}_2$, NaHCO_3 , 0-4 °C, 1 h; (iii) $\text{BH}_3 \cdot \text{THF}$, THF, reflux, 24 h; (iv) HCl/EtOAc .

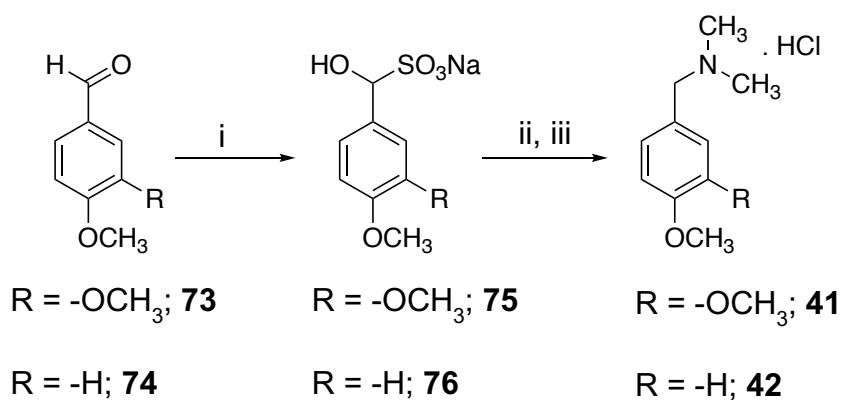
Scheme 9. Preparation of compound **40**.^a



Reagents and conditions:^a (i) EDCI , Et_3N , $(\text{CH}_3)_2\text{NH} \cdot \text{HCl}$, CH_2Cl_2 , rt, 24 h; (ii) $\text{BH}_3 \cdot \text{THF}$, THF, reflux, overnight; (iii) HCl/EtOAc .

The smallest of the series, benzylamines **41** and **42**, belonging to the benzylamine scaffold, were synthesized in 2 steps (Scheme 10). The aldehydes, **73** and **74** were converted into their sodium bisulfite adducts, **75** and **76** as a form of purification. A reductive amination was carried out on the adducts **75** and **76** using sodium cyanoborohydride and the hydrochloride of dimethylamine, yielding the products **41** and **42**.

Scheme 10. Preparation of compounds, **41** and **42**.^a



Reagents and conditions:^a (i) NaHSO₃ in H₂O, EtOH, 30-35 °C for 16 h, 4 °C for 4 h; (ii) NaCNBH₃, (CH₃)₂NH·HCl, rt, 20 h; (iii) HCl/Et₂O, Et₂O.

All target molecules were synthesized as hydrochloride salts, purified and characterized by methods such as, proton nuclear magnetic resonance (¹H NMR), infrared (IR) spectroscopy and C, H, N analyses (where required), and mass spectrometry (MS) (where required). The melting points of solid intermediates were also recorded and compared to literature (where reported).

Specific Aim 2: To study the molecular interactions of galantamine and its deconstructed analogs with the human $\alpha 7$ nAChR by molecular modeling

a. Generate 3-dimensional homology models of the human $\alpha 7$ nAChR

1. Amino acid sequence alignment

Although certain residues in the ECD of $\alpha 7$ nAChRs have been identified as being important for galantamine's PAM action, the interaction of its deconstructed analogs needs to be studied. Currently, there is no crystal structure of the human $\alpha 7$ nAChR and hence, a need to generate homology models. The crystal structure of the *Lymnaea stagnalis*-AChBP (*Ls*-AChBP)-human $\alpha 7$ nAChR chimera, which shares 64% identity with the ECD of the human $\alpha 7$ nAChR, serves as an ideal template for this purpose. In particular, the *Ls*-AChBP-human $\alpha 7$ nAChR co-crystallized with epibatidine was used (PDB ID: 3SQ6). The primary amino-acid sequences for the human $\alpha 7$ nAChR for the purpose of alignment with the template was obtained as a FASTA file from the Universal Protein Resource database (UniProt; Accession code: P36544). The software ClustalO was used for aligning the amino acid sequence of the target protein to that of the template. The first 23 amino acids from the N-terminus of the human $\alpha 7$ nAChR were truncated because the residues corresponding to these were absent in the crystal structure of the *Ls*-AChBP-human $\alpha 7$ nAChR chimera (Figure 26). Additionally, none of the residues in this region were deemed important for interacting with galantamine.¹⁰⁷

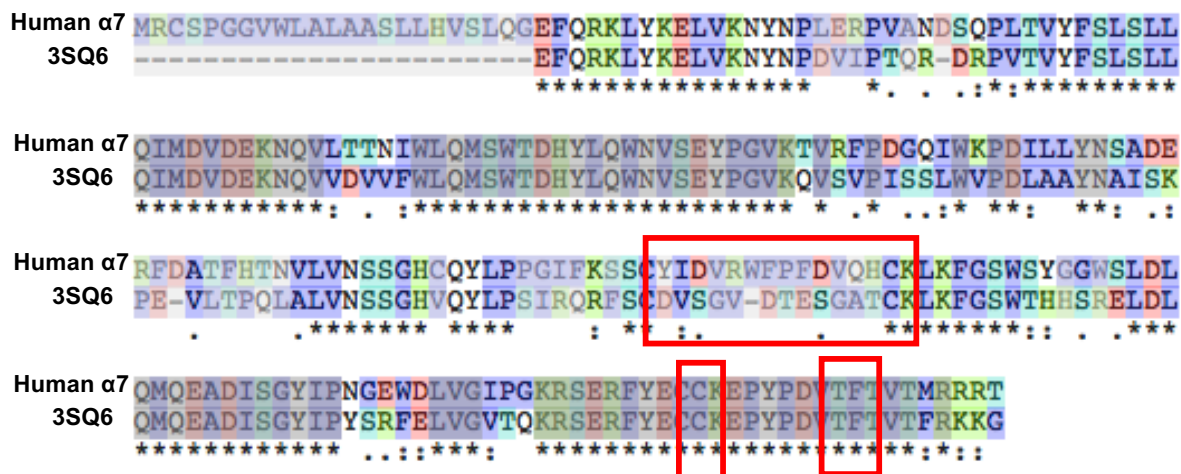


Figure 26. Sequence alignment of the template, *Ls*-AChBP-human $\alpha 7$ nAChR chimera (3SQ6) and the receptor of interest, human $\alpha 7$ nAChR. The conserved amino acids are denoted by asterisks (*), while colons (:), and periods (.) indicate strongly and weakly conserved residues, respectively. Amino acids that were compared to the template as part of alignment are indicated in red boxes.

The two cysteine residues, Cys150 and Cys164 from the human $\alpha 7$ nAChR, which form the characteristic Cys-loop were matched with those of the template (Figure 26). The vicinal cysteines, Cys212 and Cys213 were also matched with the template (Figure 26). The residues Val220, Thr221, and Phe223 considered to be important¹⁰⁷ for the potentiating effect of galantamine at $\alpha 7$ nAChR are conserved between the template and the desired protein sequence (Figure 26). The residue Val220 is an Ile196 residue in the chicken $\alpha 7$ nAChRs-5HT₃ chimera on which the mutagenesis studies were performed.¹⁰⁷ Since the orthosteric binding site is located at the interface of two subunits of the ECD, the homology models were built as dimers. The software Modeller 9.12 was employed for

the generation of 100 homology models of the human $\alpha 7$ nAChRs which were energy-minimized using Sybylx2.1.

2. Structure validation

To support our homology models, the agonist epibatidine (**13**, Figure 7) was docked to the 100 homology models of the human $\alpha 7$ nAChR. The interactions in the docking solutions were then compared to those seen in the crystal structure of the *Ls*-AChBP-human $\alpha 7$ nAChR chimera.

In the chimera crystal structure, the azabicyclo ring of epibatidine is observed to be located at the center of the “aromatic cage” (Figure 27A).¹⁶⁹ Epibatidine’s bridging amino group forms cation- π interactions with the indole ring of Trp145.¹⁶⁹ The amine also forms hydrogen bonds with the back bone carbonyl group of Trp145 and the hydroxyl oxygen atom of Tyr91.¹⁶⁹ Additionally, the chloropyridine ring participates in an edge-to-face interaction with the indole ring of Trp145.¹⁶⁹ From the complementary subunit, residues Gln114, Leu106 and Leu104 surround the chloro atom of epibatidine to participate in potential halogen bonds (Figure 27 A).¹⁶⁹ In the homology model of the human $\alpha 7$ nAChR, the docked epibatidine, as in the crystal structure, is located in the aromatic cage of the ligand-binding domain (Figure 27 B). The azabicyclo amino group of epibatidine forms hydrogen bonds with Trp145 and Tyr91 (Figure 27B). In the human $\alpha 7$ nAChR homology model, unlike the chimera crystal structure, the Leu104 is replaced by an asparagine residue (Asn104) while Trp146 corresponds to Ser146. The chlorine atom of the

chloropyridine group, similar to the pose in the crystal structure, is oriented towards Gln114 and Leu106. Additionally, the backbone carbonyl group of Asn104 is in the vicinity of the chloro group (Figure 27). Despite the close proximity of the chlorine atom of epibatidine and carbonyl oxygen atom of Asn104 (3.5 Å), a halogen bond seems unlikely due to an unfavorable geometry (Figure 27 B).

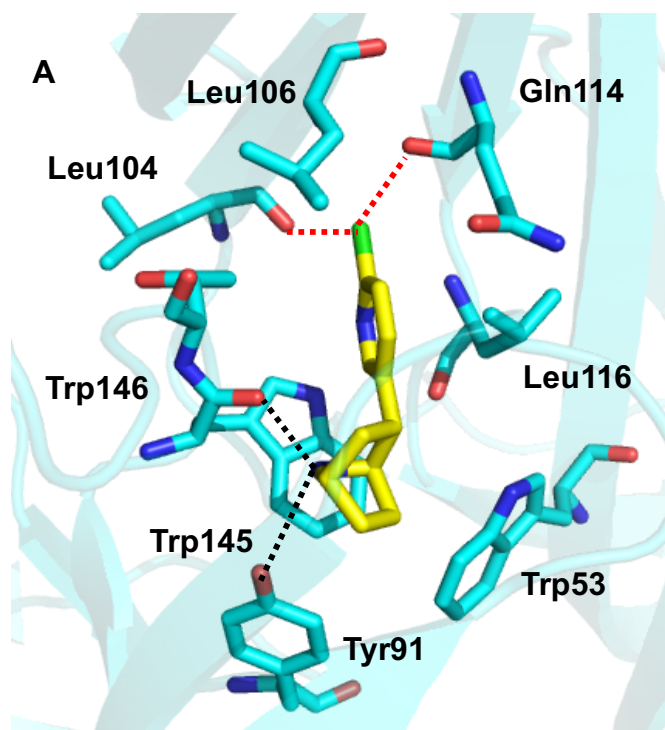
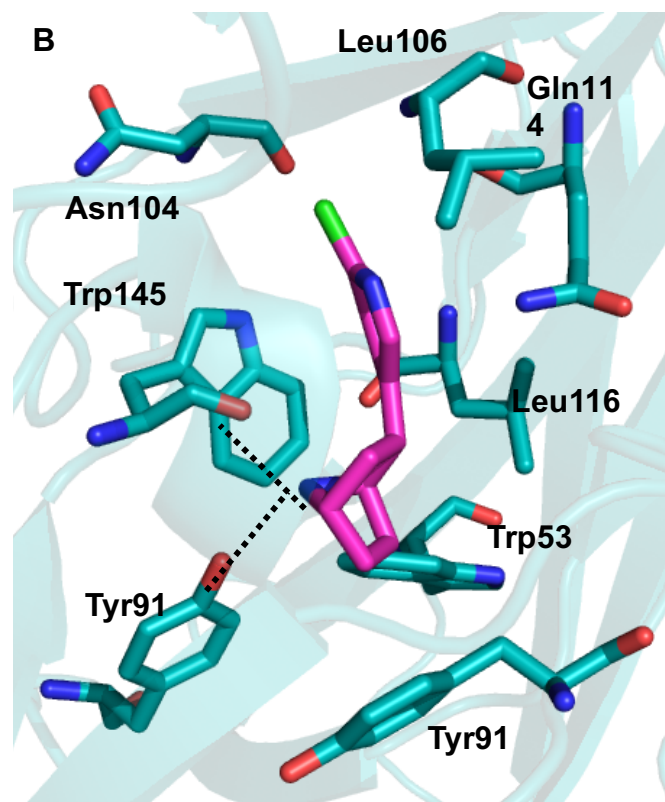


Figure 27. A. Structure of epibatidine (**13**, yellow-colored sticks) located at the center of the “aromatic cage” in the crystal structure of the chimera *Ls*-AChBP-human $\alpha 7$ nAChR. The amine from the azabicyclo group and the chloropyridine of epibatidine participate in a number of interactions with the surrounding residues of the aromatic cage. Hydrogen bonds (h-bonds) are denoted by black dotted lines while halogen-bonds are denoted by red, dotted lines. The residues of the receptor are denoted by teal-colored sticks or cartoon.



B. Epibatidine (**13**, magenta-colored sticks) docked in the homology model of the human $\alpha 7$ nAChR. The azabicyclo amino group retains the h-bonds with Trp145 and Tyr91. The chlorine atom of the chloropyridine ring of epibatidine is also oriented towards Leu106 and Gln114 as seen in the crystal structure.

The structures of the generated homology models were further validated by plotting a Ramachandran plot (Figure 28). A Ramachandran plot shows the distribution of amino acids of a particular protein into four types of areas; most favored, additional allowed, generously allowed or disallowed.¹⁹⁸ The plot (Figure 28) for the human $\alpha 7$ nAChR homology model indicates that 89.5% of the residues were in the favored regions while 96.1% were in the allowed region. There were 16 amino acids which were outliers in the plot. However, none of those residues is part of the site deemed important for binding of galantamine.

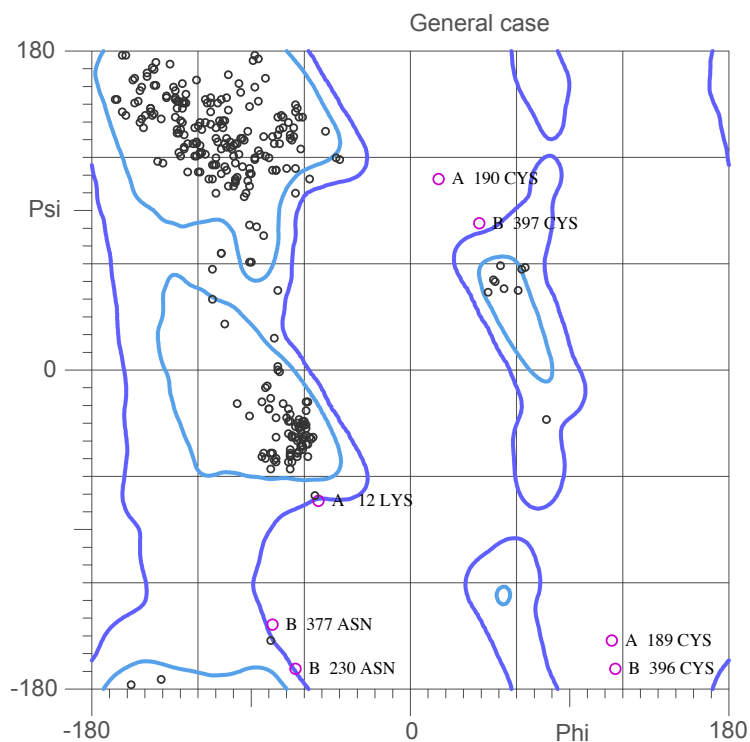


Figure 28. A Ramachandran plot for the human $\alpha 7$ nAChR homology model. The psi and phi values indicate the dihedral angles of the backbone of the amino acids in the protein. The plot distributes the amino acids according to their dihedral angles into energetically favourable or unfavourable regions.

3. Docking studies

In order to study interactions with the receptor, galantamine and its deconstructed analogs were docked in the 100 homology models of the human $\alpha 7$ nAChR.

The docking results of galantamine (**3**) revealed that the molecule was capable of interacting in primarily two different modes as highlighted in Figure 29.

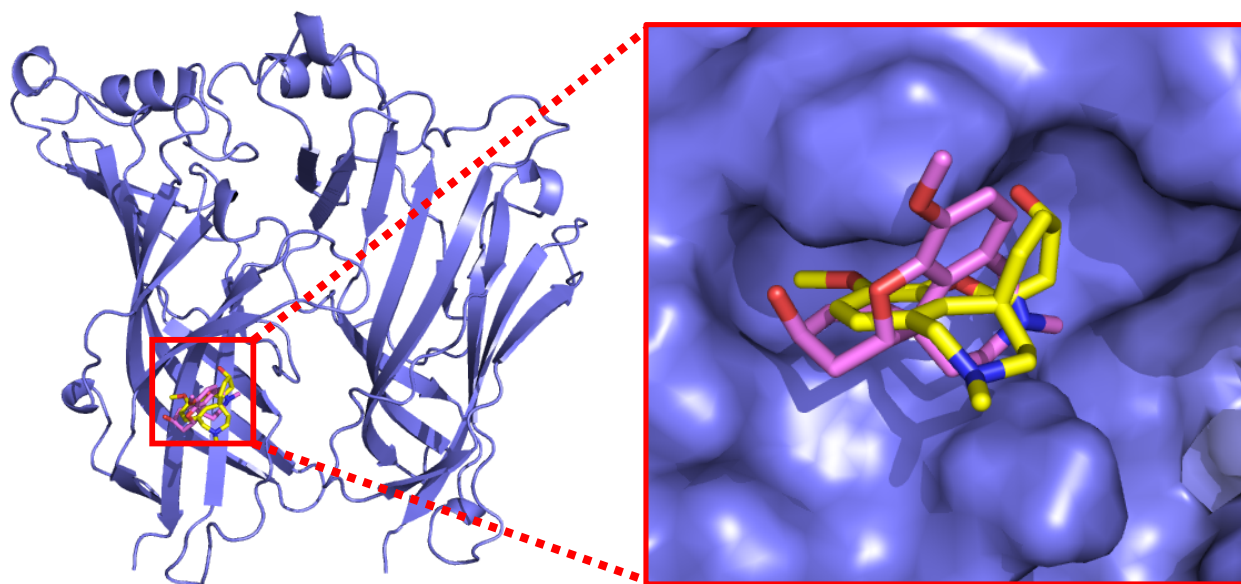


Figure 29. The homology model (dimer) of the human $\alpha 7$ nAChR is displayed on the left as a slate-colored cartoon. The image also highlights two molecules of galantamine (**3**), in yellow- (mode-1) and magenta- (mode-2) colored sticks, docked near the residue, Thr221. A close-up image on the right sheds light on the differences between the two docking poses.

In mode-I of galantamine (**3**) (Figure 30A), the molecule is oriented in a way that the oxygen atoms from the hydroxyl group, dihydrofuran ring, and the methoxy group face

the docking site (principal subunit). The nitrogen atom on the other hand, is oriented away from the docking site on the principal subunit and towards the subunit interface.

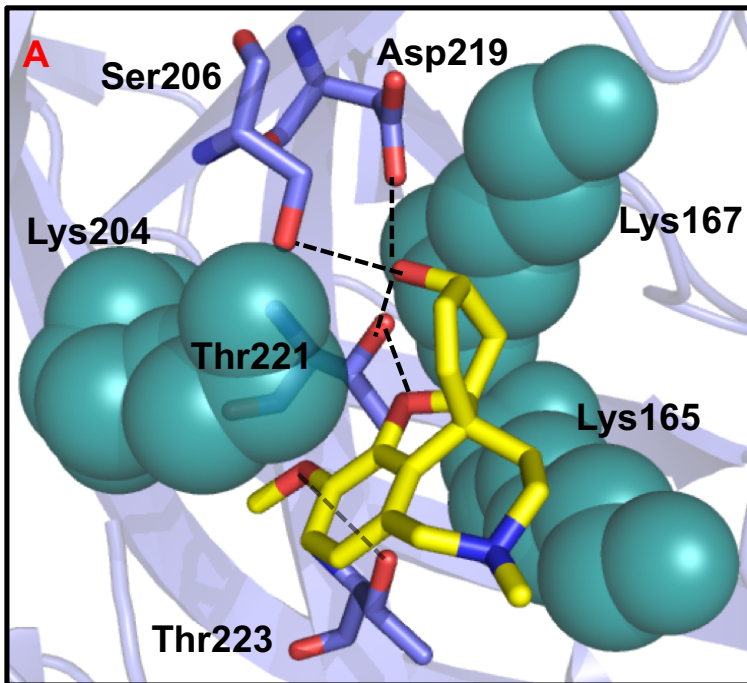
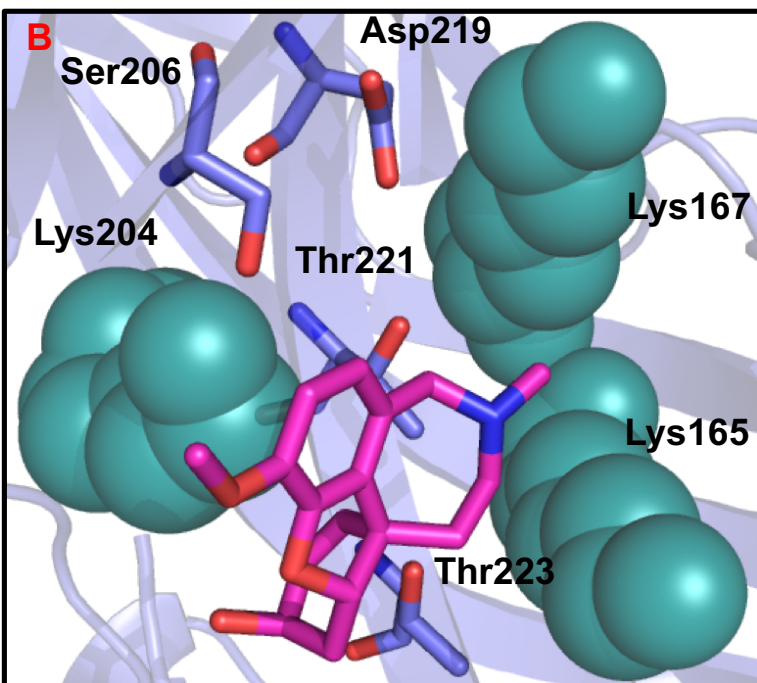


Figure 30. Docking modes-I and -II of galantamine at the human $\alpha 7$ nAChR. The amino acids of the protein are denoted by slate-colored sticks. Image A denotes galantamine in mode-I (yellow-colored sticks) while image B denotes galantamine in mode-II (magenta-colored sticks). The surrounding Lys residues, 165, 167 and 204 are represented by teal-colored spheres to emphasize their “pincer-like” arrangement around Thr221.



A. Structure of galantamine in docking mode-I wherein the three oxygen atoms of the molecule are oriented towards Thr221 or docking site. Hydrogen bonds are denoted by black-dotted lines.

B. Structure of galantamine in docking mode-II wherein the oxygen atoms are oriented away from Thr221 and towards the subunit interface.

In mode-I (Figure 30A), galantamine seems to participate in hydrogen bonds with the surrounding residues. The oxygen atom from the hydroxyl group in galantamine is capable of forming hydrogen bonds with the oxygen atoms of Asp219, Ser206, and Thr221 of the principal subunit (Figure 30A). Also within hydrogen-bonding distance from Thr221 is the dihydrofuran oxygen atom, while the methoxy group oxygen atom forms a hydrogen bond with the oxygen atom of Thr223 (Figure 30A). The protonated tertiary nitrogen atom of galantamine is surprisingly oriented away from the docking site, forgoing a possible ionic interaction with a nearby Asp219 (Figure 30A). In this mode, the nitrogen atom faces the subunit interface, and does not make any significant interactions with any amino acids (Figure 30A). In mode-II (Figure 30B), the tertiary nitrogen atom faces the docking site with Thr221 while the three oxygen atoms are oriented away from it. Unlike mode-I, galantamine in mode-II does not participate in any hydrogen bonds with the amino acids of the docking site (Figure 30).

In order to quantify and study the type of interactions between galantamine and the nAChR, hydrophobic interaction (HINT)¹⁹⁹ analysis was employed for both of these modes. HINT analysis takes into account both hydrophobic and electrostatic interactions between any two molecules.¹⁹⁹ In this case, the quality of interactions between the ligand galantamine and the protein, $\alpha 7$ nAChR was quantified. The total HINT score is a summation of polar and hydrophobic interactions.¹⁹⁹ Polar interactions include favorable acid/base and hydrogen bond interactions.¹⁹⁹ They also take into account unfavorable

(clashing) interactions such as acid/acid and base/base.¹⁹⁹ In general, the better the HINT score, the better is the interaction between the ligand and the protein. The total HINT score for the interactions of galantamine and the nAChR in mode-I and II were 393 and 261, respectively (Table 2). Despite possessing similar HINT scores, there was a marked difference in the polar component of the HINT score in the two modes (Table 2). In mode-I, the multiple hydrogen bonds formed by the oxygen atoms of galantamine with the residues of $\alpha 7$ nAChR contribute to a high polar interaction score. These hydrogen-bonding interactions are absent in mode-II (Table 2) leading to a poor polar interaction score. Owing to the favorable hydrogen-bonding interactions observed in mode-I, the probability of this pose is higher than that of mode-II. Further a comparison to the homology model of the chicken $\alpha 7$ nAChR in the literature¹⁰⁶ reveals a docking pose very similar to mode-I described here. In their homology model, Luttmann et al.¹⁰⁶ displayed a docking pose of galantamine wherein the oxygen atoms in galantamine were oriented towards Thr221 (Thr197 in chicken $\alpha 7$ nAChR), Asp219 (Asp195) and Lys167 (Lys143). All of these residues are also observed in the galantamine docking site in our human $\alpha 7$ nAChR homology model.

Table 2. HINT scores of mode-I and mode-II of galantamine and the human $\alpha 7$ nAChR homology model

Galantamine	Mode-I	Mode-II
Total HINT Score	393	106
Hydrophobic	411	367
Polar	718 (Thr221, Thr223, Asp219, Ser206)	129

The two deconstructed analogs, which retain most of the features of galantamine (**3**) are lycoramine (**6**) and the deshydroxygalantamine (**44**). Lycoramine (**6**) docks in a manner similar to mode-I of galantamine (Figure 30) (Figure 31). It retains all of the interactions of galantamine (**3**) with the receptor as observed in mode-I (Figure 30A).

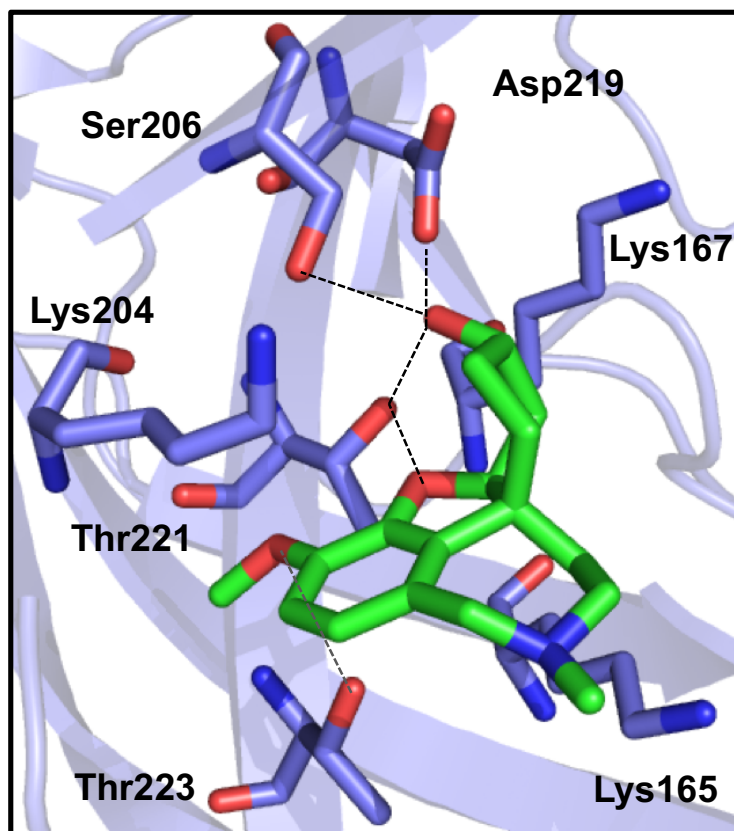


Figure 31. Structure of lycoramine (**6**) (green-colored sticks) docked at the site surrounding Thr221. The amino acid residues are displayed as slate-colored sticks or cartoon. Dashed black lines indicate hydrogen bonds.

For deshydroxygalantamine (**44**), the absence of the hydroxyl group costs it hydrogen-bonding opportunities with Thr221 and Thr223 (Figure 32). The molecule is “flipped” 180 degrees such that the methoxy group oxygen atom is now towards the inside of the ECD,

while the cyclohexyl group is on the outside (Figure 32). This is in contrast to what is observed with galantamine (in Mode-I; Figure 30A) and lycoramine (**6**, Figure 31).

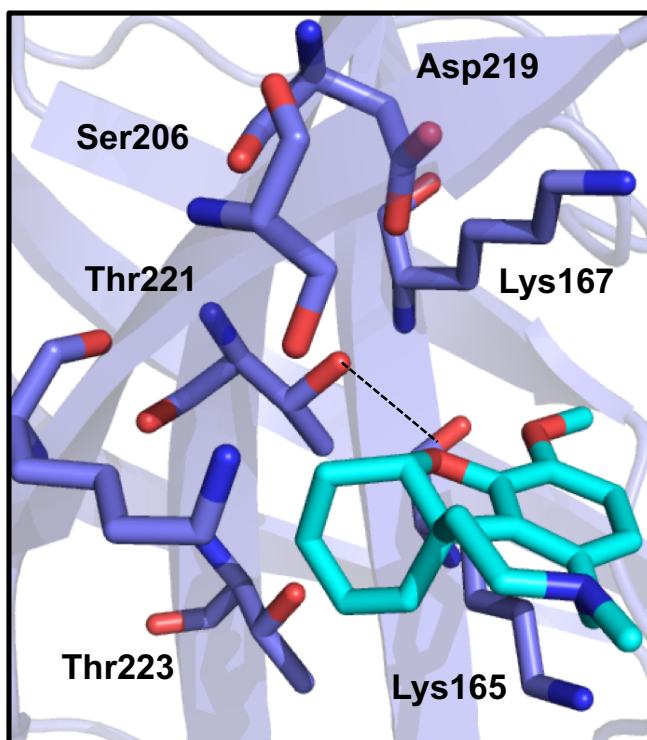


Figure 32. Structure of deshydroxygalantamine (**44**; cyan-colored sticks) docked at the site surrounding Thr221. The amino acid residues are displayed as slate-colored sticks or cartoon. Dashed black lines indicate hydrogen bonds.

Apart from galantamine (**3**), lycoramine (**6**) and deshydroxygalantamine (**44**) described so far, only the benzazepine analogs **37** and **38** and furobenzazepine **34** have the tertiary nitrogen atom constrained in an azepine ring. Even though the furobenzazepine **34** analog lacks the complete cyclohexenol portion of galantamine (**3**), it still docks with the remainder of the oxygen atoms oriented towards the docking site (Figure 33). Even without the hydroxyl group, the molecule still shows a preference for interacting similar to its parent molecule (Figure 33 and Figure 30A, respectively). The same can be observed

for the benzazepine analogs (Figure 33). The dihydrofuran oxygen atom in the furobenzazepine **34** analog forms a hydrogen bond with the hydroxyl oxygen atom of Thr223 while the methoxy group oxygen atom is also within hydrogen-bonding distance from the terminal amine of Lys165 (Figure 33). On the other hand, the benzazepine analogs **37** and **38** participate in hydrogen bonding with Thr221 and/or Lys167 (Figure 33).

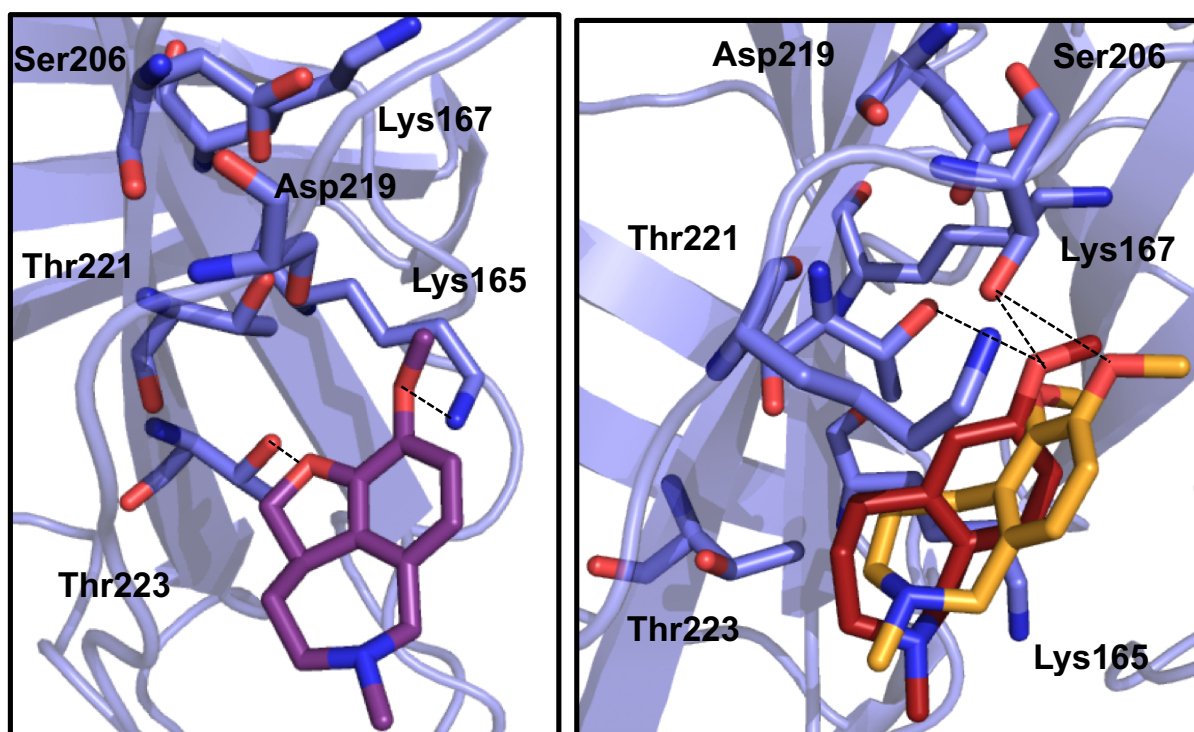


Figure 33. Structures of furobenzazepine **34** and benzazepines **37** and **38** docked at the site surrounding Thr221. The ligands and the amino acid residues are displayed as purple-, maroon- and mustard-colored and slate-colored sticks, respectively. Dashed black lines indicate hydrogen bonds.

The remainder of the deconstructed analogs are ones which have the deconstructed or cleaved form of the azepine ring. These analogs are the ones belonging to the benzofuran scaffold **35**, **36** and **50-52**, the phenylpropylamines **39** and **40**, and the structurally smallest of the series, benzylamines **41** and **42**. A trend is observed with these analogs that have an unconstrained amine group. The flexibility afforded by the benzylamine chain in **36**, **41** and **42**, the propylamine chain in **39** and **40**, the ethylamine chain in **35** and **50-52**, seems to allow the molecules to form an ionic interaction with Asp219, while maintaining the hydrogen bonds between their oxygen atoms and Thr223 (Figure 34-36).

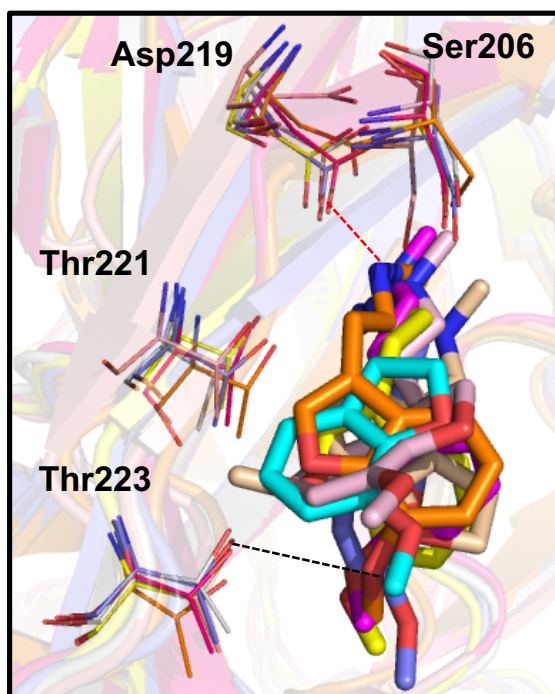


Figure 34. Structures of the benzofuran analogs **35-R** isomer (salmon pink), **35-S** isomer (magenta), **51** (orange), **50** (yellow), **36** (wheat); **52-R** isomer (blue), **52-S** isomer (cyan) docked at the site surrounding Thr221. The amino acid residues are displayed as colored sticks.

Dashed black lines indicate hydrogen bonds. Red dashed lines indicate ionic-enforced hydrogen bonds.

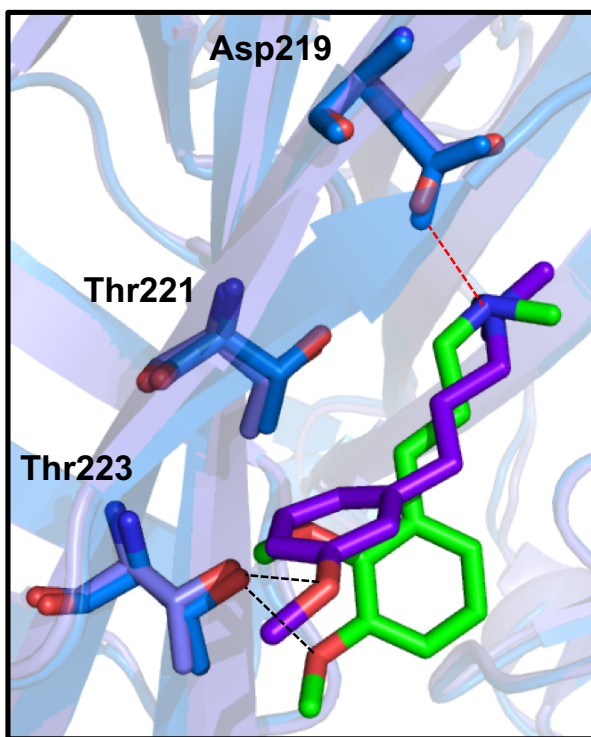


Figure 35. Structures of the phenylpropylamines **39** (green) and **40** (purple) docked at the site surrounding Thr221.

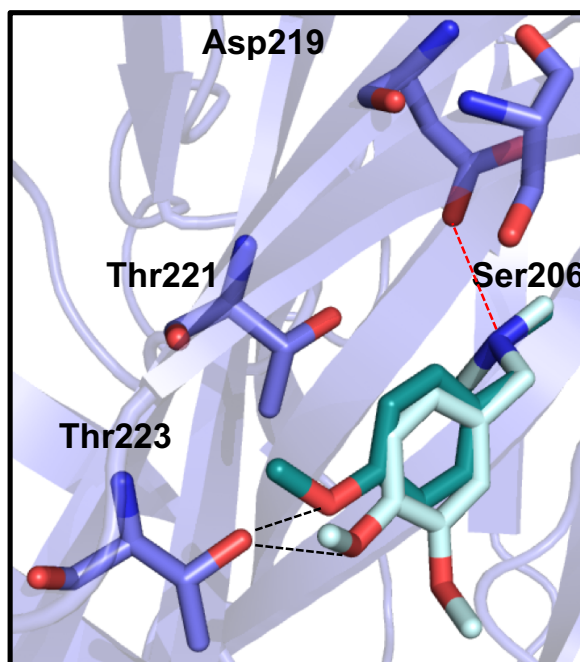
The propylamine nitrogen atom participates in an ionic interaction with the oxygen atom of Asp219 while the methoxy oxygen atoms of the analogs form hydrogen bonds with Thr223.

Dashed black lines indicate hydrogen bonds. Red dashed lines indicate ionic interactions.

Figure 36. Structures of the benzylamines **41** (light green) and **42** (teal) docked at the site surrounding Thr221.

The benzylamine nitrogen atom participates in an ionic interaction with the oxygen atom of Asp219 while the methoxy oxygen atoms of the analogs form hydrogen bonds with Thr223.

Dashed black lines indicate hydrogen bonds. Red dashed lines indicate ionic interactions.



There is a trend in terms of how the deconstructed analogs belonging to varying scaffolds interact with the docking site surrounding Thr221. The analogs which have a nitrogen atom constrained in an azepine ring, tend to dock similarly to galantamine. By retaining the docking mode and interactions of the parent molecule, perhaps **6**, **34**, **37**, **38** and **44** will display pharmacological actions that are similar to that of galantamine's. On the other hand, deconstruction of the azepine ring, results in analogs, **35**, **36**, **39**, **40**, **41**, **42**, **50**, **51**, and **52** which dock differently than galantamine. However, all of these analogs dock similarly to one another, with the nitrogen atom of the flexible alkylamine chain forming ionic interactions with the Asp219 near the allosteric site, while being within hydrogen bonding distance to Thr223. Although their interactions and docking mode in the receptor is different than galantamine, these "non-constrained" analogs still form ionic and hydrogen bonds with the receptor.

The molecules that dock similar to galantamine share the same interactions that galantamine displays with the homology model of the human $\alpha 7$ nAChR. Hence, these molecules might retain galantamine's PAM activity at the receptor. In contrast, molecules that display a different docking pose than galantamine, may or may not retain galantamine's PAM activity at the receptor. Biological data will be required to confirm these observations and predictions. All compounds have been submitted for evaluation. However, biological data are still forthcoming.

Specific Aim 3: To determine a pharmacological profile of galantamine and its deconstructed analogs at human $\alpha 7$ nAChRs by two-electrode voltage clamp techniques.

A preliminary screening (n=1) of compounds was carried out in a TEVC assay with human $\alpha 7$ nAChRs expressed in *X. laevis* oocytes. Galantamine and a representative analog belonging to each of the chemical scaffolds, benzofuran **35** and **50**, benzazepine **37**, phenylpropylamine **39**, benzylamine **41** and modified galantamine, lycoramine (**6**) were chosen for this purpose. The compounds were diluted with ND-96 buffer serially and screened at concentrations of 1 μ M and 100 μ M. Unexpectedly, galantamine (**3**) was also able to evoke an ACh-like response for $\alpha 7$ nAChRs (Figure 37). The response elicited by the compounds were normalized against the response elicited by 100 μ M ACh. All of the compounds seemed to elicit an ACh-like response at the two concentrations tested.

This is in contrast to an article reporting the TEVC study of galantamine (at 0.1 and 1 μ M) on ACh-evoked currents in human $\alpha 7$ nAChRs expressed in *X. laevis* oocytes.²³ In their study, galantamine could not activate the ion channels on its own. However, galantamine was found to activate single channel currents in nAChRs in cultured rat hippocampal neurons and mouse fibroblasts.^{91,95}

It is important to note that the compounds were screened only once in our study at the human $\alpha 7$ nAChRs expressed in *X. laevis* oocytes. More detailed and conclusive studies need to be conducted on these analogs. Additionally, problems were encountered in terms of getting the ion channel to express effectively in the frog oocytes.

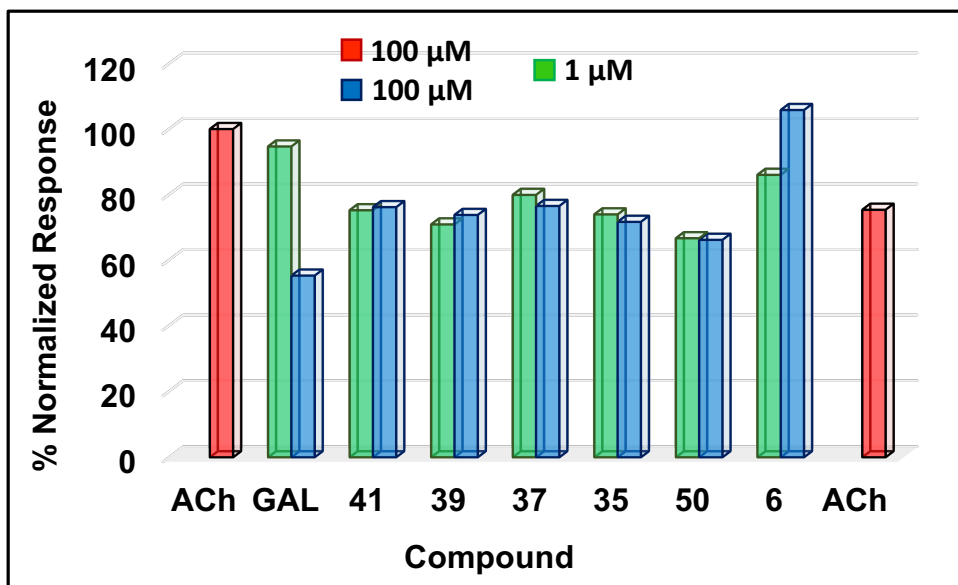


Figure 37. Electrophysiological data on galantamine and some of its deconstructed analogs at human $\alpha 7$ nAChRs expressed in *X. laevis* oocytes.

This agonist-like effect exhibited by galantamine and its deconstructed analogs was observed in an experiment that was performed only once and, hence, it is possible that it might be a false positive. A clamped oocyte might move around the chamber, due to the force of the sample injections, resulting in further impalement from the microelectrodes, causing higher leak currents. A test for checking false positives would be to expose the oocyte to an injection of only the buffer, and a response in this case would indicate that

the agonist-like responses with the samples could possibly be due to the leak currents from the impaled oocyte.

From the preliminary study (Figure 37), we determined that galantamine as well as its deconstructed analogs were capable of activating the receptors on their own. Galantamine is reported in the literature as being capable of activating single channel currents at nAChRs. However, overall, the literature tips in favor of galantamine being a PAM (i.e., lacking agonist-like activity of its own) in whole-cell currents of nAChRs. Mutagenesis data¹⁰⁷ indicate that the residue most important for galantamine's potentiating effect is Thr221, which is located near the agonist binding site (Figure 38).

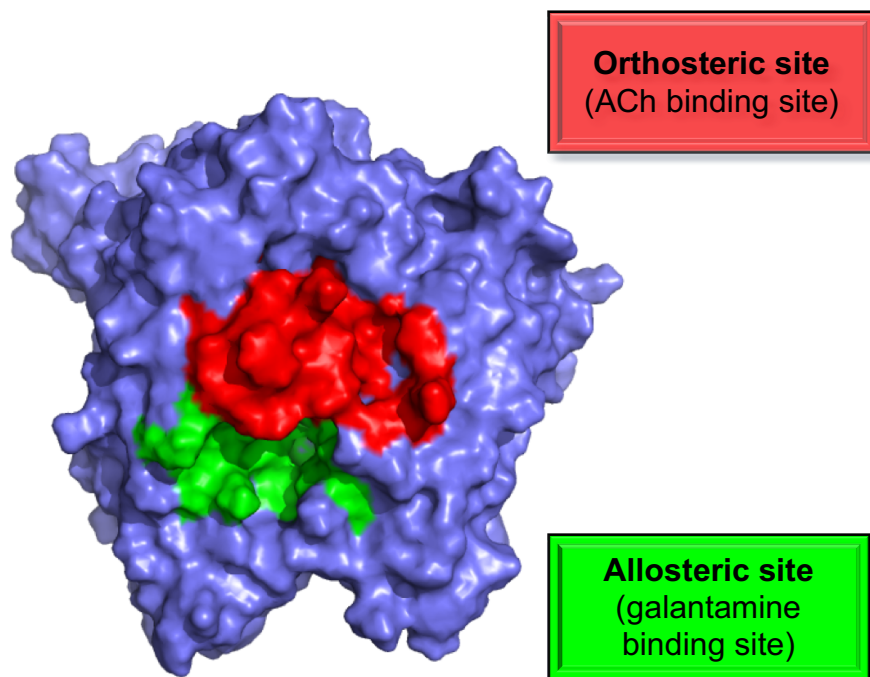


Figure 38. The homology model of two ECD subunits of the human $\alpha 7$ nAChR (slate-colored surface) displaying the orthosteric binding site (red-colored surface) and the galantamine binding site (green-colored surface).

The amino acid residues defining the orthosteric binding site shown in Figure 38 are based on the orthosteric binding site determined from the crystal structures of AChBP co-crystallized with nAChR ligands.^{131,200} Previous studies have also indicated that at high concentrations (10 μ M), galantamine inhibits agonist-evoked currents.^{23,102} Since the binding site of galantamine is close to the agonist binding site, it is possible that a high concentration causes a direct block of the orthosteric site. If this is probable, then galantamine could also be able to reach and possibly interact with the orthosteric site in the absence of an agonist. This is supported by the crystal structure of *Ac*-AChBP co-crystallized with galantamine, wherein galantamine seems to interact with the ACh-binding site.²⁰¹ From the single run of the preliminary screening we conducted, galantamine and its deconstructed analogs show promise as potential agonists. However, it remains to be seen whether they will also act as PAMs at the human α 7 nAChRs. Given its classification as a PAM, it is possible that galantamine and its deconstructed analogs could potentially be ago-PAMs. Detailed biological evaluation is forthcoming and will shed light on whether these molecules are indeed ago-PAMs.

V. CONCLUSIONS

Of the methods to alleviate the cholinergic deficit associated with AD, positive allosteric modulation of $\alpha 7$ nAChRs would seemingly represent a unique and underexplored approach. An advantage that a PAM offers over nAChR agonists, is that it is not capable of causing receptor desensitization due to prolonged exposure. Also, a PAM does not exert an effect of its own and only potentiates the existing concentrations of the endogenous ligand.

The goal of this project was to identify a pharmacophore of galantamine for the human $\alpha 7$ nAChRs. We have employed a three-pronged approach: “deconstruction”, homology modeling and docking studies, incipient screening of our molecules using a two-electrode voltage clamp electrophysiological technique.

The deconstruction approach resulted in molecules (highlighted in Figure 39), that served as abbreviated forms of galantamine.

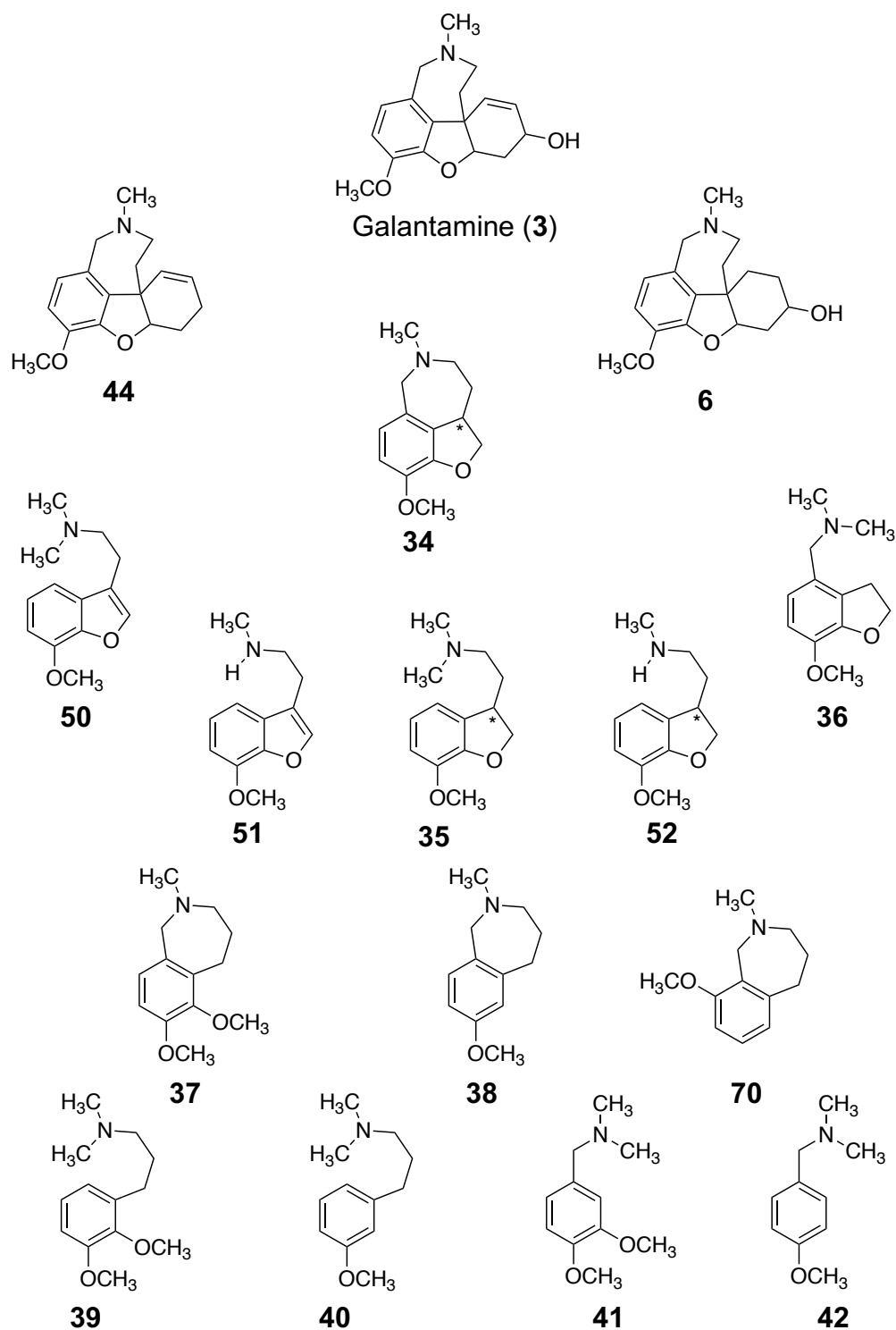


Figure 39. The deconstructed analogs of galantamine. Except for compound **44**, all others were synthesized successfully. Also added are those molecules which were not part of the originally proposed molecules or “true” deconstructions but served as positional isomers **70** or eliminated chirality **50** and **51**.

The overlap between the structures of codeine and galantamine, the crystal structure of galantamine with human recombinant AChE and SAR data of galantamine for AChE, all served as guides for the decision to synthesize **6** and **44**. Although involving only a few reactions from commercially available galantamine hydrobromide, the synthesis of the two molecules proved challenging. At the time of our biological evaluation by TEVC, we submitted the free base form of lycoramine (**6**). Since then, we have synthesized the more water-soluble hydrochloride salt of **6**. Although we were unsuccessful in synthesizing **44**, its intermediate **45** was isolated after many failed attempts. If the synthetic route for **45** can be optimized to afford better yields, then the synthesis of compound **44** may be attempted again. Apart from these, other challenges that arose in synthesizing the remainder of the deconstructed analogs were overcome by employing different reaction conditions or an altogether alternate approach.

To understand how galantamine and our deconstructed analogs could interact with the receptor, we generated the homology models of the human $\alpha 7$ nAChR and docked the molecules to the galantamine-binding site (area around Thr221) at the subunit interface. Modeling studies indicate at least two plausible binding modes for galantamine. Based on their HINT scores and on comparison to previously published modeling studies,¹⁰⁶ the docking of galantamine where the three oxygen atoms are oriented towards the binding site, and the tertiary nitrogen atom pointing towards the subunit interface seems to be preferential. Interestingly, the docking of the deconstructed analogs displayed two different trends. Analogs **6**, **34**, **37**, **38**, and **44** that had a nitrogen atom constrained in an

tetrahydroazepine ring docked similarly to galantamine, with the oxygen atoms oriented towards the docking site and the nitrogen pointing towards the subunit interface. As with galantamine, the interactions of these molecules to the receptor, primarily involved their oxygen atoms forming hydrogen bonds with either Thr221, Thr223, Lys165, Lys167 and/or Ser206 of the receptor. In contrast to this, the interactions in analogs **35**, **36**, **50-52**, and **39-42** with the receptor involved both, the oxygen atoms as well as the unconstrained nitrogen atom. The oxygen atoms in these analogs retained galantamine's hydrogen bond interactions with Thr223 while the flexible alkylamine chain allowed an additional ionic interaction of the nitrogen atom with Asp219. Overall, these analogs displayed a different docking mode and participated in interactions that are shared but not identical to galantamine and the receptor.

All of the deconstructed analogs seem to interact with the residues of the docking site, even though they exhibit two distinct docking modes. Although differently, these molecules are capable of interacting with the same site as galantamine and as a result, they might still be able to activate or modulate the receptor similarly. Therefore, any trend in probable binding modes cannot dictate the functional activity of these molecules.

A TEVC screening of galantamine and its deconstructed analogs in its incipient stages was conducted against the human $\alpha 7$ nAChRs expressed in *X. laevis* oocytes. Even after multiple attempts, successful expression of the human $\alpha 7$ nAChR in the oocytes could not be achieved. The expression was attempted in several batches of purchased oocytes,

and by attempting variations in buffer concentrations. Due to the challenges faced, expression could be achieved in only one batch of oocytes and the data presented in this dissertation, reflect that. Previous studies have indicated that galantamine could potentiate anatoxin-evoked currents in α -Bgtx-sensitive nAChRs in rat hippocampal neurons.⁹² Additionally, galantamine's PAM effect on agonists in the chimera of α 7-5HT₃ receptor in HEK293 cells and TRex-293 cells has also been reported.¹⁰² Several studies have reported the ability of galantamine to activate single-channel currents but not whole cells.⁹⁴ The literature findings are summarized in Table 3.

Table 3. Literature reports for galantamine as an agonist, a PAM, and an antagonist. The focus has been on the effect of galantamine on $\alpha 7$ nAChRs or in some cases, α -BgTx-sensitive nAChRs.

Receptor	Cell line/expression system	[Galantamine] or GAL	Agonist used	Response	Galantamine classified as?
α -BgTx and MLA sensitive nAChRs	Cultured rat hippocampal neurons ⁹¹	1-10 μ M	None GAL action abolished by FK1 but not MLA or α -BgTx	Evoked single-channel currents	Agonist
	PC-12 cells ⁹⁴	50 μ M			
α -BgTx sensitive nAChRs ⁹²	cultured rat hippocampal neurons	1 μ M	Anatoxin (10 μ M)	potentiated 59% of agonist-evoked currents	PAM
$\alpha 7/5HT_3$ chimera ^{101,102}	HEK-293 cells	0.5 μ M	ACh	EC ₅₀ (ACh) = 2.3 μ M ¹⁰¹ ; 2.5 μ M ¹⁰² EC ₅₀ (ACh + GAL) = 0.9 μ M ^{101,102}	PAM
			ACh	EC ₅₀ (ACh) = 3.8 μ M EC ₅₀ (ACh + GAL) = 2.4 μ M	
$\alpha 7/5HT_3$ chimera ¹⁰⁷	TRex-293	0.5 μ M	Nicotine	EC ₅₀ (Nicotine) = 2.4 μ M EC ₅₀ (Nicotine + GAL) = 0.9 μ M	PAM
			Epibatidine	EC ₅₀ (Epibatidine) = 5.2 μ M EC ₅₀ (Epibatidine + GAL) = 3.3 μ M	
Human $\alpha 7$ nAChRs ²³	<i>Xenopus laevis</i> oocytes	0.1 μ M	ACh	EC ₅₀ (ACh) = 305 μ M EC ₅₀ (ACh + GAL) = 189 μ M	PAM
Chicken/mouse $\alpha 7$ nAChR/5HT ₃ chimera ¹⁰²	HEK-293 cells	> 10 μ M	--	--	Antagonist or inhibitor
Human $\alpha 7$ nAChRs ²³	<i>Xenopus laevis</i> oocytes				

The variation between our results and those reported earlier might be due to the different cell lines, expression systems or even different electrophysiological techniques used. Biological evaluation of galantamine and its analogs at human $\alpha 7$ nAChR at the time of

submission of this dissertation is ongoing. The data which is forthcoming from these studies, might shed light on the functional activities of galantamine and its deconstructed analogs. Perhaps it might also be of value to test these compounds in human $\alpha 7$ nAChRs expressed in HEK-293 cells as a form of comparison. This could give us further information about the influence of various expression systems on activity of compounds.

VI. EXPERIMENTAL

A. Synthesis

All of the compounds were characterized by melting point (where reported in the literature), spectroscopic techniques such as proton nuclear magnetic resonance (^1H NMR), mass spectrometry (MS), and infrared spectroscopy (IR). The uncorrected melting points (mp) were determined in either a Thomas Hoover or a MEL TEMP apparatus using glass-walled capillary tubes. The ^1H NMR spectra of compounds were obtained by using a Bruker Avance III (400 MHz) or a Bruker ARX (400 MHz) spectrometer. The position of the peaks in the spectra were reported in parts per million (ppm) with tetramethylsilane (TMS) as an internal standard. Additionally, the splitting patterns (s = singlet, d = doublet, t = triplet, q = quartet, dd = doublet of doublets, and m = multiplet), coupling constant (J , in Hz) and integration of peaks were also specified. The IR spectra were obtained on a Thermo Nicolet iS10FT-IR instrument and the MS was obtained on a Perkin Elmer Acion 2 TOF instrument. The final compounds that were sent for biological evaluation were synthesized as water-soluble hydrobromide or hydrochloride salts. The purity of the final

compounds was evaluated based on elemental analyses (Atlantic Microlabs Inc.; Norcross, GA) for C, H, and N atoms and observed values were within $\pm 0.4\%$ of theoretical values. The reactions were monitored by thin-layer chromatography (TLC) on silica-gel plates (dimensions 250 μm , 2.5 x 10 cm; Analtech Inc. Newark, DE). Flash column chromatography was performed on a CombiFlash Rf+ Lumen (Teledyne Isco Inc. Lincoln, NE) and the columns were pre-filled with silica gel (Silica Gel 230-400 mesh, RediSep Rf Normal-Phase Silica Flash column, Teledyne Isco Inc., Lincoln, NE).

{{(4a*S*,6*R*,8a*S*)-4a,5,9,10,11,12-Hexahydro-3-methoxy-11-methyl-6*H*-benzofuro[3a3,2-*ef*][2]-benzazepin-6-ol} (Galantamine; 3)

The procedure followed was similar to the one reported in the literature.²⁵

Ammonium hydroxide (3 mL) was added in a dropwise manner at 0 °C (ice-bath) to a stirred solution of galantamine hydrobromide (0.30 g, 0.8 mmol) in H₂O (10 mL). The solution was allowed to stirred at 0 °C for 30 min and at room temperature for 2 h. The aqueous solution was extracted with Et₂O (3 x 15 mL) and the combined organic portion was dried (Na₂SO₄) and evaporated under reduced pressure to give 0.13 g (56%) of **3** as a white solid: mp 125-127 °C (lit.²⁵ mp 127-128 °C); ¹H NMR (DMSO-*d*₆) δ 1.18 (s, 1H, -CH), 1.48-1.50 (m, 1H, -CH), 1.91-2.10 (m, 2H, -CH), 2.33 (s, 3H, NCH₃), 2.60-2.64 (m, 1H, -CH), 2.97 (m, 1H, -CH), 3.17-3.24 (m, 1H, -CH), 3.59-3.64 (d, *J* = 14.9 Hz, 1H, -CH), 3.77 (s, 3H, -OCH₃), 4.00-4.08 (m, 2H, -CH), 4.55 (s, 1H, -CH), 2.03 (m, 2H, CH=CH), 6.55-6.61 (m, 2H, ArH).

{{(4a*S*,6*R*,8a*S*)-4a,5,7,8,9,10,11,12-Octahydro-3-methoxy-11-methyl-6*H*-benzofuro[3a3,2-*ef*][2]-benzazepin-6-ol} Hydrochloride (Lycoramine; 6)

The procedure followed was similar to the one reported in the literature²⁵ but the hydrochloride salt was not previously reported.

Pd/C (10%; 0.03 g) was added portion wise to a solution of **3** (0.13 g, 0.5 mmol) in anhydrous MeOH (10 mL). The reaction mixture was reduced in a Parr hydrogenator at 40 psi for 22 h, filtered through celite and the filtrate was evaporated under reduced pressure to yield a turbid oil. A residue was obtained which was purified using column chromatography (silica gel; acetone/MeOH, 90:10 to 80:20) to yield a sticky yellow residue.

A saturated solution of gaseous HCl in EtOH was added in a dropwise manner to a stirred solution of the residue in EtOH (2 mL) till acidic (pH ~12). To this, excess Et₂O was added and resulting suspension was stirred overnight. The sticky solid collected upon filtration was hygroscopic and was crystallized from acetone-H₂O to yield yellow crystals (0.02 g) mp ~80 °C (fuses). While filtering, a white solid (0.03 g) precipitated from the filtrate (mother liquor) which was subsequently collected by filtration. The melting point and TLC (in iodine) of the two solids indicated that the solid from the mother liquor was more homogeneous. Hence, it was further characterized by ¹H NMR and CHN analyses: mp 152 °C (fuses); ¹H-NMR (CDCl₃) δ 1.32-1.36 (m, 1H, -CH), 1.59-1.65 (m, 1H, -CH), 1.73-1.76 (m, 2H, -CH), 1.96-2.17 (m, 5H, -CH), 2.94 (s, 2H, -CH), 3.47-3.51 (m, 1H, -CH), 3.66 (br s, 1H, -CH), 3.78 (s, 3H, -OCH₃), 4.12-4.45 (m, 2H, -CH), 4.46 (s, 1H, -CH), 4.56-4.59 (d, *J* = 13.8 Hz, 2H, -CH), 6.76-6.78 (d, *J* = 8.2 Hz, 1H, ArH), 6.83-6.85 (d, *J* = 8.3 Hz, 1H, ArH), 10.13 (br s, 0.5H, NH⁺), 11.40 (br s, 0.5H, NH⁺). Anal. Calcd for (C₁₇H₂₃NO₃·HCl·H₂O) C, 59.38; H, 7.62; N, 4.07. Found: C, 59.31; H, 7.30; N, 4.05.

The free base of **6** was also synthesized according to the following procedure. The product obtained was sent for biological evaluation.

Pd/C (10%, 0.02 g) was added to a solution of **3** (0.07 g, 0.2 mmol) in anhydrous MeOH (10 mL). The reaction mixture was reduced in a Parr hydrogenator at 40 psi for 22 h. The reaction mixture was filtered through Celite and the filtrate was evaporated to dryness under reduced pressure to yield a turbid oil. The oil was purified using column chromatography (silica gel; acetone/MeOH, 100:0 to 80:20) to yield a sticky, white residue. The residue was dissolved in hot Et₂O, filtered and the filtrate was evaporated to dryness under reduced pressure to give 0.02 g (28%) of **6** (free base) as a white solid: mp 108-112 °C (lit.²⁵ mp 108-110 °C); ¹H NMR (DMSO-*d*₆) δ 1.19 (s, 1H, -CH), 1.46-1.52 (m, 1H, -CH), 1.59-1.95 (m, 7H, -CH), 2.32 (s, 3H, NCH₃), 2.42-2.46 (m, 1H, -CH), 2.98-3.06 (m, 1H, -CH), 3.15-3.21 (t, *J* = 12.84 Hz, -CH), 3.57-3.60 (d, 1H, *J* = 15 Hz, -CH), 3.79 (s, 3H, -OCH₃), 3.96-4.03 (m, 2H, -CH), 4.30-4.31 (t, *J* = 3.02 Hz, 1H, -OH), 6.53-6.54 (d, *J* = 8.16 Hz, -ArH), 6.58-6.60 (d, *J* = 8.2 Hz, ArH).

7-Methoxy-2-methyl-1,2,3,4,4a,5-hexahydrobenzofuro[4,3-cd]azepine

Hydrochloride (34)

A 1M solution of BH₃ in THF (2.5 mL, 2.3 mmol) was added in a dropwise manner to a solution of **56** (0.50 g, 2.1 mmol) in anhydrous THF (6 mL) at 0 °C (ice-bath) under an N₂ atmosphere. The resulting clear solution was heated at reflux and allowed to stir

overnight. The reaction mixture was allowed to cool to room temperature and quenched carefully at 0 °C (ice-bath) by addition of HCl (6N) till acidic (pH ~ 3). The reaction mixture was then heated to evaporate THF, until THF could no longer be detected by smell. The residue was cooled to 0 °C (ice-bath) and a solution of NaOH (1N, to pH 12) was added in a dropwise manner. The aqueous portion was extracted with CH₂Cl₂ (3 x 30 mL). The combined organic portion was dried (Na₂SO₄) and evaporated to dryness under reduced pressure to yield a crude turbid oil.

The crude oil was dissolved in EtOAc (2 mL) and cooled to 0 °C (ice-bath) followed by the addition of a saturated solution of gaseous HCl in EtOAc to acidic pH ~ 3. The white solid that precipitated upon addition of HCl/EtOAc was collected by filtration and washed with Et₂O and then recrystallized from ethanol to yield 0.04 g (20%) of **34** as white crystals: mp 256-258 °C; ¹H NMR (DMSO-*d*₆) δ 1.92-2.04 (m, 2H, -CH₂), 2.47 (s, 3H, NCH₃), 3.51 (s, 2H, -CH₂), 3.82 (s, 4H, -OCH₃ and -CH), 4.08-4.11 (d, 1H, *J* = 28.4 Hz, -CH), 4.18-4.23 (t, 1H, *J* = 8.8 Hz, -CH), 4.41-4.44 (d, *J* = 14.8 Hz, -CH), 4.85-4.90 (t, *J* = 9.6 Hz, -CH), 6.63-6.69 (m, 2H, ArH), 13.15 (s, 1H, H⁺). Anal. Calcd for (C₁₃H₁₇NO₂·HCl) C, 61.05; H, 7.09; N, 5.48. Found: C, 60.83; H, 7.18; N, 5.39.

***N,N*-Dimethyl-2,3-dihydro-7-methoxy-3-benzofuranethylamine (35)**

Pd/C (10%; 0.08 g) was added to a solution of **50** (0.15 g, 0.6 mmol) in glacial acetic acid (10 mL). The reaction mixture was reduced in a Parr hydrogenator at 30 psi for 18 h. The

reaction mixture was filtered and the filtrate was evaporated under reduced pressure to yield a residue. The residue was dissolved in H₂O (20 mL), basified with NaOH (5N, pH ~ 12) and extracted with CH₂Cl₂ (3 x 30 mL). The combined organic portion was dried (Na₂SO₄) and evaporated under reduced pressure to afford a pale-yellow oil. A saturated solution of gaseous HCl in Et₂O was added to a stirred solution of the oil in Et₂O (3 mL) to give a white solid which upon recrystallization from EtOH yielded 0.07 g (44%) of **35** as a white solid: mp 189-191 °C; ¹H NMR (DMSO-*d*₆) δ 1.90-2.11 (m, 2H, -CH₂), 2.52 (s, 6H, -N(CH₃)₂), 3.02-3.14 (m, 2H, -CH₂), 3.50-3.57 (m, 1H, -CH), 3.77 (s, 3H, -OCH₃), 4.25-4.29 (m, 1H, -CH), 4.57-4.62 (t, 1H, *J* = 9.02 Hz), 6.83-6.90 (m, 3H, ArH), 10.49 (s, 2H, -NH₂⁺); Anal. Calcd for (C₁₃H₁₉NO₂·HCl) C, 60.58; H, 7.82; N, 5.43. Found: C, 60.58; H, 7.82; N, 5.50.

4-(*N,N*-Dimethylamino)methyl-7-methoxy-2,3-dihydrobenzofuran (36)

Zinc chloride (0.09 g, 0.6 mmol) was added portion-wise and aqueous formaldehyde (37%, 1 mL, 12.3 mmol) was added dropwise to a stirred solution of **62** (0.23 g, 1.3 mmol) in MeOH (10 mL). Sodium cyanoborohydride (0.08 g, 1.2 mmol) was added portion-wise to the reaction mixture at 0 °C (ice-bath) and the reaction mixture was allowed to stir at room temperature for 24 h. The reaction mixture was quenched by the careful addition of NaOH (1N, 30 mL) and extracted with CH₂Cl₂ (3 x 30 mL). The combined organic portion was dried (Na₂SO₄) and evaporated to dryness under reduced pressure to afford a yellow oil. A saturated solution of gaseous HCl in EtOH was added in a dropwise manner to a

stirred solution of the oil in EtOH (4 mL) to give a white solid. Recrystallization of the solid from acetone/H₂O yielded 0.10 g (33%) of **36** as a white solid: mp 190-195 °C; ¹H NMR (CDCl₃) δ 2.68 (d, 6H, *J* = 4.96 Hz, N-CH₃), 3.36 (t, 2H, *J* = 8.74 Hz, -CH₂), 3.82 (s, 3H, -OCH₃), 3.96 (d, 2H, *J* = 5.28 Hz, -CH₂N), 4.61 (t, 2H, *J* = 8.78 Hz, -CH₂), 6.74 (d, 1H, *J* = 8.32 Hz, ArH), 6.95 (d, 1H, *J* = 8.32 Hz, ArH), 12.50 (s, 1H, NH⁺). Anal. Calcd for (C₁₂H₁₇NO₂·HCl) C, 59.14; H, 7.44; N, 5.75. Found: C, 59.02; H, 7.35; N, 5.75.

6,7-Dimethoxy-2-methyl-1,3,4,5-tetrahydro-2H-benzo[c]azepine Hydrochloride (37)

A 1M solution of BH₃ in THF (9 mL, 8.4 mmol) was added in a dropwise manner to a stirred solution of **65** (0.50 g, 2.1 mmol) in anhydrous THF (14 mL) at 0 °C (ice-bath) under an N₂ atmosphere. The reaction mixture was heated at reflux and allowed to stir overnight, cooled to room temperature and quenched at 0 °C (ice-bath) by the careful addition of HCl (6N) till acidic (pH ~ 3). The reaction mixture was then heated to evaporate the THF, until THF could no longer be detected by smell. The residue was cooled to 0 °C (ice-bath) and a solution of NaOH (3N) was added in a dropwise manner until basic (pH ~ 12) and extracted with Et₂O (3 x 30 mL). The combined organic portion was dried (Na₂SO₄) and evaporated to dryness under reduced pressure to yield 0.48 g of a crude yellow oil.

A saturated solution of gaseous HCl in EtOAc was added in a dropwise manner to a solution of the crude yellow oil in EtOAc until the solution was acidic (pH ~ 3). The white

solid that precipitated upon addition of HCl/EtOAc was collected by filtration and washed with Et₂O. Recrystallization of the solid from acetone yielded 0.1 g (20%) of **37** as white crystals: mp 198-200 °C; ¹H NMR (DMSO-*d*₆) δ 1.84 (s, 2H, -CH₂), 2.58 (s, 3H, NCH₃), 2.95 (s, 2H, -CH₂), 3.39 (m, 2H, -CH₂), 3.63 (s, 3H, OCH₃), 3.78 (s, 3H, OCH₃) 4.36 (s, 2H, -CH₂), 6.88-6.91 (d, *J* = 11.6 Hz, 1H, ArH), 7.12-7.15 (d, *J* = 10.8 Hz, 1H, ArH), 10.72 (s, 1H, NH⁺); Anal. Calcd for (C₁₃H₁₉NO₂·HCl) C, 60.58; H, 7.82; N, 5.43. Found: C, 60.74; H, 7.89; N, 5.36.

7-Methoxy-2-methyl-1,3,4,5-tetrahydro-2*H*-benzo[*c*]azepine Hydrochloride (38)

A 1M solution of BH₃ in THF (4 mL, 3.9 mmol) was added in a dropwise manner to a stirred solution of **68** (0.20 g, 1.0 mmol) in anhydrous THF (2 mL) at 0 °C (ice-bath) under an N₂ atmosphere. The reaction mixture was heated at reflux and allowed to stir overnight, allowed to cool to room temperature and quenched by the careful addition of a solution of HCl (15%) at 0 °C (ice-bath) until acidic (pH ~ 3). The resulting solution was heated to evaporate the THF followed by the addition of NaOH (3N) in a dropwise manner at 0 °C (ice-bath) until the solution was basic (pH ~ 12). The aqueous portion was extracted with EtOAc (3 x 30 mL). The combined organic portion was dried (Na₂SO₄) and evaporated to dryness under reduced pressure to yield 0.17 g of a crude yellow oil.

A saturated solution of gaseous HCl in EtOH was added in a dropwise manner to a stirred solution of the crude yellow oil in EtOH until the solution was acidic (pH ~ 3). The EtOH

was evaporated to dryness under reduced pressure to afford a white powder which upon recrystallization from acetone yielded 0.05 g (23%) of **38** as white crystals: mp 210-212 °C; ¹H NMR (DMSO-*d*₆) δ 1.92 (br s, 2H, -CH₂), 2.65 (s, 3H, NCH₃), 2.95 (s, 2H, -CH₂), 3.36-3.49 (m, 2H, -CH₂), 3.79 (s, 3H, -OCH₃), 4.36-4.45 (d, *J* = 34.44 Hz, 2H, -CH₂), 6.82-6.85 (dd, *J* = 2.66, 8.24 Hz, 1H, ArH), 6.88-6.89 (d, *J* = 2.64 Hz, 1H, ArH), 7.35-7.37 (d, *J* = 8.32 Hz, 1H, ArH), 10.71 (br s, 1H, NH⁺); Anal. Calcd for (C₁₂H₁₇NO·HCl) C, 63.28, H, 7.96, N, 6.15. Found: C, 63.06; H, 7.94; N, 6.11.

3-(2,3-Dimethoxyphenyl)-*N,N*-dimethylpropylamine Hydrochloride (39)

A 1M solution of BH₃ in THF (9 mL, 9.3 mmol) was added in a dropwise manner to **71** (0.60 g, 2.3 mmol) at 0 °C (ice-bath) and under an N₂ atmosphere. The clear reaction mixture was heated at reflux and allowed to stir for 24 h, allowed to cool to room temperature and quenched at 0 °C (ice-bath) by the careful addition of HCl (6N) until acidic (pH ~ 3). The resulting solution was heated until the THF had evaporated and the THF could no longer be detected by smell. The residue was cooled to 0 °C (ice-bath) and a solution of NaOH (5N) was added in a dropwise manner until basic (pH ~ 12) and extracted with CHCl₃ (3 x 30 mL). The combined organic portion was dried (Na₂SO₄) and evaporated to dryness under reduced pressure to yield 0.45 g of a crude yellow oil.

A saturated solution of gaseous HCl in EtOAc was added in a dropwise manner to a solution of the oil in EtOAc until the solution was acidic (pH ~ 3). The white solid which

precipitated was allowed to stir in Et₂O overnight and subsequently collected by filtration. Recrystallization of the solid from EtOH yielded 0.17 g (28%) of **39** as white crystals: mp 159-162 °C; ¹H NMR (DMSO-*d*₆) δ 1.90-1.94 (m, 2H, -CH₂), 2.58-2.68 (m, 2H, -CH₂), 2.91 (s, 6H, -N(CH₃)₂), 3.74 (s, 3H, -OCH₃), 3.80 (s, 3H, -OCH₃), 6.80-6.82 (d, *J* = 7.6 Hz, 1H, ArH), 6.92-6.94 (d, *J* = 7.4 Hz, 1H, ArH), 6.99-7.03 (t, *J* = 8 Hz, 1H, ArH), 10.17 (br s, 1H, NH⁺); Anal. Calcd for (C₁₃H₂₁NO₂·HCl) C, 60.11; H, 8.54; N, 5.39. Found: C, 60.05; H, 8.69; N, 5.38.

3-(3-Methoxyphenyl)-*N,N*-dimethylpropylamine Hydrochloride (40)

The compound is reported in the literature but synthesized here by a different route.²⁰²

A 1M solution of BH₃ in THF (24 mL, 23.5 mmol) was added in a dropwise manner to **72** (1.22 g, 5.9 mmol) at 0 °C (ice-bath) and under an N₂ atmosphere. The clear reaction mixture was heated at reflux and allowed to stir for 36 h. The reaction mixture was allowed to cool to room temperature and quenched by the careful addition of HCl (6N) until acidic (pH ~ 3). The resulting solution was heated until the THF had evaporated and could no longer be detected by smell. The residue was cooled to 0 °C (ice-bath) and a solution of NaOH (5N) was added in a dropwise manner until basic (pH ~ 12). The aqueous portion was extracted with CHCl₃ (3 x 60 mL) and the combined organic portion was dried (Na₂SO₄) and evaporated to dryness under reduced pressure to yield 0.45 g of a crude oil.

A saturated solution of gaseous HCl in EtOAc was added dropwise to a stirred solution of the crude oil in EtOAc until the solution was acidic (pH ~ 3). A solid precipitated, which was collected by filtration and washed with Et₂O. Recrystallization of the solid from absolute EtOH yielded 0.56 g (42%) of **40** as white crystals: mp 127-129 °C (lit.²⁰² mp 122-124 °C); ¹H NMR (DMSO-*d*₆) δ 1.97-2.01 (m, 2H, -CH₂), 2.59-2.63 (t, *J* = 7.6 Hz, 2H, -CH₂), 2.75-2.76 (m, 6H, -NCH₃), 2.99-3.03 (t, *J* = 8.2 Hz, 2H, -CH₂), 3.75 (s, 3H, -OCH₃), 6.78-6.82 (m, 3H, ArH), 7.21-7.25 (t, *J* = 8 Hz, 1H, ArH), 10.51 (br s, 1H, NH⁺).

3,4-Dimethoxybenzyl-*N,N*-dimethylamine Hydrochloride (41)

The compound was synthesized by the procedure reported in the literature.^{203,204}

Compound **75** (1.00 g, 3.7 mmol) was added portion-wise to a stirred solution of CH₃NH₂·HCl (0.30 g, 3.3 mmol) in anhydrous MeOH (11 mL) at room temperature under an N₂ atmosphere. Sodium cyanoborohydride (0.50 g, 8.2 mmol) was added portion wise to the stirred solution of the reaction mixture which was cooled to 0 °C (ice-bath). The reaction mixture was allowed to stir at room temperature for 20 h, quenched by the careful addition of NaOH (5N, 30 mL), and extracted with EtOAc (3 x 10 mL). The combined organic portion was dried (MgSO₄) and evaporated to dryness under reduced pressure to yield a yellow oil (5.80 g). A saturated hydrochloric acid solution in anhydrous Et₂O was added dropwise to the yellow oil until acidic (pH ~ 2) and the precipitate was collected by

filtration to yield 0.52 g (61%) of **41** as a white solid: mp 202-204 °C (lit.²⁰⁴ mp 202-203 °C); ¹H NMR (DMSO-*d*₆) δ 10.69 (s, 1H, NH, ex. D₂O), 7.23 (s, 1H, ArH), 6.99 (s, 2H, ArH), 4.05 (s, 2H, CH₂), 3.77-3.79 (d, *J* = 8 Hz, 6H, OCH₃), 2.58 (s, 6H, N(CH₃)₂).

4-Methoxybenzyl-*N,N*-dimethylamine Hydrochloride (42)

The compound is reported in the literature but was synthesized by a different method.^{203,205}

Compound **76** (1.10 g, 4.7 mmol) was added portion-wise to a stirred solution of dimethylamine hydrochloride (0.30 g, 4.2 mmol) in anhydrous MeOH (10 mL) at room temperature under an N₂ atmosphere. Sodium cyanoborohydride (0.70 g, 10.5 mmol) was added portion wise to the reaction mixture which was cooled to 0 °C (ice-bath). The reaction mixture was allowed to stir at room temperature for 20 h, quenched by the careful addition of NaOH (5N, 30 mL), and extracted with EtOAc (2 x 30 mL). The combined organic portion was washed with NaOH (5N, 30 mL) and evaporated under reduced pressure to yield a sticky, yellow residue. The residue was dissolved in HCl (15%, 30 mL) and extracted with CH₂Cl₂ (30 mL). The aqueous portion was basified with NaOH (15%, 30 mL), extracted with EtOAc (30 mL) and evaporated under reduced pressure to yield a pale-yellow oil.

A saturated solution of HCl in anhydrous Et₂O was added in a dropwise manner until acidic (pH ~ 2) and the precipitate was collected by filtration to yield a white solid. Recrystallization of this crude solid from acetone afforded 0.07 g (7%) of **42** as light brown crystals: mp 157-159 °C (lit.²⁰⁵ mp 152 °C); ¹H NMR (DMSO-*d*₆) δ 10.61 (s, 1H, NH ex D₂O), 7.48-7.50 (d, *J* = 8 Hz, 2H, ArH), 7.00-7.02 (d, *J* = 8 Hz, 2H, ArH), 4.18-4.19 (d, *J* = 4 Hz, 2H, CH₂), 3.78 (s, 3H, CH₃), 2.64-2.65 (d, *J* = 4 Hz, 6H, N-CH₃).

3-Deoxy-3-chlorogalantamine (45)

Thionyl chloride (10 mL, 0.1 mmol) was added dropwise to **3** (0.11 g, 0.4 mmol) and the reaction mixture was heated at reflux and allowed to stir for 24 h. The reaction mixture was allowed to cool and the thionyl chloride was evaporated to dryness under reduced pressure. H₂O (15 mL) was added to this residue and extracted with Et₂O (3 x 15 mL). NH₄OH was added in a dropwise manner at 0 °C (ice-bath) to the aqueous portion till basic (pH ~12) and extracted with Et₂O (3 x 15 mL). A residue was obtained at the interface of the aqueous and organic phase, which was collected by filtration and which was purified by column chromatography (silica gel; acetone) to afford 0.01 g (1%) of **45** as a clear yellow oil. MS calculated [M+H]⁺: 306.1261 MS found [M+H]⁺: 306.1285.

Ethyl-(7-methoxy-1-benzofuran-3-yl)acetate (47)

The reaction conditions followed were similar to those reported in the literature for similar analogs.¹⁸⁹

Carbethoxymethylene triphenylphosphorane (8.50 g, 24.3 mmol) was added portion-wise to a stirred solution of commercially available 7-methoxybenzofuran-3-one (**46**) (1.00 g, 6.1 mmol) in anhydrous toluene (48 mL) at 0 °C (ice-bath), under an N₂ atmosphere. The reaction mixture was heated at reflux for 24 h, allowed to cool to room temperature and the toluene was evaporated under reduced pressure to give a reddish-brown residue. The residue was separated using column chromatography (silica gel; hexanes/EtOAc, 0:100 to 100:0) to afford 1.01 g (71%) of **47** as a yellow oil. ¹H NMR (DMSO-*d*₆) δ 1.21-1.25 (t, 3H, *J* = 7.1 Hz, -CH₃), 3.79-3.80 (d, 2H, *J* = 0.64 Hz, -CH₂), 3.96 (s, 3H, -OCH₃), 4.12-4.17 (m, 2H, -CH₂), 6.96-6.98 (dd, 1H, *J* = 1.58, 7.2 Hz, ArH), 7.17-7.23 (m, 2H, ArH), 7.91 (s, 1H, ArH).

7-Methoxy-3-(2-hydroxyethyl)benzofuran (48)

The procedure followed was similar to one reported in the literature for similar analogs.^{191,206}

A solution of **47** (0.33 g, 1.4 mmol) in anhydrous THF (2 mL) was added in a dropwise manner to a cooled (salt-ice bath) suspension of LiAlH₄ (0.06 g, 1.7 mmol) in anhydrous

THF (12 mL) under an N₂ atmosphere. The reaction mixture was stirred at room temperature for 1 h. The reaction was quenched carefully by the dropwise addition of cold water to the cooled (ice-salt bath) reaction mixture. The contents were filtered using celite and the filtrate was evaporated to dryness under reduced pressure to yield a crude residue. Water (20 mL) was added to the residue and the aqueous portion was extracted with CHCl₃ (3 x 30 mL). The combined organic portion was dried (Na₂SO₄) and evaporated to dryness under reduced pressure to afford 0.25 g (93%) of **48** as a yellow oil. ¹H NMR (DMSO-*d*₆) δ 2.79-2.83 (dt, 2H, *J* = 0.84, 6.88 Hz, -CH₂), 3.69-3.74 (m, 2H, -CH₂), 3.95 (s, 3H, -OCH₃), 4.74-4.77 (t, 1H, *J* = 5.34 Hz, -OH), 6.93-6.96 (dd, 1H, *J* = 1.2, 7.32 Hz, ArH), 7.17-7.24 (m, 2H, ArH), 7.78 (s, 1H, furan ArH).

7-Methoxy-3-(2-*p*-toluenesulfonylethyl)benzofuran (49)

Triethylamine (0.7 mL, 5.2 mmol) was added in a dropwise manner to a stirred solution of **48** in anhydrous CH₂Cl₂ (8 mL) followed by the addition of *p*-toluenesulfonyl chloride (0.30 g, 1.6 mmol) at 0 °C (ice-bath) and under an N₂ atmosphere. The reaction mixture was stirred at room temperature for 16 h. An additional portion of *p*-toluenesulfonyl chloride (0.03 g) was then added to the reaction mixture and stirred for another 6 h. The reaction mixture was evaporated under reduced pressure to yield a crude residue which was separated by column chromatography (silica gel; hexanes/EtOAc, 0:100 to 100:0) to afford 0.38 g (85%) of **49** as white crystals: mp 67-73 °C; ¹H NMR (DMSO-*d*₆) δ 2.40 (s, 3H, Ar-CH₃), 2.98-3.01 (t, 2H, *J* = 6.1 Hz, -CH₂), 3.96 (s, 3H, -OCH₃), 4.30-4.33 (t, 2H, *J*

= 6.26 Hz, -CH₂), 6.93-6.95 (dd, 1H, *J* = 0.88, 7.64 Hz, ArH), 7.09-7.17 (m, 2H, ArH), 7.34-7.36 (d, 2H, *J* = 8.04 Hz, ArH), 7.65-67 (d, 2H, *J* = 8.28 Hz, ArH), 7.74 (s, 1H, ArH).

***N,N*-Dimethyl-7-methoxy-3-benzofuranethylamine (50)**

The compound was synthesized via a different method in the literature.¹⁸⁸ The synthetic route followed in our case, was similar to the reported procedure for synthesizing **51**.^{186,187} Dimethylamine (40 wt. % in H₂O, 2.5 mL, 22.2 mmol) and K₂CO₃ (0.19 g, 1.4 mmol) were added to a solution of **49** in DMF (3.5 mL) in a sealed tube. The sealed tube was then stirred for 3 h at 120 °C (oil-bath) and then allowed to cool to room temperature. The reaction mixture was diluted with H₂O (10 mL) and extracted with EtOAc (3 x 15 mL). The combined organic portion was washed with H₂O (2 x 30 mL), dried (Na₂SO₄) and evaporated to dryness under reduced pressure to afford 0.19 g (94%) of a yellow oil. A saturated solution of gaseous HCl in EtOAc was added in a dropwise manner to a solution of the oil in anhydrous EtOAc (2 mL) till the solution was acidic (pH ~ 3). The precipitate was collected by filtration and dried to yield 0.19 g (81%) of **50** as a yellow solid: mp 188-190 °C (lit.¹⁸⁸ mp 189-190 °C); ¹H NMR (DMSO-*d*₆) δ 2.86 (s, 6H, -N(CH₃)₂), 3.11-3.15 (t, 2H, *J* = 8.16 Hz, -CH₂), 3.35-3.40 (m, overlaps with H₂O peak, 2H, -CH₂), 3.97 (s, 3H, -OCH₃), 6.99-7.01 (d, 1H, *J* = 7.52 Hz, ArH), 7.23-7.27 (t, 1H, *J* = 7.86 Hz, ArH), 7.34-7.36 (dd, 1H, *J* = 0.84, 7.8 Hz, ArH), 7.92 (s, 1H, ArH), 10.49 (s, 1H, NH⁺).

***N*-Methyl-7-methoxy-3-benzofuranethylamine Hydrochloride (51)**

The compound (free base) is reported in the literature as an oil.^{186–188}

Methylamine (40 wt. % in H₂O, 3 mL, 38.6 mmol) and K₂CO₃ (0.60 g, 4.5 mmol) were added to a solution of **49** (1.05 g, 3.0 mmol) in DMF (4 mL) in a sealed tube. The reaction mixture in the sealed tube was stirred for 1 h at 120 °C (oil-bath) and cooled to room temperature. The reaction mixture was diluted with H₂O (50 mL) and extracted with EtOAc (4 x 30 mL). The combined organic portion was washed with H₂O (3 x 100 mL), dried (Na₂SO₄) and evaporated to dryness under reduced pressure to afford 1.00 g of a yellow oil. A saturated solution of gaseous HCl in EtOAc was added dropwise to a solution of the oil in anhydrous EtOAc (5 mL) till the solution was acidic (pH ~ 3). The precipitate was collected by filtration and dried to yield a crude yellow solid which upon recrystallization from absolute EtOH yielded 0.32 g (41%) of **51** as white crystals: mp 159-161 °C; ¹H NMR (DMSO-*d*₆) δ 2.62 (s, 3H, N-CH₃), 3.05-3.08 (t, 2H, *J* = 7.7 Hz, -CH₂), 3.20-3.09 (t, 2H, *J* = 4.1 Hz, -CH₂), 3.97 (s, 3H, -OCH₃), 6.98-7.00 (d, 1H, *J* = 4.22 Hz, ArH), 7.23-7.27 (t, 1H, *J* = 4.22 Hz, ArH), 7.31-7.34 (dd, 1H, *J* = 0.94, 7.84 Hz, ArH), 7.91 (s, 1H, ArH), 8.98 (s, 2H, -NH₂⁺); Anal. Calcd for (C₁₂H₁₆NO₂·HCl) C, 59.63; H, 6.67; N, 5.79. Found: C, 59.38; H, 6.63; N, 5.80.

***N*-Methyl-2,3-dihydro-7-methoxy-3-benzofuranethylamine Hydrochloride (52)**

Pd/C (10%; 0.10 g) was added to a solution of **51** (0.20 g, 0.9 mmol) in glacial acetic acid (20 mL). The reaction mixture was reduced in a Parr hydrogenator at 30 psi for 18 h. The reaction mixture was filtered and the filtrate was evaporated under reduced pressure to yield an oily residue. The residue was dissolved in H₂O (20 mL), basified with NaOH (5N, pH ~ 12) and extracted with CH₂Cl₂ (3 x 30 mL). The combined organic portion was dried (Na₂SO₄) and evaporated under reduced pressure to afford a pale-yellow oil. A saturated solution of gaseous HCl in Et₂O was added to a stirred solution of the oil in Et₂O (3 mL) to give a white solid which upon recrystallization from EtOH yielded 0.18 g (53%) of **51** as off-white solid: mp 148-150 °C; ¹H NMR (DMSO-*d*₆) δ 1.83-1.92 (m, 1H, -CH), 2.00-2.09 (m, 1H, -CH), 2.57 (s, 3H, -NCH₃), 2.86-3.04 (m, 2H, -CH₂), 3.57-3.61 (m, 1H, -CH), 3.80 (s, 3H, -OCH₃), 4.26-4.30 (m, 1H, -CH), 4.61-4.65 (t, 1H, *J* = 8.98 Hz, -CH), 6.86-6.89 (m, 3H, ArH), 8.88 (s, 2H, -NH₂⁺); Anal. Calcd for (C₁₂H₁₇NO₂·HCl) C, 59.14; H, 7.44; N, 5.75. Found: C, 58.97; H, 7.19; N, 5.74.

7-Methoxy-benzofuran-3-yl acetic acid (53)

The procedure followed was similar to one reported in the literature for a similar analog.²⁰⁷

A solution of 1N NaOH was added in a dropwise manner to a stirred solution of **47** (1.00 g, 6.1 mmol) in MeOH (10 mL) at 0 °C (ice-bath) until basic (pH~12) and allowed to stir at room temperature overnight. The aqueous portion was extracted with CH₂Cl₂ (3 x 30

mL). The combined aqueous portion was acidified with HCl (6N) till acidic (pH ~ 2), followed by an extraction with CH₂Cl₂ (3 x 30 mL). The combined organic portion was dried (Na₂SO₄) and evaporated under reduced pressure to afford 0.88 g (100%) of **53** as a white solid: mp 136-138 °C; ¹H NMR (DMSO-*d*₆) δ 3.70 (s, 2H, -CH₂), 3.96 (s, 3H, -OCH₃), 6.95-6.98 (dd, 1H, *J* = 2.34, 6.54 Hz, ArH), 7.19-7.21 (m, 2H, ArH), 7.89 (s, 1H, ArH), 12.49 (s, 1H, -OH).

7-Methoxy-3-(*N*-methylacetamide)benzofuran (54)

Thionyl chloride (2 mL, 28.0 mmol) was added in a dropwise manner at 0 °C (ice-bath) to **53** (0.10 g, 0.5 mmol) under an N₂ atmosphere. The reaction mixture was allowed to stir at room temperature for 4 h, and then evaporated to dryness under reduced pressure to yield the crude intermediate as an amber oil that was used in the next step reaction without further characterization. A solution of 7-methoxy-benzofuran-3-yl acetyl chloride in anhydrous THF (6 mL) was added in a dropwise manner at 0 °C (ice-bath) to a saturated solution of CH₃NH₂ in THF (10 mL). The reaction mixture was allowed to stir overnight at room temperature. The THF was evaporated under reduced pressure to give an oily residue to which H₂O (30 mL) and extracted with CH₂Cl₂ (3 x 30 mL). The combined organic portion was dried (Na₂SO₄) and evaporated to dryness under reduced pressure to yield 0.10 g (91%) of **54** as an off-white solid: mp 142-145 °C; ¹H NMR (DMSO-*d*₆) δ 2.62-2.64 (d, 3H, *J* = 4.64 Hz, NCH₃), 3.51 (s, 3H, -CH₂), 3.96 (s, 3H, -OCH₃), 6.94-6.97 (m, 1H, ArH), 7.21 (m, 2H, ArH), 7.82 (s, 1H, ArH), 7.99 (s, 1H, NH).

Compound **54** can also be synthesized using the following procedures,

A. A solution of **47** (0.11 g, 0.4 mmol) in THF (~2 mL) was added to a saturated solution of methylamine in THF (3.5 mL), in a sealed tube. The reaction mixture in the sealed tube was stirred for 6 days at 66 °C (oil-bath), cooled to room temperature and evaporated to dryness under reduced pressure to yield an oily residue. The residue was purified by column chromatography (silica gel; CH₂Cl₂/MeOH, 100:0 to 80:20) to afford 0.02 g (18%) of **54** as a white solid. The white solid was confirmed to be **54** by running a TLC with the previously synthesized and characterized batch of **54**.

B. Anhydrous DMF (0.05 mL) was added in a dropwise manner at 0 °C (ice-bath) to a stirred solution of oxalyl chloride (0.2 mL, 2.3 mmol) and **53** (0.15 g, 0.7 mmol) in anhydrous CH₂Cl₂ (10 mL), under an N₂ atmosphere. The reaction mixture was allowed to stir overnight at room temperature. The reaction mixture was evaporated to dryness under reduced pressure to yield a yellow oily residue. The residue was diluted with anhydrous CH₂Cl₂ (10 mL) and added in a dropwise manner at 0 °C (ice-bath) to a stirred and saturated solution of CH₃NH₂ in THF (10 mL). The reaction mixture was allowed to stir at 0-4 °C (ice-bath) for 1 h. The reaction mixture was evaporated under reduced pressure to remove the THF to yield a semi-solid residue, which was quenched by the careful addition of HCl (1N, 30 mL) and extracted with CH₂Cl₂ (3 x 30 mL). The combined organic portion was dried (Na₂SO₄) and evaporated to dryness under reduced pressure to yield 0.15 g (94%) of **54** as a white solid: mp 153-154 °C.

C. Oxalyl chloride (3 mL, 35.0 mmol) was added in a dropwise manner at 0 °C (ice-bath) to a stirred solution of **53** (0.10 g, 0.5 mmol) under an N₂ atmosphere. The reaction mixture was allowed to stir at room temperature for 4 h, and the oxalyl chloride was evaporated to dryness under reduced pressure to yield the crude intermediate as an amber oil that was used in the next step reaction without further characterization. A solution of 7-methoxy-benzofuran-3-yl acetyl chloride in anhydrous CH₂Cl₂ (12 mL) was added in a dropwise manner at 0 °C (ice-bath) to a saturated solution of CH₃NH₂ in THF (10 mL). The reaction mixture was allowed to stir overnight at room temperature. The THF was evaporated under reduced pressure to give an oily residue, which was diluted with H₂O (30 mL) and extracted with CH₂Cl₂ (3 x 30 mL). The combined organic portion was dried (Na₂SO₄) and evaporated to dryness under reduced pressure to yield 0.11 g (71%) of **54** as a white solid: mp 151-154 °C.

2,3-Dihydro-7-methoxy-3-(*N*-methylacetamide)benzofuran (55)

Pd/C (10%; 0.14 g) was added to a solution of **54** (0.27 g, 1.2 mmol) in MeOH (20 mL). The reaction mixture was reduced in a Parr hydrogenator at 30 psi for 36 h. The reaction mixture was filtered over Celite and the filtrate was evaporated under reduced pressure to yield 0.25 g (90%) of **55** as an off-white solid: mp 119-122 °C; ¹H NMR (DMSO-*d*₆) δ 2.29-2.35 (m, 1H, -CH), 2.55-2.56 (d, 1H, *J* = 5.92 Hz, -CH), 2.59-2.60 (s, 3H, *J* = 4.6 Hz, -NCH₃), 3.75 (s, 4H, -OCH₃ and -CH), 4.15-4.19 (dd, 1H, *J* = 6.74, 9.02 Hz, -CH), 4.60-4.65 (t, 1H, *J* = 9.02 Hz, -CH), 6.77-6.82 (m, 3H, ArH), 7.86-7.87 (d, 1H, *J* = 3.96 Hz, -

NH).

7-Methoxy-2-methyl-1,2,4a,5-tetrahydrobenzofuro[4,3-cd]azepin-3(4H)-one (56)

Paraformaldehyde (0.08 g) was added portion-wise and trifluoroacetic acid (0.5 mL, 5.0 mmol) was added in a dropwise manner at 0 °C (ice-bath) to a stirred solution of **55** (0.12 g, 0.5 mmol) in 1,2-dichloroethane (15 mL). The reaction mixture was allowed to stir at room temperature overnight and quenched by the careful addition of saturated aqueous solution of NaHCO₃ (30 mL). The aqueous portion was extracted with CH₂Cl₂ (3 x 30 mL). The combined organic portion was dried (Na₂SO₄) and evaporated to dryness under reduced pressure to yield 0.05 g (39%) of **56** as a white solid: mp 104-108 °C; ¹H NMR (DMSO-d₆) δ 2.72-2.82 (m, 2H, -CH₂), 3.68-3.73 (m, 1H, -CH), 3.95-4.01 (m, 1H, -CH), 4.11-4.15 (d, 1H, *J* = 16.44 Hz, -CH), 4.57-4.61 (d, 1H, *J* = 16.44 Hz, -CH), 4.70-4.75 (t, 1H, *J* = 8.36 Hz, -CH), 6.54-6.56 (d, 1H, *J* = 8.16 Hz, ArH), 6.62-6.64 (d, 1H, *J* = 8.16 Hz, ArH).

4-Bromo-2-(2,2-diethoxyethoxy)methoxy benzene (58)

The compound is reported in literature and was synthesized by a similar procedure.²⁰⁸

Potassium carbonate (3.50 g, 25.0 mmol) and 1-bromo-2,2-diethoxyethane (4 mL, 25.0 mmol) were added portion-wise to a solution of 5-bromo-2-methoxyphenol, (**57**) (5.00 g,

25.0 mmol) in anhydrous THF (14 mL) at 0 °C (ice-bath) under an N₂ atmosphere. The reaction mixture was heated at reflux with a dry ice condenser for 2 h, allowed to cool to room temperature, quenched by the careful addition of NaOH (1N, 50 mL) and extracted with CH₂Cl₂ (3 x 30 mL). The combined organic portion was washed with H₂O (3 x 100 mL) and brine (20 mL), dried (Na₂SO₄) and evaporated to dryness under reduced pressure to afford 6.95 g (64%) of **58** as a clear amber oil. ¹H NMR (CDCl₃) δ 1.28 (m, 6H, -CH₃), 3.67 (m, 2H, -CH₂), 3.80 (m, 2H, -CH₂), 3.88 (s, 3H, -OCH₃), 4.08 (m, 2H, -CH₂), 4.91 (s, 1H, -CH), 6.78 (d, 1H, *J* = 8.28 Hz, ArH), 7.08 (m, 2H, ArH).

4-Bromo-7-methoxybenzofuran (59)

The compound is reported in literature and was synthesized by a similar procedure.²⁰⁸

A solution of **58** (4.3 g, 13.5 mmol) in chlorobenzene (10 mL) was added in a dropwise manner to a stirred solution of polyphosphoric acid (6.84 g) in chlorobenzene (25 mL) at 80 °C under an N₂ atmosphere. The reaction mixture was heated for 1 h at 120 °C, with an attachment of a dry ice condenser. The reaction was allowed to cool to room temperature, followed by the careful addition of NaOH (1N) till basic (pH ~ 12) and extracted with CH₂Cl₂ (3 x 30 mL). The combined organic portion was dried (Na₂SO₄) and evaporated to dryness under reduced pressure to yield an amber oil which was purified by column chromatography (silica gel; hexanes/EtOAc, 100:0 to 90:10) to afford 1.2 g

(40%) of **59** as a yellow oil. $^1\text{H NMR}$ (CDCl_3) δ 3.93 (s, 3H, $-\text{OCH}_3$), 6.62 (d, 1H, $J = 8.44$ Hz, ArH), 6.72 (d, 1H, $J = 2.12$ Hz, ArH), 7.21 (d, 1H, ArH), 7.58 (d, 1H, $J = 2.12$ Hz, ArH).

4-Cyano-7-methoxybenzofuran (**60**)

The compound is reported in the literature but was synthesized by a different procedure.²⁰⁹

Copper (I) cyanide (0.5 g, 5.8 mmol) was added portion-wise to a stirred solution of **59** (1.1 g, 4.8 mmol) in anhydrous DMF (15 mL) at 0 °C (ice-bath) under an N_2 atmosphere. The reaction mixture was heated at reflux for 24 h, allowed to cool to room temperature, quenched carefully by a dropwise addition into ice-cold H_2O (50 mL) and extracted with CH_2Cl_2 (3 x 30 mL). The combined organic portion was washed with H_2O (3 x 100 mL), brine (30 mL) dried (Na_2SO_4) and evaporated to dryness under reduced pressure to yield a yellow residue which was purified by column chromatography (silica gel; hexanes/EtOAc, 100:0 to 95:5) to afford 0.33 g (40%) of **60** as a white solid: mp 92-94 °C; $^1\text{H NMR}$ ($\text{DMSO}-d_6$) δ 4.13 (s, 3H, $-\text{OCH}_3$), 6.89 (d, 1H, $J = 8.28$ Hz, ArH), 7.03 (s, 1H, ArH), 7.60 (d, 1H, $J = 8.28$ Hz, ArH), 7.82 (s, 1H, ArH).

Compound **60** can also be synthesized by the following procedure,

Zinc cyanide (1.69 g, 14.4 mmol) and $\text{Pd}(\text{PPh}_3)_4$ (0.76 g, 0.7 mmol) were added portion-wise to a stirred solution of **59** (0.83 g, 3.7 mmol) in anhydrous DMF (14 mL) at 0 °C (ice-

bath) under an N₂ atmosphere. The reaction mixture was heated at 100 °C for 22 h, allowed to cool to room temperature, quenched carefully by a dropwise addition into ice-cold H₂O (50 mL) to yield a white suspension. The solid was filtered and the filtrate was extracted with CH₂Cl₂ (3 x 30 mL). The combined organic portion was washed with H₂O (3 x 100 mL) and brine (30 mL), dried (Na₂SO₄) and evaporated to dryness under reduced pressure to yield a yellow oily residue which was purified by column chromatography (silica gel; hexanes/EtOAc, 100:0 to 80:20) to afford 0.12 g (18%) of **60** as a white solid: mp 92-94 °C; The same reaction, at a 300 mg and at a 600 mg scale of **59** afforded 50% and 44% of **60**, respectively.

4-Aminomethyl-7-methoxybenzofuran Hydrochloride (61)

The procedure followed was reported in the literature for a similar analog.²¹⁰

A solution of **60** (0.33 g, 2.0 mmol) in anhydrous THF (6 mL) was added in a dropwise manner at -4 °C (salt-ice bath) to a suspension of LiAlH₄ (0.14 g, 3.6 mmol) in anhydrous THF (10 mL) under an N₂ atmosphere. The reaction mixture was allowed to stir at room temperature for 1 h and quenched carefully by the dropwise addition of ice-cold H₂O (1 mL), NaOH (1N, 1 mL) and another addition of cold H₂O (1 mL) to the cooled (ice-salt bath) reaction mixture. The precipitate was filtered through Celite and the filtrate was evaporated to dryness under reduced pressure to yield a crude residue. To the residue, H₂O (20 mL) was added and extracted with CH₂Cl₂ (3 x 30 mL). The combined organic

portion was dried (Na_2SO_4) and evaporated to dryness under reduced pressure to afford a brown oil. A saturated solution of gaseous HCl in EtOAc was added in a dropwise manner to a stirred solution of the oil in EtOAc (3 mL) to give 0.29 g (71%) of **61** as a green solid: mp $>210\text{ }^\circ\text{C}$ (decomposed/charred); $^1\text{H NMR}$ ($\text{DMSO-}d_6$) δ 3.40 (s, 3H, -OCH₃), 4.23 (m, 2H, -CH₂), 7.02 (d, 1H, $J = 8.16\text{ Hz}$, ArH), 7.28 (s, 1H, ArH), 7.35 (d, 1H, $J = 8.12\text{ Hz}$, ArH), 8.07 (s, 1H, ArH), 8.40 (br s, 3H, NH⁺ and NH₂).

4-Aminomethyl-7-methoxy-2,3-dihydrobenzofuran (62)

Pd/C (10%; 0.14 g) was added portion-wise to a solution of **61** (0.29 g, 1.3 mmol) in MeOH (25 mL). The reaction mixture was reduced in a Parr hydrogenator at 35 psi for 24 h, filtered over celite and the filtrate was evaporated to dryness under reduced pressure to yield a white solid. mp $241\text{-}245\text{ }^\circ\text{C}$. NaOH (1N) was added in a dropwise manner to a solution of the solid in MeOH (2 mL) till basic (pH ~ 12) and the aqueous portion was extracted with CH_2Cl_2 (3 x 30 mL). The combined organic portion was dried (Na_2SO_4) and evaporated to dryness under reduced pressure to afford 0.23 g (96%) of **62** as a yellow solid: mp $80\text{-}90\text{ }^\circ\text{C}$; $^1\text{H NMR}$ (CDCl_3) δ 3.13 (t, 2H, $J = 8.74\text{ Hz}$, -CH₂), 3.69 (s, 2H, CH₂N), 3.79 (s, 3H, -OCH₃), 4.56 (t, 2H, $J = 8.76\text{ Hz}$, -CH₂), 6.67 (m, 2H, ArH).

3-(2,3-Dimethoxyphenyl)-N-methylpropanamide (64)

The procedure followed was reported in the literature for a similar compound.¹⁹⁷

Thionyl chloride (2 mL, 31.7 mmol) was added in a dropwise manner at 0 °C (ice-bath) to a stirred solution of commercially available 3-(2,3-dimethoxyphenyl)propionic acid (**63**) (0.63 g, 3.0 mmol) under an N₂ atmosphere. The stirred reaction mixture was heated at reflux for 2 h, allowed to cool to room temperature and the SOCl₂ was evaporated to dryness under reduced pressure to yield 3-(2,3-dimethoxyphenyl)propionyl chloride as an amber oil. The reaction was monitored by IR (diamond, cm⁻¹) 1690 cm⁻¹ (acid carbonyl). A solution of 3-(2,3-dimethoxyphenyl)propionyl chloride in anhydrous CH₂Cl₂ (30 mL) was added in a dropwise manner at 0 °C (ice-bath) to a solution of saturated aqueous NaHCO₃ (10 mL) and CH₃NH₂ (40% w/v in H₂O, 1 mL, 14.2 mmol). The reaction mixture was allowed to stir at 0-4 °C (ice-salt bath) for 1 h. The reaction was quenched by the careful addition of saturated aqueous NaHCO₃ (30 mL) and extracted with CH₂Cl₂ (3 x 15 mL). The combined organic portion was dried (Na₂SO₄) and evaporated to dryness under reduced pressure to yield 0.65 g of an orange crude residue, which was purified by column chromatography (silica gel; hexanes/EtOAc; 100:0 to 0:100) to afford 0.55 g (81%) of **64** as a white solid: mp 107-111 °C; ¹H NMR (DMSO-*d*₆) δ 2.31-2.35 (t, *J* = 7.72 Hz, 2H, -CH₂), 2.58-2.59 (d, *J* = 4.6 Hz, 3H, NHCH₃), 2.78-2.82 (t, *J* = 7.3 Hz, 2H, -CH₂), 3.75 (s, 3H, -OCH₃), 3.81 (s, 3H, -OCH₃), 6.77-6.79 (dd, *J* = 1.44, 7.60 Hz, 1H, ArH), 6.89-6.92 (dd, *J* = 1.49, 8.16 Hz, ArH), 6.98-7.02 (t, *J* = 7.86 Hz, ArH), 7.75 (br s, 1H, NH).

6,7-Dimethoxy-2-methyl-1,3,4,5-tetrahydro-2H-benzo[c]azepin-3-one (65)

The procedure followed was reported in literature for a similar compound.¹⁹⁷

Paraformaldehyde (0.33 g) was added portion-wise, and CF₃COOH (2 mL, 24.8 mmol) was added in a dropwise manner at 0 °C (ice-bath) to a stirred solution of **64** (0.54 g, 2.4 mmol) in CH₂Cl₂ (50 mL). The reaction mixture was allowed to stir at room temperature for 24 h, quenched by the careful addition of saturated aqueous solution of NaHCO₃ (30 mL) and extracted with CH₂Cl₂ (3 x 15 mL). The combined organic portion was dried (Na₂SO₄) and evaporated to dryness under reduced pressure to yield 0.54 g (96%) of **65** as a white solid: mp 108-111 °C; ¹H NMR (DMSO-*d*₆) δ 2.81-2.85 (m, 2H, -CH₂), 2.89 (s, 3H, NHCH₃), 2.95-2.98 (t, 2H, *J* = 6.84 Hz, -CH₂), 3.72 (s, 3H, -OCH₃), 3.81 (s, 3H, -OCH₃), 4.51 (s, 2H, -CH₂), 6.86-6.88 (d, 1H, *J* = 8.36 Hz, ArH), 6.95-6.97 (d, *J* = 8.36 Hz, ArH).

3-(3-Methoxyphenyl)-*N*-methylpropanamide (67)

The compound is reported in the literature and the same procedure was followed.¹⁹⁷

1-Ethyl-3-(3-dimethylaminopropyl)carbodiimide (EDCI) (2.06 g, 10.8 mmol) and Et₃N (6 mL, 45.2 mmol) were added portion-wise to a stirred solution of 3-(3-methoxyphenyl)propionic acid (**66**) (1.81 g, 10.0 mmol) and CH₃NH₂·HCl (2.06 g, 30.5 mmol) in anhydrous CH₂Cl₂ (40 mL). The reaction was allowed to stir at room temperature

for 6 h and quenched by the careful addition of HCl (1N, 100 mL) and extracted with CH₂Cl₂ (3 x 40 mL). The combined organic portion was dried (Na₂SO₄) and evaporated to dryness under reduced pressure to yield a crude yellow oil which was purified by column chromatography (silica gel; CHCl₃/MeOH; 100:0 to 80:20) to afford 0.91 g (47%) of **67** as a pale-yellow oil. ¹H NMR (DMSO-*d*₆) δ 2.36-2.40 (t, *J* = 7.82 Hz, 2H, -CH₂), 2.59-2.60 (d, *J* = 4.6 Hz, 3H, NCH₃), 2.79-2.83 (t, *J* = 7.8 Hz, 2H, -CH₂), 3.76 (s, 3H, -OCH₃), 6.76-6.80 (m, 3H, ArH), 7.19-7.23 (t, *J* = 7.96 Hz, 1H, ArH), 7.74 (br s, 1H, NH).

7-Methoxy-2-methyl-1,3,4,5-tetrahydro-2*H*-benzo[c]azepin-3-one (*p*-isomer; **68)**

The procedure followed was reported in the literature for a similar compound.¹⁹⁷

Paraformaldehyde (0.33 g) and CF₃COOH (2 mL, 27.4 mmol) were added portion wise at 0 °C (ice-bath) to a stirred solution of **67** (0.52 g, 2.7 mmol) in 1,2-dichloroethane (60 mL). The reaction mixture was stirred at room temperature for 4 h, quenched by the careful addition of saturated aqueous solution of NaHCO₃ (75 mL) and extracted with CH₂Cl₂ (3 x 100 mL). The combined organic portion was dried (Na₂SO₄) and evaporated to dryness under reduced pressure to give a yellow oil. The two positional isomers, 7-methoxy-2-methyl-1,3,4,5-tetrahydro-2*H*-benzo[c]azepine-3-one and 9-methoxy-2-methyl-1,3,4,5-tetrahydro-2*H*-benzo[c]azepine-3-one were separated by column chromatography (silica gel; hexanes/EtOAc; 100:0 to 0:100). Subsequently this afforded 0.26 g (47%) of 7-methoxy-2-methyl-1,3,4,5-tetrahydro-2*H*-benzo[c]azepine-3-one (**68** '*p*-

isomer') as white crystals: mp 117-119 °C (lit.¹⁹⁷ mp 107-107.5 °C); ¹H NMR (DMSO-*d*₆) δ 2.80-2.84 (t, *J* = 6.94 Hz, 2H, -CH₂), 2.90 (s, 3H, NCH₃), 3.02-3.06 (t, *J* = 6.92 Hz, 2H, -CH₂), 3.75 (s, 3H, -OCH₃), 4.50 (s, 2H, -CH₂), 6.71-6.76 (m, 2H, ArH), 7.15-7.17 (d, *J* = 8.28 Hz, 1H, ArH)

Both, the *p*- and the *o*-positional isomers are known and except for the method of separation of the two isomers, the reaction was followed according to the literature procedure. The literature procedure reported using preparative HPLC, while column chromatography was used for separation in case of **68**.

9-Methoxy-2-methyl-1,3,4,5-tetrahydro-2*H*-benzo[*c*]azepin-3-one (*o*-isomer; **69)**

The procedure followed was reported in the literature for a similar compound.¹⁹⁷

Paraformaldehyde (0.33 g) and CF₃COOH (2 mL, 27.4 mmol) were added portion wise at 0 °C (ice-bath) to a stirred solution of **67** (0.52 g, 2.7 mmol) in 1,2-dichloroethane (60 mL). The reaction mixture was allowed to stir at room temperature for 4 h, quenched by the careful addition of saturated aqueous solution of NaHCO₃ (75 mL) and extracted with CH₂Cl₂ (3 x 100 mL). The combined organic portion was dried (Na₂SO₄) and evaporated to dryness under reduced pressure to give a yellow oil. The two positional isomers, 7-methoxy-2-methyl-1,3,4,5-tetrahydro-2*H*-benzo[*c*]azepine-3-one and 9-methoxy-2-methyl-1,3,4,5-tetrahydro-2*H*-benzo[*c*]azepine-3-one were separated by column chromatography (silica gel; hexanes/EtOAc; 100:0 to 0:100). Subsequently this afforded

0.04 g (6%) of 9-methoxy-2-methyl-1,3,4,5-tetrahydro-2*H*-benzo[*c*]azepine-3-one (**69** 'o-isomer') as a white solid: mp 60 °C; ¹H NMR (DMSO-*d*₆) δ 2.77-2.80 (t, *J* = 6.88 Hz, 2H, -CH₂), 2.90 (s, 3H, NCH₃), 3.02-3.06 (t, *J* = 6.80 Hz, 2H, -CH₂), 3.75 (s, 3H, -OCH₃), 4.64 (s, 2H, -CH₂), 6.78-6.81 (d, *J* = 7.6 Hz, 1H, ArH), 6.87-6.89 (d, *J* = 8.2 Hz, 1H, ArH), 7.19-7.22 (t, *J* = 7.92 Hz, 1H, ArH).

Both the *p*- and the *o*-positional isomers are known and except for the method of separation of the two isomers, the reaction was followed according to the literature procedure. The literature procedure reported using preparative HPLC, while column chromatography was used for separation of **68** and **69**. Also, **68** (*o*-isomer) was reported as a yellow oil.

9-Methoxy-2-methyl-1,3,4,5-tetrahydro-2*H*-benzo[*c*]azepine (70**)**

A 1M solution of BH₃ in THF (1 mL, 1.2 mmol) was added in a dropwise manner to a stirred solution of **69** (0.06 g, 0.3 mmol) in anhydrous THF (2 mL) at 0 °C (ice-bath) under an N₂ atmosphere. The clear reaction mixture was heated at reflux and allowed to stir overnight, then cooled to room temperature and quenched by the careful addition of HCl (6N) at 0 °C (ice-bath) until acidic (pH ~ 3). The reaction mixture was heated to evaporate the THF until THF could no longer be detected by smell. The residue was cooled to 0 °C (ice-bath) and a solution of NaOH (3N) was added in a dropwise manner until basic (pH ~ 12) followed by extraction with Et₂O (3 x 30 mL). The combined organic portion was

dried (Na_2SO_4) and evaporated to dryness under reduced pressure to yield 0.48 g of a crude yellow oil.

A saturated solution of gaseous HCl in EtOAc was added in a dropwise manner to a solution of the crude yellow oil in EtOAc until the solution was acidic (pH \sim 3). The white solid that precipitated upon addition of gaseous HCl/EtOAc was collected by filtration and washed with Et_2O . Recrystallization of the white solid from acetone yielded 0.01 g (15%) of **70** as white crystals: mp 199-200°C; ^1H NMR ($\text{DMSO}-d_6$) δ 1.91 (br s, 2H, $-\text{CH}_2$), 2.61 (s, 3H, NCH_3), 2.99 (br s, 2H, $-\text{CH}_2$), 3.35-3.46 (m, 2H, $-\text{CH}_2$), 3.86 (s, 3H, $-\text{OCH}_3$), 4.49 (s, 2H, $-\text{CH}_2$), 6.68-6.91 (d, $J = 7.44$ Hz, 1H, ArH), 7.01-7.03 (d, $J = 8.4$ Hz, 1H, ArH), 7.33-7.34 (t, $J = 7.94$ Hz, 1H, ArH), 10.92 (br s, 1H, NH^+); Anal. Calcd for ($\text{C}_{12}\text{H}_{17}\text{NO}\cdot\text{HCl}$) C, 63.28; H, 7.96; N, 6.15. Found: C, 63.51; H, 7.96; N, 6.12.

3-(2,3-Dimethoxyphenyl)-*N,N*-dimethylpropanamide (71)

The procedure followed was reported in the literature for a similar compound.¹⁹⁷

Thionyl chloride (1 mL, 13.78 mmol) was added in a dropwise manner at 0 °C (ice-bath) to 3-(2,3-dimethoxyphenyl) propionic acid (**63**) (0.68 g, 3.2 mmol) under an N_2 atmosphere. The reaction mixture was heated at reflux and allowed to stir for 2 h, allowed to cool to room temperature and the thionyl chloride was evaporated to dryness under reduced pressure to yield the crude intermediate as an amber oil which was used in the

next reaction without further characterization. A solution of 3-(2,3-dimethoxyphenyl)propionyl chloride in anhydrous CH_2Cl_2 (30 mL) was added in a dropwise manner at 0 °C (ice-bath) to a stirred solution of saturated aqueous NaHCO_3 (10 mL) and $(\text{CH}_3)_2\text{NH}_2$ (40% w/v in H_2O , 2 mL, 15.1 mmol). The reaction mixture was allowed to stir at 0-4 °C for 1 h, quenched by the careful addition of saturated aqueous NaHCO_3 (30 mL) and extracted with CH_2Cl_2 (3 x 15 mL). The combined organic portion was dried (Na_2SO_4) and evaporated to dryness under reduced pressure to yield a crude amber residue, which was purified by column chromatography (silica gel; hexanes/EtOAc; 100:0 to 0:100) to afford 0.55 g (71%) of **71** as an amber oil. ^1H NMR ($\text{DMSO}-d_6$) δ 2.77-2.79 (t, J = 4.26 Hz, 2H, $-\text{CH}_2$), 2.85 (s, 3H, $-\text{NCH}_3$), 2.97 (s, 3H, $-\text{NCH}_3$), 3.76 (s, 3H, $-\text{OCH}_3$), 3.82 (s, 3H, $-\text{OCH}_3$), 6.82-6.84 (dd, J = 1.42, 7.54 Hz, 1H, ArH), 6.91-6.91 (d, J = 1.48 Hz, 1H, ArH), 6.93-6.98 (t, J = 10.68 Hz, 1H, ArH). ^1H NMR (CD_3CN) 2.55-2.59 (t, J = 7.96 Hz, 2H, $-\text{CH}_2$) is visible which in DMSO overlapped with the $\text{DMSO}-d_6$ peak (~2.54 ppm).

3-(3-Methoxyphenyl)-*N,N*-dimethylpropanamide (72)

The compound is reported in literature²¹¹ as a colorless oil but the procedure followed was similar to another reported method.¹⁹⁷

In a two-neck flask, 1-ethyl-3-(3-dimethylaminopropyl)carbodiimide (EDCI) (2.06 g, 10.8 mmol) and Et_3N (6 mL, 45.2 mmol) were added portion-wise to a stirred solution of 3-(3-

methoxyphenyl)propionic acid (**66**) (1.81 g, 10.0 mmol) and CH₃NH₂·HCl (2.46 g, 30.2 mmol) in anhydrous CH₂Cl₂ (40 mL) under an N₂ atmosphere. The reaction was allowed to stir at room temperature for 24 h and quenched by the careful addition of HCl (1N, 50 mL) and extracted with CH₂Cl₂ (3 x 20 mL). The combined organic portion was dried (Na₂SO₄) and evaporated to dryness under reduced pressure to yield a crude yellow oil which was purified by column chromatography (silica gel; CH₂Cl₂/MeOH; 100:0 to 90:10) to afford 1.21 g (58%) of **72** as a pale-yellow oil. ¹H NMR (DMSO-*d*₆) δ 2.60-2.63 (t, *J* = 7.78 Hz, 2H, -CH₂), 2.78-2.82 (t, *J* = 7.76 Hz, 2H, -CH₂), 2.85 (s, 3H, -NCH₃), 2.96 (s, 3H, -NCH₃), 3.76 (s, 3H, -OCH₃), 6.76-6.79 (m, 1H, ArH), 6.83-6.85 (m, 2H, ArH), 7.19-7.23 (t, *J* = 8.1 Hz, 1H, ArH)

Sodium 1-hydroxy-1-(3,4-dimethoxyphenyl)methanesulfonate (75)

The procedure followed was reported in the literature.²⁰³

A solution of sodium bisulfite (1.00 g, 9.6 mmol) in H₂O (2 mL) was added in a dropwise manner to a stirred solution of veratraldehyde (**73**) (1.60 g, 9.6 mmol) in EtOH (19 mL) at room temperature. The resulting suspension was allowed to stir at 30-35 °C for 16 h and subsequently at 4-5 °C for 4 h. The precipitate was collected by filtration, washed with hexane (3 x 15 mL) and dried to yield 2.10 g (88%) of **75** as a white solid: mp 155-160 °C; The starting material was an oil and the product was collected as a solid. The *r_f* values (0.77) were identical for both the starting material and product in EtOH:NH₄OH (9.5:0.5)

solvent system and there were no other products formed. Based on this, the product was not characterized further and was used in the next step.

Compound **75** is reported in the literature but not its melting point.

Sodium 1-hydroxy-1-(4-methoxyphenyl)methanesulfonate (76)

The compound is reported in literature²¹² but was synthesized by a different method here.²⁰³

A solution of sodium bisulfite (1.00 g, 9.6 mmol) in H₂O (1.9 mL) was added in a drop wise manner to a stirred solution of anisaldehyde (**74**) (1.30 g, 9.6 mmol) in EtOH (19 mL) at room temperature. The resulting suspension was allowed to stir at 30-35 °C for 16 h and subsequently at 4-5 °C for 4 h. The precipitate was collected by filtration, washed with hexane (3 x 15 mL) and dried to yield 2.0 g (88%) of **76** as a white solid: mp 158-164 °C (lit.²¹² mp 155-157 °C).

B. Electrophysiology – Two-electrode voltage clamp

To gain hands-on experience on the two-electrode voltage clamp technique in electrophysiology, I spent the Summer of 2017 in Dr. Marvin K. Schulte's laboratory in the University of Sciences, Philadelphia. Here, I conducted preliminary screening on some of my deconstructed analogs under the training and guidance of Dr. Schulte's graduate

student, Laura DeCristafano. The protocol followed is well established in their laboratory.^{213–215}

1. Expression and cRNA microinjection:

Xenopus laevis ovarian lobes were purchased from Xenopus 1 (Dexter, MI). The lobes were then shaken gently for around 20-30 mins at room temperature in 1.5 mg/mL collagenase (Sigma type II, Sigma-Aldrich) in order to facilitate the removal of follicular cells. The oocytes were stored in Barth's buffer composed of 88 mM NaCl, 1mM KCl, 0.4 mM CaCl₂, 0.33 mM Ca(NO₃)₂, 0.8 mM MgSO₄, 5 mM Tris, 2.4 mM NaHCO₃ at pH 7.4 with gentamycin (final concentration of 0.1 mg/mL). Healthy-looking stage IV oocytes were chosen for microinjection with cRNAs and recording.

The synthetic cRNAs for human $\alpha 7$ were prepared using the mMMESSAGE mMACHINE™ High Yield Capped RNA Transcription Kit (Ambion, TX). Each oocyte was injected with 50 nL cRNA at a concentration of 300 ng/ μ L. The injected oocytes were then incubated for 48 hours in Barth's buffer at 19 °C to allow sufficient expression of human $\alpha 7$ nAChRs. After incubation, healthy oocytes were chosen for electrophysiological recordings.

2. Two-electrode voltage clamp recording and data collection:

The electrophysiological recordings were carried out by a TEVC set-up at -60 mV. The set-up consisted of an automated system with an OC-725C oocyte clamp amplifier (Warner Instruments, CT, US) that was connected to an axon instruments data

acquisition system. The software CLAMPEX was used for data acquisition while CLAMPFIT was used for analyses. Both the current and recording electrodes were filled with a 3M KCl solution and had resistances of $\sim 1\text{ M}\Omega$. A vertical flow chamber of volumes $\sim 280\ \mu\text{L}$ was used to hold the individual oocytes, which were perfused with the ND-96 recording buffer (96 mM NaCl, 2mM KCl, 1 mM MgCl_2 , 1.8 mM CaCl_2 , and 2 mM phosphate buffer at pH 7.4) at a rate of 5-6 mL/min by a peristaltic pump. Solutions of the agonist, ACh along with galantamine and its deconstructed analogs were prepared in ND-96 buffer. The solutions of the compounds were serially diluted to appropriate concentrations and injected into the recording chamber at the rate of 20 mL/min via a Gilson Autosampler. All the data were analyzed in GraphPad Prism.

Molecular Modeling

1. 3D-overlap of molecules

Galantamine (**3**) and codeine (**8**) were sketched and energy minimized in SYBYLX-2.1 (Tripos International). The molecules were overlapped in SYBYLX-2.1 using the multifit option. The atoms chosen in both the molecules for alignment were the methoxy oxygen atoms, the centroids of the phenyl ring, the hydroxyl oxygen atoms, the dihydrofuran oxygen atoms and the tertiary nitrogen atoms.

2. Generation of homology models

The primary amino acid sequence of the human $\alpha 7$ nAChR was obtained from the Universal Protein Resource (UniProt; accession code: P36544).²¹⁶ The sequence of the template, chimera *Ls-AChBP* – human $\alpha 7$ nAChR¹⁶⁹ was obtained as a FASTA file from the Protein Databank (PDB) at <http://www.rcsb.org>. The template was prepared by removal of water molecules, ligands and other molecules such as surfactants that were employed for crystallization. Hence, only the residues for two subunits were retained. The sequences of template and the protein of interest were aligned using Clustal O.²¹⁷ The first three amino acids from the protein of interest were removed after alignment as there was a lack of complementary amino acids on the template. Two truncated amino acid sequences of the protein of interest were aligned to two amino acid sequences of the template dimer. One hundred 3D homology models of the human $\alpha 7$ nAChR were generated using Modeller v9.12 (University of California San Francisco, San Francisco, CA)²¹⁸ using the crystal structure of the chimera of *Ls-AChBP* – human $\alpha 7$ nAChR co-crystallized with epibatidine (PDB ID: 3SQ6) as the template. The homology models were supported by docking the agonist epibatidine. Additionally, Ramachandran plots¹⁹⁸ were generated to determine the percentage of amino acids that fell under the most favored, additional allowed region, generously allowed region and disallowed regions. Of the 16 disallowed amino acids, none were in the site reported to be important for the binding of galantamine.

3. Docking studies:

Galantamine and its deconstructed analogs were sketched and energy minimized using Gasteiger-Hückel charges and a dielectric constant of 4.0 in SYBYLX-2.1 (Tripos International). The molecules were docked in the homology models of the human $\alpha 7$ nAChR using GOLD Suite 5.3 (Cambridge Crystallographic Data Centre, Cambridge, UK),²¹⁹ an automated genetic algorithm docking program with GOLD score as the chosen scoring function. The docking site was defined as a spherical region, 6 Å around the C α of Thr221 of human $\alpha 7$ nAChR. The docking solutions with similar poses were grouped together using a script. The clusters were inspected visually and a model was chosen based on the orientation and interactions of the ligand with the docking site. The chosen model/s were merged with the protein and their energy was minimized using the Tripos Force Field (Gasteiger-Hückel charges, distance-dependent dielectric constant = 4.0) in SYBYL X-2.1 (Tripos International).

The Hydrophobic Interaction (HINT)¹⁹⁹ scores of the minimized ligand-receptor complexes were determined using the HINT program in SYBYL x 8.1, to quantify the interactions observed in the homology modeling studies. The protein was partitioned using the dictionary option while the ligand was partitioned using the calculate option in the default settings. The atom-based breakdown of the HINT score was analyzed to

determine the contributions of the individual atoms to the interactions with amino acid residues at the binding region of the human $\alpha 7$ nAChR.

BIBLIOGRAPHY

Bibliography

1. Stelzmann, R. A.; Schnitzlein, H. N.; Murtagh, F. R. An English translation of Alzheimer's 1907 paper, "Über eine eigenartige Erkrankung der Hirnrinde". *Clin. Anat.* **1995**, *8*, 429-431.
2. Roberson, E. D.; Mucke, L. 100 years and counting: Prospects for defeating Alzheimer's disease. *Science* **2006**, *314*, 781-784.
3. Alzheimer's Association. 2017 Alzheimer's disease facts and figures. *Alzheimer's Dement.* **2017**, *13*, 325-373.
4. Lott, I. T.; Dierssen, M. Cognitive deficits and associated neurological complications in individuals with Down's syndrome. *Lancet Neurol.* **2010**, *9*, 623-633.
5. Ortman, J. M.; Velkoff, V. A.; Hogan, H. (2014) An aging nation: The older population in the United States. Population estimates and projections prepared by the U.S. Department of Commerce. Economics and Statistics Administration. U.S. Census Bureau.
6. Latest medication for memory loss. Alzheimer's association. https://www.alz.org/alzheimers_disease_standard_prescriptions.asp#types (accessed Jan 20, 2018).
7. Bartus, R. T.; Dean, R. L., 3rd; Beer, B.; Lippa, A. S. The cholinergic hypothesis of geriatric memory dysfunction. *Science* **1982**, *217*, 408-417.
8. Contestabile, A. The history of the cholinergic hypothesis. *Behav. Brain Res.* **2011**, *221*, 334-340.
9. Hardy, J. A.; Higgins, G. A. Alzheimer's disease: The amyloid cascade hypothesis. *Science* **1992**, *256*, 184-185.
10. Maccioni, R. B.; Farías, G.; Morales, I.; Navarrete, L. The revitalized tau hypothesis on Alzheimer's disease. *Arch. Med. Res.* **2010**, *41*, 226-231.
11. de la Torre, J. C. The vascular hypothesis of Alzheimer's disease: Bench to bedside and beyond. *Neurodegener. Dis.* **2010**, *7*, 116-121.
12. Zotova, E.; Nicoll, J. A. R.; Kalaria, R.; Holmes, C.; Boche, D. Inflammation in Alzheimer's disease: Relevance to pathogenesis and therapy. *Alzheimer's Res. Ther.* **2010**, *2*, 1-9.
13. Markesbery, W. R. Oxidative stress hypothesis in Alzheimer's disease. *Free Radical Biol. Med.* **1997**, *23*, 134-147.

14. Puglielli, L.; Tanzi, R. E.; Kovacs, D. M. Alzheimer's disease: The cholesterol connection. *Nat. Neurosci.* **2003**, *6*, 345-351.
15. Current Alzheimer's treatments. Alzheimer's Association: https://www.alz.org/research/science/alzheimers_disease_treatments.asp (accessed April 23, 2018)
16. Mehta, M.; Adem, A.; Sabbagh, M. New acetylcholinesterase inhibitors for Alzheimer's disease. *Int. J. Alzheimer's Dis.* **2012**, *2012*, 1-8.
17. Whitehouse, P. J.; Martino, A. M.; Marcus, K. A.; Zweig, R. M.; Singer, H. S.; Price, D. L.; Kellar, K. J. Reductions in acetylcholine and nicotine binding in several degenerative diseases. *Arch. Neurol.* **1988**, *45*, 722-724.
18. Nordberg, A.; Winblad, B. Reduced number of [³H]nicotine and [³H]acetylcholine binding sites in the frontal cortex of Alzheimer brains. *Neurosci. Lett.* **1986**, *72*, 115-120.
19. Bencherif, M.; Lippiello, P. M. Alpha7 neuronal nicotinic receptors: The missing link to understanding Alzheimer's etiopathology? *Med. Hypotheses* **2010**, *74*, 281-285.
20. Wang, H.-Y.; Lee, D. H. S.; Davis, C. B.; Shank, R. P. Amyloid peptide A β ₁₋₄₂ binds selectively and with picomolar affinity to α 7 nicotinic acetylcholine receptors. *J. Neurochem.* **2000**, *75*, 1155-1161.
21. Lilienfeld, S. Galantamine - A novel cholinergic drug with a unique dual mode of action for the treatment of patients with Alzheimer's disease. *CNS Drug Rev.* **2002**, *8*, 159-176.
22. Thomsen, T.; Kaden, B.; Fischer, J. P.; Bickel, U.; Barz, H.; Gusztony, G.; Cervos-Navarro, J.; Kewitz, H. Inhibition of acetylcholinesterase activity in human brain tissue and erythrocytes by galanthamine, physostigmine and tacrine. *Eur. J. Clin. Chem. Clin. Biochem.* **1991**, *29*, 487-492.
23. Texidó, L.; Ros, E.; Marin-Satué, M.; López, S.; Aleu, J.; Marsal, J.; Solsona, C. Effect of galantamine on the human α 7 neuronal nicotinic acetylcholine receptor, the *Torpedo* nicotinic acetylcholine receptor and spontaneous cholinergic synaptic activity. *Br. J. Pharmacol.* **2005**, *145*, 672-678.
24. Cheung, J.; Rudolph, M. J.; Burshteyn, F.; Cassidy, M. S.; Gary, E. N.; Love, J.; Franklin, M. C.; Height, J. J. Structures of human acetylcholinesterase in complex with pharmacologically important ligands. *J. Med. Chem.* **2012**, *55*, 10282-10286.
25. Han, S. Y.; Sweeney, J. E.; Bachman, E. S.; Schweiger, E. J.; Forloni, G.; Coyle, J. T.; Davis, B. M.; Joullié, M. M. Chemical and pharmacological characterization of galanthamine, an acetylcholinesterase inhibitor, and its derivatives. A potential application in Alzheimer's disease? *Eur. J. Med. Chem.* **1992**, *27*, 673-687.
26. What is Alzheimer's? https://alz.org/alzheimers_disease_what_is_alzheimers.asp (accessed Jan 19, 2018).
27. Holland, A. J.; Oliver, C. Down's syndrome and the links with Alzheimer's disease. *J. Neurol., Neurosurg. Psychiatry* **1995**, *59*, 111-114.
28. Wisniewski, K. E.; Wisniewski, H. M.; Wen, G. Y. Occurrence of neuropathological changes and dementia of Alzheimer's disease in Down's syndrome. *Ann. Neurol.* **1985**, *17*, 278-282.

29. Alzheimer's Disease in People with Down Syndrome. <http://www.nia.nih.gov/health/alzheimers-disease-people-down-syndrome> (accessed Jan 19, 2018).
30. Katzman, R. The prevalence and malignancy of Alzheimer disease. A major killer. *Arch. Neurol.* **1976**, *33*, 217-218.
31. Burns, A.; Iliffe, S. Dementia. *Br. Med. J.* **2009**, *338*, 405-409.
32. Barker, W. W.; Luis, C. A.; Kashuba, A.; Luis, M.; Harwood, D. G.; Loewenstein, D.; Waters, C.; Jimison, P.; Shepherd, E.; Sevush, S.; Graff-Radford, N.; Newland, D.; Todd, M.; Miller, B.; Gold, M.; Heilman, K.; Doty, L.; Goodman, I.; Robinson, B.; Pearl, G.; Dickson, D.; Duara, R. Relative frequencies of Alzheimer disease, Lewy body, vascular and frontotemporal dementia, and hippocampal sclerosis in the state of Florida brain bank. *Alzheimer Dis. Assoc. Disord.* **2002**, *16*, 203-212.
33. Feldman, H. H.; Woodward, M. The staging and assessment of moderate to severe Alzheimer disease. *Neurology* **2005**, *65*, S10-S17.
34. Burns, A.; Iliffe, S. Alzheimer's disease. *Br. Med. J.* **2009**, *338*, 467-471.
35. Bird, T. D. Alzheimer Disease Overview. In *GeneReviews*; Adam, M. P., Ardinger, H. H., Pagon, R. A., Wallace, S. E., Bean, L. J., Stephens, K., Amemiya, A., Eds.; University of Washington, Seattle: Seattle, 1993-2018.
36. Selkoe, D. J. Alzheimer disease: Mechanistic understanding predicts novel therapies. *Ann. Intern. Med.* **2004**, *140*, 627-638.
37. Bertram, L.; Lill, C. M.; Tanzi, R. E. The genetics of Alzheimer disease: Back to the future. *Neuron* **2010**, *68*, 270-281.
38. Bagyinszky, E.; Youn, Y. C.; An, S. S. A.; Kim, S. The genetics of Alzheimer's disease. *Clin. Interv. Aging* **2014**, *9*, 535-551.
39. Tanzi, R. E.; Bertram, L. New frontiers in Alzheimer's disease genetics. *Neuron* **2001**, *32*, 181-184.
40. Piaceri, I.; Nacmias, B.; Sorbi, S. Genetics of familial and sporadic Alzheimer disease. *Front. Biosci., Elite Ed.* **2013**, *5*, 167-177.
41. Davies, P.; Maloney, A. J. F. Selective loss of central cholinergic neurons in Alzheimer's disease. *Lancet* **1976**, *308*, 1403.
42. Perry, E. K.; Gibson, P. H.; Blessed, G.; Perry, R. H.; Tomlinson, B. E. Neurotransmitter enzyme abnormalities in senile dementia: Choline acetyltransferase and glutamic acid decarboxylase activities in necropsy brain tissue. *J. Neurol. Sci.* **1977**, *34*, 247-265.
43. Bowen, D. M.; Smith, C. B.; White, P.; Davison, A. N. Neurotransmitter-related enzymes and indices of hypoxia in senile dementia and other abiotrophies. *Brain* **1976**, *99*, 459-496.
44. Davis, K. L.; Mohs, R. C.; Marin, D.; Purohit, D. P.; Perl, D. P.; Lantz, M.; Austin, G.; Haroutunian, V. Cholinergic markers in elderly patients with early signs of Alzheimer disease. *J. Am. Med. Assoc.* **1999**, *281*, 1401-1406.
45. Francis, P. T.; Palmer, A. M.; Snape, M.; Wilcock, G. K. The cholinergic hypothesis of Alzheimer's disease: A review of progress. *J. Neurol. Neurosurg. Psychiatry* **1999**, *66*, 137-147.

46. Drachman, D. A.; Leavitt, J. Human memory and the cholinergic system. *Arch. Neurol.* **1974**, *30*, 113-121.
47. Perry, E. K.; Morris, C. M.; Court, J. A.; Cheng, A.; Fairbairn, A. F.; McKeith, I. G.; Irving, D.; Brown, A.; Perry, R. H. Alteration in nicotine binding sites in Parkinson's disease, Lewy body dementia and Alzheimer's disease: Possible index of early neuropathology. *Neuroscience* **1995**, *64*, 385-395.
48. Schröder, H.; Giacobini, E.; Struble, R. G.; Zilles, K.; Maelicke, A. Nicotinic cholinergic neurons of the frontal cortex are reduced in Alzheimer's disease. *Neurobiol. Aging* **1991**, *12*, 259-262.
49. Rylett, R. J.; Ball, M. J.; Colhoun, E. H. Evidence for high affinity choline transport in synaptosomes prepared from hippocampus and neocortex of patients with Alzheimer's disease. *Brain Res.* **1983**, *289*, 169-175.
50. Craig, L. A.; Hong, N. S.; McDonald, R. J. Revisiting the cholinergic hypothesis in the development of Alzheimer's disease. *Neurosci. Biobehav. Rev.* **2011**, *35*, 1397-1409.
51. Selkoe, D. J. The molecular pathology of Alzheimer's disease. *Neuron* **1991**, *6*, 487-498.
52. Glenner, G.; Harada, M.; Isersky, C.; Cuatrecasas, P.; Page, D.; Keiser, H. Human amyloid protein: Diversity and uniformity. *Biochem. Biophys. Res. Commun.* **1970**, *41*, 1013-1019.
53. Glenner, G. G.; Wong, C. W. Alzheimer's disease: Initial report of the purification and characterization of a novel cerebrovascular amyloid protein. *Biochem. Biophys. Res. Commun.* **1984**, *120*, 885-890.
54. Kang, J.; Lemaire, H-G.; Unterbeck, A.; Salbaum, J. M.; Masters, C. L.; Grzeschik, K-H.; Multhaup, G.; Beyreuther, K.; Müller-Hill, B. The precursor of Alzheimer's disease amyloid A4 protein resembles a cell-surface receptor. *Nature* **1987**, *325*, 733-736.
55. Mattson, M. P. Pathways towards and away from Alzheimer's disease. *Nature* **2004**, *430*, 631-639.
56. Masters, C. L.; Simms, G.; Weinman, N. A.; Multhaup, G.; McDonald, B. L.; Beyreuther, K. Amyloid plaque core protein in Alzheimer disease and Down syndrome. *Proc. Natl. Acad. Sci. U. S. A.* **1985**, *82*, 4245-4249.
57. Glenner, G. G.; Wong, C. W. Alzheimer's disease and Down's syndrome: Sharing of a unique cerebrovascular amyloid fibril protein. *Biochem. Biophys. Res. Commun.* **1984**, *122*, 1131-1135.
58. Reiman, E. M. Alzheimer's disease: Attack on amyloid- β protein. *Nature* **2016**, *537*, 36-37.
59. Hardy, J. Selkoe, D. J. The amyloid hypothesis of Alzheimer's disease: Progress and problems on the road to therapeutics. *Science* **2002**, *297*, 353-356.
60. Drachman, D. A. The amyloid hypothesis, time to move on: Amyloid is the downstream result, not cause, of Alzheimer's disease. *Alzheimer's Dementia* **2014**, *10*, 372-380.

61. Morris, G. P.; Clark, I. A.; Vissel, B. Inconsistencies and controversies surrounding the amyloid hypothesis of Alzheimer's disease. *Acta. Neuropathol. Commun.* **2014**, *2*, 1-21.
62. Grundke-Iqbal, I.; Iqbal, K.; Tung, Y-C.; Quinlan, M.; Wisniewski, H. M.; Binder, L. I. Abnormal phosphorylation of the microtubule-associated protein τ (tau) in Alzheimer cytoskeletal pathology. *Proc. Natl. Acad. Sci. U. S. A.* **1986**, *83*, 4913-4917.
63. Kosik, K. S.; Joachim, C. L.; Selkoe, D. J. Microtubule-associated protein tau (τ) is a major antigenic component of paired helical filaments in Alzheimer disease. *Proc. Natl. Acad. Sci. U. S. A.* **1986**, *83*, 4044-4048.
64. Braak, H.; Braak, E. Neuropathological staging of Alzheimer-related changes. *Acta. Neuropathol.* **1991**, *82*, 239-259.
65. Mudher, A.; Lovestone, S. Alzheimer's disease - do tauists and baptists finally shake hands? *Trends Neurosci.* **2002**, *25*, 22-26.
66. Lansdall, C. J. An effective treatment for Alzheimer's disease must consider both amyloid and tau. *Biosci. Horiz.* **2014**, *7*, 1-11.
67. de la Torre, J. C.; Mussivand, T. Can disturbed brain microcirculation cause Alzheimer's disease? *Neurol. Res.* **1993**, *15*, 146-153.
68. Hofman, A.; Ott, A.; Breteler, M. M. B.; Bots, M. L.; Slooter, A. J. C.; van Harskamp, F.; van Duijn, C. N.; van Broeckhoven, C. Grobbee, D. E. Atherosclerosis, apolipoprotein E, and prevalence of dementia and Alzheimer's disease in the Rotterdam study. *Lancet* **1997**, *349*, 151-154.
69. Simons, M.; Keller, P.; Dichgans, J.; Schulz, J. B. Cholesterol and Alzheimer's disease: Is there a link? *Neurology* **2001**, *57*, 1089-1093.
70. Griffin, W. S. T.; Stanley, L. C.; Ling, C.; White, L.; MacLeod, V.; Perrot, L. J.; White, C. L., III; Araoz, C. Brain interleukin 1 and S-100 immunoreactivity are elevated in Down syndrome and Alzheimer disease. *Proc. Natl. Acad. Sci. U. S. A.* **1989**, *86*, 7611-7615.
71. Eikelenboom, P.; Stam, F. C. Immunoglobulins and complement factors in senile plaques. An immunoperoxidase study. *Acta. Neuropathol. (Berl)* **1982**, *57*, 239-242.
72. Rogers, J.; Cooper, N. R.; Webster, S.; Schultz, J.; McGeer, P. L.; Styren, S. D.; Civin, W. H.; Brachova, L.; Bradt, B.; Ward, P.; Lieberburg, I. Complement activation by β -amyloid in Alzheimer disease. *Proc. Natl. Acad. Sci. U. S. A.* **1992**, *89*, 10016-10020.
73. Lue, L-F.; Brachova, L.; Civin, W. H.; Rogers, J. Inflammation, A β deposition, and neurofibrillary tangle formation as correlates of Alzheimer's disease neurodegeneration. *J. Neuropathol. Exp. Neurol.* **1996**, *55*, 1083-1088.
74. McGeer, P. L.; McGeer, E. G. Inflammation of the brain in Alzheimer's disease: Implications for therapy. *J. Leukocyte Biol.* **1999**, *65*, 409-415.
75. Rogers, J.; Shen, Y. A perspective on inflammation in Alzheimer's disease. *Ann. N. Y. Acad. Sci.* **2000**, *924*, 132-135.
76. Harman, D. Free radical theory of aging: Alzheimer's disease pathogenesis. *Age* **1995**, *18*, 97-119.

77. Christen, Y. Oxidative stress and Alzheimer disease. *Am. J. Clin. Nutr.* **2000**, *71*, 621S-629S.
78. Praticò, D. Oxidative stress hypothesis in Alzheimer's disease: A reappraisal. *Trends Pharmacol. Sci.* **2008**, *29*, 609-615.
79. Čolović, M. B.; Krstić, D. Z.; Lazarević-Pašti, T. D.; Bondžić, A. M.; Vasić, V. M. Acetylcholinesterase inhibitors: Pharmacology and toxicology. *Curr. Neuropharmacol.* **2013**, *11*, 315-335.
80. Heinrich, M.; Teoh, H. L. Galanthamine from snowdrop – the development of a modern drug against Alzheimer's disease from local Caucasian knowledge. *J. Ethnopharmacol.* **2004**, *92*, 147-162.
81. Janssen, B.; Schafer, B. Galantamine. *ChemTexts* **2017**, *3*, 1-21.
82. Noble, B. The Iliad and The Odyssey (Barnes & Noble Collectible Editions) <https://www.barnesandnoble.com/w/barnes-noble-leatherbound-classics-the-iliad-and-the-odyssey-homer/1106658791> (accessed Feb 25, 2018).
83. Plaitakis, A.; Duvoisin, R. C. Homer's moly identified as *Galanthus nivalis* L.: Physiologic antidote to stramonium poisoning. *Clin. Neuropharmacol.* **1983**, *6*, 1-5.
84. Proskurnina, N. F.; Yakovieva, A. Ob alkaloidakh Galanthus woronowi. 2. O vydelenni novogo alkaloida. *Zhurnal Obshchei Khimii Russ. J. Gen. Chem.* **1953**, *22*, 1899-1902.
85. Scott, L. J.; Goa, K. L. Galantamine. A review of its use in Alzheimer's disease. *Drugs* **2000**, *60*, 1095-1122.
86. Thomsen, T.; Kewitz, H. Selective inhibition of human acetylcholinesterase by galanthamine in vitro and in vivo. *Life Sci.* **1990**, *46*, 1553-1558.
87. Darvesh, S.; Walsh, R.; Kumar, R.; Caines, A.; Roberts, S.; Magee, D.; Rockwood, K.; Martin, E. Inhibition of human cholinesterases by drugs used to treat Alzheimer disease. *Alzheimer Dis. Assoc. Disord.* **2003**, *17*, 117-126.
88. Dvir, H.; Silman, I.; Harel, M.; Rosenberry, T. L.; Sussman, J. L. Acetylcholinesterase: From 3D structure to function. *Chem.-Biol. Interact.* **2010**, *187*, 10-22.
89. Bartolucci, C.; Perola, E.; Pilger, C.; Fels, G.; Lamba, D. Three-dimensional structure of a complex of galanthamine (Nivalin®) with acetylcholinesterase from *Torpedo californica*: Implications for the design of new anti-Alzheimer drugs. *Proteins* **2001**, *42*, 182-191.
90. Greenblatt, H. M.; Kryger, G.; Lewis, T.; Silman, I.; Sussman, J. L. Structure of acetylcholinesterase complexed with (-)-galanthamine at 2.3 Å resolution. *FEBS Lett.* **1999**, *463*, 321-326.
91. Pereira, E. F. R.; Reinhardt-Maelicke, S.; Schrattenholz, A.; Maelicke, A.; Albuquerque, E. X. Identification and functional characterization of a new agonist site on nicotinic acetylcholine receptors of cultured hippocampal neurons. *J. Pharmacol. Exp. Ther.* **1993**, *265*, 1474-1491.
92. Schrattenholz, A.; Pereira, E. F. R.; Roth, U.; Weber, K-H.; Albuquerque, E. X.; Maelicke, A. Agonist responses of neuronal nicotinic acetylcholine receptors are

- potentiated by a novel class of allosterically acting ligands. *Mol. Pharmacol.* **1996**, 49, 1-6.
93. Maelicke, A.; Schrattenholz, A.; Schröder, H. Modulatory control by non-competitive agonists of nicotinic cholinergic neurotransmission in the central nervous system. *Semin. Neurosci.* **1995**, 7, 103-114.
 94. Storch, A.; Schrattenholz, A.; Cooper, J. C.; Ghani, E. M. A.; Gutbrod, O.; Weber, K-H.; Reinhardt, S.; Lobron, C.; Hermsen, B.; Šoškič, V.; Pereira, E. F. R.; Albuquerque, E. X.; Methfessel, C.; Maelicke, A. Physostigmine, galanthamine and codeine act as 'noncompetitive nicotinic receptor agonists' on clonal rat pheochromocytoma cells. *Eur. J. Pharmacol.* **1995**, 290, 207-219.
 95. Pereira, E. F. R.; Alkondon, M.; Reinhardt, S.; Maelicke, A.; Peng, X.; Lindstrom, J.; Whiting, P.; Albuquerque, E. X. Physostigmine and galanthamine: Probes for a novel binding site on the $\alpha 4\beta 2$ subtype of neuronal nicotinic acetylcholine receptors stably expressed in fibroblast cells. *J. Pharmacol. Exp. Ther.* **1994**, 270, 768-778.
 96. Maelicke, A.; Coban, T.; Schrattenholz, A.; Schröder, B.; Reinhardt-Maelicke, S.; Storch, A.; Godovac-Zimmermann, J.; Methfessel, C.; Pereira, E. F. R.; Albuquerque, E. X. Physostigmine and neuromuscular transmission. *Ann. Acad. N. Y. Sci.* **1993**, 631, 140-154.
 97. Okonjo, K. O.; Kuhlmann, J.; Maelicke, A. A second pathway of activation of the *Torpedo* acetylcholine receptor channel. *Eur. J. Biochem.* **1991**, 200, 671-677.
 98. Kuhlmann, J.; Okonjo, K. O.; Maelicke, A. Desensitization is a property of the cholinergic binding region of the nicotinic acetylcholine receptor, not of the receptor-integral ion channel. *FEBS Lett.* **1991**, 279, 216-218.
 99. Filho, J. M. J. M. C.; Birks, J. Physostigmine for dementia due to Alzheimer's disease. *Cochrane DB Syst. Rev.* **2001**, 2, 1-81.
 100. Orhan, G.; Orhan, I.; Subutay-Oztekin, N.; Ak, F.; Sener, B. Contemporary anticholinesterase pharmaceuticals of natural origin and their synthetic analogues for the treatment of Alzheimer's disease. *Recent Pat. CNS Drug Discovery* **2009**, 4, 43-51.
 101. Maelicke, A.; Schrattenholz, A.; Samochocki, M.; Radina, M.; Albuquerque, E. X. Allosterically potentiating ligands of nicotinic receptors as a treatment strategy for Alzheimer's disease. *Behav. Brain Res.* **2000**, 113, 199-206.
 102. Samochocki, M.; Höffle, A.; Fehrenbacher, A.; Jostock, R.; Ludwig, J.; Christner, C.; Radina, M.; Zerlin, M.; Ullmer, C.; Pereira, E. F. R.; Lübbert, H.; Albuquerque, E. X.; Maelicke, A. Galantamine is an allosterically potentiating ligand of neuronal nicotinic but not of muscarinic acetylcholine receptors. *J. Pharmacol. Exp. Ther.* **2003**, 305, 1024-1036.
 103. Akk, G.; Steinbach, J. H. Galantamine activates muscle-type nicotinic acetylcholine receptors without binding to the acetylcholine-binding site. *J. Neurosci.* **2005**, 25, 1992-2001.
 104. Schrattenholz, A.; Godovac-Zimmermann, J.; Schäfer, H.-J.; Albuquerque, E. X.; Maelicke, A. Photoaffinity labeling of *Torpedo* acetylcholine receptor by physostigmine. *Eur. J. Biochem.* **1993**, 216, 671-677.

105. Schröder, B.; Reinhardt-Maelicke, S.; Schratzenholz, A.; McLane, K. E.; Kretschmer, A.; Conti-Tronconi, B. M.; Maelicke, A. Monoclonal antibodies FK1 and WF6 define two neighboring ligand binding sites on *Torpedo* acetylcholine receptor α -polypeptide. *J. Biol. Chem.* **1994**, *269*, 10407-10416.
106. Luttmann, E.; Ludwig, J.; Höffle-Maas, A.; Samochocki, M.; Maelicke, A.; Fels, G. Structural model for the binding sites of allosterically potentiating ligands on nicotinic acetylcholine receptors. *ChemMedChem* **2009**, *4*, 1874-1882.
107. Ludwig, J.; Höffle-Maas, A.; Samochocki, M.; Luttmann, E.; Albuquerque, E. X.; Fels, G.; Maelicke, A. Localization by site-directed mutagenesis of a galantamine binding site on $\alpha 7$ nicotinic acetylcholine receptor extracellular domain. *J. Recept. Signal Transduction* **2010**, *30*, 469-483.
108. Iorga, B.; Herlem, D.; Barré, E.; Guillou, C. Acetylcholine nicotinic receptors: Finding the putative binding site of allosteric modulators using the “blind docking” approach. *J. Mol. Model.* **2005**, *12*, 366-372.
109. Santos, M. D.; Alkondon, M.; Pereira, E. F. R.; Aracava, Y.; Eisenberg, H. M.; Maelicke, A.; Albuquerque, E. X. The nicotinic allosteric potentiating ligand galantamine facilitates synaptic transmission in the mammalian central nervous system. *Mol. Pharmacol.* **2002**, *61*, 1222-1234.
110. Geerts, H.; Guillaumat, P.-O.; Grantham, C.; Bode, W.; Anciaux, K.; Sachak, S. Brain levels and acetylcholinesterase inhibition with galantamine and donepezil in rats, mice, and rabbits. *Brain Res.* **2005**, *1033*, 186-193.
111. Bores, G. M.; Huger, F. P.; Petko, W.; Mutlib, A. E.; Camacho, F.; Rush, D. K.; Selk, D. E.; Wolf, V.; Kosley, R. W. Jr.; Davis, L.; Vargas, H. M. Pharmacological evaluation of novel Alzheimer’s disease therapeutics: Acetylcholinesterase inhibitors related to galanthamine. *J. Pharmacol. Exp. Ther.* **1996**, *277*, 728-738.
112. Bickel, U.; Thomsen, T.; Fischer, J. P.; Weber, W.; Kewitz, H. Galanthamine: Pharmacokinetics, tissue distribution and cholinesterase inhibition in brain of mice. *Neuropharmacology* **1991**, *30*, 447-454.
113. Maelicke, A.; Albuquerque, E. X. Allosteric modulation of nicotinic acetylcholine receptors as a treatment strategy for Alzheimer’s disease. *Eur. J. Pharmacol.* **2000**, *393*, 165-170.
114. Dineley, K. T.; Pandya, A. A.; Yakel, J. L. Nicotinic ACh receptors as therapeutic targets in CNS disorders. *Trends Pharmacol. Sci.* **2015**, *36*, 96-108.
115. Gotti, C.; Zoli, M.; Clementi, F. Brain nicotinic acetylcholine receptors: Native subtypes and their relevance. *Trends Pharmacol. Sci.* **2006**, *27*, 482-491.
116. Millar, N. S.; Gotti, C. Diversity of vertebrate nicotinic acetylcholine receptors. *Neuropharmacology* **2009**, *56*, 237-246.
117. Oddo, S.; LaFerla, F. M. The role of nicotinic acetylcholine receptors in Alzheimer’s disease. *J. Physiol. (Paris)* **2006**, *99*, 172-179.
118. Gotti, C.; Clementi, F.; Fornari, A.; Gaimarri, A.; Guiducci, S.; Manfredi, I.; Moretti, M.; Pedrazzi, P.; Pucci, L.; Zoli, M. Structural and functional diversity of native brain neuronal nicotinic receptors. *Biochem. Pharmacol.* **2009**, *78*, 703-711.

119. Wallace, T. L.; Porter, R. H. P.; Targeting the nicotinic $\alpha 7$ acetylcholine receptor to enhance cognition in disease. *Biochem. Pharmacol.* **2011**, *82*, 891-903.
120. Papke, R. L. Merging old and new perspectives on nicotinic acetylcholine receptors. *Biochem. Pharmacol.* **2014**, *89*, 1-11.
121. Stokes, C.; Papke, R. L. Use of an $\alpha 3\beta 4$ nicotinic acetylcholine receptor subunit concatamer to characterize ganglionic receptor subtypes with specific subunit composition reveals species-specific pharmacologic properties. *Neuropharmacology* **2012**, *63*, 538-546.
122. Uteshev, V. V. The therapeutic promise of positive allosteric modulation of nicotinic receptors. *Eur. J. Pharmacol.* **2014**, *727*, 181-185.
123. Chatzidaki, A.; Millar, N. S. Allosteric modulation of nicotinic acetylcholine receptors. *Biochem. Pharmacol.* **2015**, *97*, 408-417.
124. Wang, H-Y.; Lee, D. H. S.; D'Andrea, M. R.; Peterson, P. A.; Shank, R. P.; Reitz, A. B. β -Amyloid₁₋₄₂ binds to $\alpha 7$ nicotinic acetylcholine receptor with high affinity. Implications for Alzheimer's disease pathology. *J. Biol. Chem.* **2000**, *275*, 5626-5632.
125. Pettit, D. L.; Shao, Z.; Yakel, J. L. β -Amyloid₁₋₄₂ peptide directly modulates nicotinic receptors in the rat hippocampal slice. *J. Neurosci.* **2001**, *21*, 1-5.
126. Lombardo, S.; Maskos, U. Role of the nicotinic acetylcholine receptor in Alzheimer's disease pathology and treatment. *Neuropharmacology* **2015**, *96*, 255-262.
127. Taly, A.; Corringer, P.-J.; Guedin, D.; Lestage, P.; Changeux, J.-P. Nicotinic receptors: Allosteric transitions and therapeutic targets in the nervous system. *Nat. Rev. Drug Discovery* **2009**, *8*, 733-750.
128. Albuquerque, E. X.; Pereira, E. F. R.; Alkondon, M.; Rogers, S. W. Mammalian nicotinic acetylcholine receptors: From structure to function. *Physiol. Rev.* **2009**, *89*, 73-120.
129. Jensen, A. A.; Frølund, B.; Liljefors, T.; Krosgaard-Larsen, P. Neuronal nicotinic acetylcholine receptors: Structural revelations, target identifications, and therapeutic inspirations. *J. Med. Chem.* **2005**, *48*, 4705-4745.
130. Collingridge, G. L.; Olsen, R. W.; Peters, J.; Spedding, M. A nomenclature for ligand-gated ion channels. *Neuropharmacology* **2009**, *56*, 2-5.
131. Fasoli, F.; Gotti, C. Structure of neuronal nicotinic receptors. In *The Neurobiology and Genetics of Nicotine and Tobacco. Current Topics in Behavioral Neurosciences*; Balfour, D. J. K., Munafò, M. R., Eds.; Springer: New York City, 2015; pp 1-18.
132. Gotti, C.; Clementi, F. Neuronal nicotinic receptors: From structure to pathology. *Prog. Neurobiol.* **2004**, *74*, 363-396.
133. Arias, H. R. Positive and negative modulation of nicotinic receptors. *Adv. Protein Chem. Struct. Biol.* **2010**, *80*, 153-203.
134. Thomsen, M. S.; Zwart, R.; Ursu, D.; Jensen, M. M.; Pinborg, L. H.; Gilmour, G.; Wu, J.; Sher, E.; Mikkelsen, J. D. $\alpha 7$ and $\beta 2$ nicotinic acetylcholine receptor subunits form heteromeric receptor complexes that are expressed in the human

- cortex and display distinct pharmacological properties. *PLoS One* **2015**, *10*, e0130572.
135. Khiroug, S. S.; Harkness, P. C.; Lamb, P. W.; Sudweeks, S. N.; Khiroug, L.; Millar, N. S.; Yakel, J. L. Rat nicotinic ACh receptor $\alpha 7$ and $\beta 2$ subunits co-assemble to form functional heteromeric nicotinic receptor channels. *J. Physiol.* **2002**, *540.2*, 425-434.
 136. Dani, J. A. Neuronal nicotinic acetylcholine receptor structure and function and response to nicotine. *Int. Rev. Neurobiol.* **2015**, *124*, 3-19.
 137. Changeux, J.-P.; Edelstein, S. J. Allosteric receptors after 30 years. *Neuron* **1998**, *21*, 959-980.
 138. Galzi, J.-L.; Bertrand, S.; Corringer, P.-J.; Changeux, J.-P.; Bertrand, D. Identification of calcium binding sites that regulate potentiation of a neuronal nicotinic acetylcholine receptor. *EMBO J.* **1996**, *15*, 5824-5832.
 139. Brown, E. M.; Vassilev, P. M.; Hebert, S. C. Calcium ions as extracellular messengers. *Cell* **1995**, *83*, 679-682.
 140. Krause, R. M.; Buisson, B.; Bertrand, S.; Corringer, P.-J.; Galzi, J.-L.; Changeux, J.-P.; Bertrand, D. Ivermectin: A positive allosteric effector of the $\alpha 7$ neuronal nicotinic acetylcholine receptor. *Mol. Pharmacol.* **1998**, *53*, 283-294.
 141. Bertrand, D.; Gopalakrishnan, M. Allosteric modulation of nicotinic acetylcholine receptors. *Biochem. Pharmacol.* **2007**, *74*, 1155-1163.
 142. Zwart, R.; De Filippi, G.; Broad, L. M.; McPhie, G. I.; Pearson, K. H.; Baldwinson, T.; Sher, E. 5-Hydroxyindole potentiates human $\alpha 7$ nicotinic receptor-mediated responses and enhances acetylcholine-induced glutamate release in cerebellar slices. *Neuropharmacology* **2002**, *43*, 374-384.
 143. Grønlien, J. H.; Håkerud, M.; Ween, H.; Thorin-Hagene, K.; Briggs, C. A.; Gopalakrishnan, M.; Malysz, J. Distinct profiles of $\alpha 7$ nAChR positive allosteric modulation revealed by structurally diverse chemotypes. *Mol. Pharmacol.* **2007**, *72*, 715-724.
 144. Williams, D. K.; Wang, J.; Papke, R. L. Positive allosteric modulators as an approach to nicotinic acetylcholine receptor-targeted therapeutics: Advantages and limitations. *Biochem. Pharmacol.* **2011**, *82*, 915-930.
 145. Faghhi, R.; Gopalakrishnan, M.; Briggs, C. A. Allosteric modulators of the $\alpha 7$ nicotinic acetylcholine receptor. *J. Med. Chem.* **2008**, *51*, 701-712.
 146. Young, G. T.; Zwart, R.; Walker, A. S.; Sher, E.; Millar, N. S. Potentiation of $\alpha 7$ nicotinic acetylcholine receptors via an allosteric transmembrane site. *Proc. Natl. Acad. Sci. U. S. A.* **2008**, *105*, 14686-14691.
 147. Collins, T.; Millar, N. S. Nicotinic acetylcholine receptor transmembrane mutations convert ivermectin from a positive to a negative allosteric modulator. *Mol. Pharmacol.* **2010**, *78*, 198-204.
 148. Collins, T.; Young, G. T.; Millar, N. S. Competitive binding at a nicotinic receptor transmembrane site of two $\alpha 7$ -selective positive allosteric modulators with differing effects on agonist-evoked desensitization. *Neuropharmacology* **2011**, *61*, 1306-1313.

149. Pereira, E. F. R.; Hilmas, C.; Santos, M. D.; Alkondon, M.; Maelicke, A.; Albuquerque, E. X. Unconventional ligands and modulators of nicotinic receptors. *J. Neurobiol.* **2002**, *53*, 479-500.
150. Alkondon, M.; Pereira, E. F. R.; Yu, P.; Arruda, E. Z.; Almeida, L. E. F.; Guidetti, P.; Fawcett, W. P.; Sapko, M. T.; Randall, W. R.; Schwarcz, R.; Tagle, D. A.; Albuquerque, E. X. Targeted Deletion of the kynurenine aminotransferase II gene reveals a critical role of endogenous kynurenic acid in the regulation of synaptic transmission via $\alpha 7$ nicotinic receptors in the hippocampus. *J. Neurosci.* **2004**, *24*, 4635-4648.
151. Rassoulpour, A.; Wu, H.-Q.; Ferré, S.; Schwarcz, R. Nanomolar concentrations of kynurenic acid reduce extracellular dopamine levels in the striatum. *J. Neurochem.* **2005**, *93*, 762-765.
152. Yoshimura, R. F.; Hogenkamp, D. J.; Li, W. Y.; Tran, M. B.; Belluzzi, J. D.; Whittemore, E. R.; Leslie, F. M.; Gee, K. W. Negative allosteric modulation of nicotinic acetylcholine receptors blocks nicotine self-administration in rats. *J. Pharmacol. Exp. Ther.* **2007**, *323*, 907-915.
153. Abdrakhmanova, G. R.; Blough, B. E.; Nesloney, C.; Navarro, H. A.; Damaj, M. I.; Carroll, F. I. In vitro and in vivo characterization of a novel negative allosteric modulator of neuronal nAChRs. *Neuropharmacology* **2010**, *59*, 511-517.
154. Dukat, M.; Wesolowska, A.; Alley, G.; Young, S.; Abdrakhmanova, G. R.; Navarro, H. A.; Young, R.; Glennon, R. A. MD-354 selectively antagonizes the antinociceptive effects of (-)nicotine in the mouse tail-flick assay. *Psychopharmacology* **2010**, *210*, 547-557.
155. Spurny, R.; Debaveye, S.; Farinha, A.; Veys, K.; Vos, A. M.; Gossas, T.; Atack, J.; Bertrand, S.; Bertrand, D.; Danielson, U. H.; Tresadern, g.; Ulens, G. Molecular blueprint of allosteric binding sites in a homologue of the agonist-binding domain of the $\alpha 7$ nicotinic acetylcholine receptor. *Proc. Natl. Acad. Sci. U. S. A.* **2015**, *112*, E2543-E2552.
156. Gill-Thind, J. K.; Dhankher, P.; D'Oyley, J. M.; Sheppard, T. D.; Millar, N. S. Structurally similar allosteric modulators of $\alpha 7$ nicotinic acetylcholine receptors exhibit five distinct pharmacological effects. *J. Biol. Chem.* **2015**, *290*, 3552-3562.
157. Gill, J. K.; Dhankher, P.; Sheppard, T. D.; Sher, E.; Millar, N. S. A series of $\alpha 7$ nicotinic acetylcholine receptor allosteric modulators with close chemical similarity but diverse pharmacological properties. *Mol. Pharmacol.* **2012**, *81*, 710-718.
158. Gill, J. K.; Savolainen, M.; Young, G. T.; Zwart, R.; Sher, E.; Millar, N. S. Agonist activation of $\alpha 7$ nicotinic acetylcholine receptors via an allosteric transmembrane site. *Proc. Natl. Acad. Sci. U. S. A.* **2011**, *108*, 5867-5872.
159. Thakur, G. A.; Kulkarni, A. R.; Deschamps, J. R.; Papke, R. L. Expedient synthesis, enantiomeric resolution, and enantiomer functional characterization of (4-(4-bromophenyl)-3a,4,5,9b-tetrahydro-3H-cyclopenta[c]quinoline-8-sulfonamide (4BP-TQS): An allosteric agonist-positive allosteric modulator of $\alpha 7$ nicotinic acetylcholine receptors. *J. Med. Chem.* **2013**, *56*, 8943-8947.

160. Glennon, R. A.; Young, R. Appendix. In *Drug discrimination: Applications to medicinal chemistry and drug studies*; 1st ed.; Glennon, R. A., Young, R., Eds.; Wiley: Hoboken, 2011; pp 235-236.
161. Brejc, K.; van Dijk, W. J.; Klaassen, R. V.; Schuurmans, M.; van der Oost, J.; Smit, A. B.; Sixma, T. K. Crystal structure of an ACh-binding protein reveals the ligand-binding domain of nicotinic receptors. *Nature* **2001**, *411*, 269-276.
162. Unwin, N. Refined structure of the nicotinic acetylcholine receptor at 4 Å resolution. *J. Mol. Biol.* **2005**, *346*, 967-989.
163. Miyazawa, A.; Fujiyoshi, Y.; Unwin, N. Structure and gating mechanism of the acetylcholine receptor pore. *Nature* **2003**, *423*, 949-955.
164. Dellisanti, C. D.; Yao, Y.; Stroud, J. C.; Wang, Z.-Z.; Chen, L. Crystal structure of the extracellular domain of nAChR α 1 bound to α -Bungarotoxin at 1.94 Å resolution. *Nat. Neurosci.* **2007**, *10*, 953-962.
165. Smit, A. B.; Syed, N. I.; Schaap, D.; van Minnen, J.; Klumperman, J.; Kits, K. S.; Lodder, H.; van der Schors, R. C.; van Elk, R.; Sorgedraeger, B.; Brejc, K.; Sixma, T. K.; Geraerts, P. M. A glia-derived acetylcholine-binding protein that modulates synaptic transmission. *Nature* **2001**, *411*, 261-268.
166. Karlin, A. The acetylcholine-binding protein: 'What's in a name?' *Pharmacogenomics J.* **2001**, *1*, 221-223.
167. Konstantakaki, M.; Tzartos, S. J.; Poulas, K.; Eliopoulos, E. Model of the extracellular domain of the human α 7 nAChR based on the crystal structure of the mouse α 1 nAChR extracellular domain. *J. Mol. Graphics and Modell.* **2008**, *26*, 1333-1337.
168. Olsen, J. A.; Balle, T.; Gajhede, M.; Ahring, P. K.; Kastrup, J. S. Molecular recognition of the neurotransmitter acetylcholine by an acetylcholine binding protein reveals determinants of binding to nicotinic acetylcholine receptors. *PLoS One* **2014**, *9*, e91232.
169. Li, S.-X.; Huang, S.; Bren, N.; Noridomi, K.; Dellisanti, C. D.; Sine, S. M.; Chen, L. Ligand-binding domain of an α 7-nicotinic receptor chimera and its complex with agonist. *Nat. Neurosci.* **2011**, *14*, 1253-1259.
170. Schapira, M.; Abagyan, R.; Totrov, M. Structural model of nicotinic acetylcholine receptor isotypes bound to acetylcholine and nicotine. *BMC Struct. Biol.* **2002**, *2*, 1-8.
171. Cheng, X.; Lu, B.; Grant, B.; Law, R. J.; McCammon, J. A. Channel opening motion of α 7 Nicotinic acetylcholine receptor as suggested by normal mode analysis. *J. Mol. Biol.* **2006**, *355*, 310-324.
172. Brannigan, G.; LeBard, D. N.; Hénin, J.; Eckenhoff, R. G.; Klein, M. L. Multiple binding sites for the general anesthetic isoflurane identified in the nicotinic acetylcholine receptor transmembrane domain. *Proc. Natl. Acad. Sci. U. S. A.* **2010**, *107*, 14122-14127.
173. Alwassil, O. I. Elaboration and design of α 7 nAChR negative allosteric modulators. Ph.D. Dissertation, Virginia Commonwealth University, Virginia, 2015.
174. Goldin, A. L. Expression of ion channels in *Xenopus* oocytes. In *Expression and Analysis of Recombinant Ion Channels: From Structural Studies to*

- Pharmacological Screening*; Clare, J. J., Trezise, D. J., Eds.; Wiley-VCH: Weinheim, 2006.
175. Bianchi, L.; Driscoll, M. *Heterologous expression of C. elegans ion channels in Xenopus oocytes*. [Online]; Schafer, W., Ambros, V., Eds.; WormBook, the online review of *C. elegans* biology: Pasadena, CA, 2006; http://www.wormbook.org/chapters/www_channelexpress/channelexpress.html (accessed April 10, 2018).
 176. Stühmer, W. Electrophysiological recording from *Xenopus* oocytes. *Methods Enzymol.* **1992**, *207*, 319-339.
 177. Baumgartner, W.; Islas, L.; Sigworth, F. J. Two-microelectrode voltage clamp of *Xenopus* Oocytes: Voltage errors and compensation for local current flow. *Biophys. J.* **1999**, *77*, 1980-1991.
 178. Di Resta, C.; Becchetti, A. Introduction to ion channels. *Adv. Exp. Med. Biol.* **2010**, *674*, 9-21.
 179. Forster, I.; Bertrand, D. Inward rectification of neuronal nicotinic acetylcholine receptors investigated by using the homomeric $\alpha 7$ receptor. *Proc. R. Soc. B.* **1995**, *260*, 139-148.
 180. López, S.; Bastida, J.; Viladomat, F.; Codina, C. Acetylcholinesterase inhibitory activity of some Amaryllidaceae alkaloids and *Narcissus* extracts. *Life Sci.* **2002**, *71*, 2521–2529.
 181. Šafratová, M.; Hošťálková, A.; Hulcová, D.; Breiterová, K.; Hrabcová, V.; Machado, M.; Fontinha, D.; Prudêncio, M.; Kuneš, J.; Chlebek, J.; Jun, D.; Hrabínová, M.; Nováková, L.; Havelek, R.; Seifrtová, M.; Opletal, .; Cahlíková, L. Alkaloids from *Narcissus Poeticus* cv. pink parasol of various structural types and their biological activity. *Archives Pharmacol. Res.* **2018**, *41*, 208-218.
 182. Trost, B. M.; Tang, W.; Toste, F. D. Divergent enantioselective synthesis of (-)-galanthamine and (-)-morphine. *J. Am. Chem. Soc.* **2005**, *127*, 14785-14803.
 183. Perissutti E.; Fiorino F.; Severino B.; Frecentese F.; Massarelli P.; Nencini C.; Santagada V.; Caliendo G. Synthesis of 6 β -D-glucosyl and 6-nitroxy (-)-galanthamine derivatives as acetylcholinesterase inhibitors. *Die Pharmazie* **2007**, *62*, 403-405.
 184. Wildman, W. C.; Brown, C. L. The structure of habranthine. *Tetrahedron Lett.* **1968**, *9*, 4573-4576.
 185. Brown, C. L. The mass spectra of montanine- and galanthamine-type alkaloids; The structures of pancracine and habranthine. Ph.D. Dissertation, Iowa State University, Ames, IA 1968.
 186. Ciganek, E. Square, K. Octahydro-1H-Benzo[4,5]furo[3,2,-e]-isoquinoline analgesic and narcotic antagonistic compounds. ZA7905221 (B), September, 24, 1980.
 187. Ciganek, E. 2,3,4,4a,5,6,7,7a-Octahydro-1H-benzofuro[3,2-e]isoquinoline: A new morphine fragment. *J. Am. Chem. Soc.* **1981**, *103*, 6261-6262.
 188. Jung, M. E.; Abrecht, S. Improved synthesis of 3-substituted 7-methoxybenzofurans. Useful intermediates for the preparation of morphine analogs of organic chemistry. *J. Org. Chem.* **1988**, *53*, 423-425.

189. Kozikowski, A. P.; Gaisina, I. N.; Yuan, H.; Petukhov, P. A.; Blond, S. Y.; Fedolak, A.; Caldarone, B.; McGonigle, P. Structure-based design leads to the identification of lithium mimetics that block mania-like effects in rodents. Possible new GSK-3 β therapies for bipolar disorders. *J. Am. Chem. Soc.* **2007**, *129*, 8328-8332.
190. Gaisina, I. N.; Gallier, F.; Ougolkov, A. V.; Kim, K. H.; Kurome, T.; Guo, S.; Holzle, D.; Luchini, D. N.; Blond, S. Y.; Billadeau, D. D.; Kozikowski, A. P. From a natural product lead to the identification of potent and selective benzofuran-3-yl-(indol-3-yl)maleimides as glycogen synthase kinase 3 β inhibitors that suppress proliferation and survival of pancreatic cancer cells. *J. Med. Chem.* **2009**, *52*, 1853-1863.
191. Albanese-Walker, J.; Rossen, K.; Reamer, R. A.; Volante, R. P.; Reider, P. J. Synthesis of benzofuroquinoline for α -2 adrenoceptor antagonist MK-912: An O-analogue of the Pictet-Spengler reaction. *Tetrahedron Lett.* **1999**, *40*, 4917-4920.
192. Nerozzi, F. Heterogeneous catalytic hydrogenation. Platinum group metals as hydrogenation catalysts in a two-day course. *Platin. Met. Rev.* **2012**, *56*, 236-241.
193. Yasuhiko, K.; Matsumoto, T.; Uchikawa, O.; Fujii, N.; Tarui, N. Furoisoquinoline derivatives, process for producing the same and use thereof. US6924292 (B2), August, 2, 2005.
194. Youn, S. W. The Pictet-Spengler reaction: Efficient carbon-carbon bond forming reaction in heterocyclic synthesis. *Org. Prep. Proced. Int.* **2009**, *38*, 505-591.
195. Guillou, C.; Beunard, J.-L.; Gras, E.; Thal, C. An efficient total synthesis of (\pm)-galanthamine. *Angew. Chem., Int. Ed.* **2001**, *40*, 4745-4746.
196. Koelsch, C. F.; Whitney, A. G. The Rosenmund-von Braun nitrile synthesis. *J. Org. Chem.* **1941**, *06*, 795-803.
197. So, M.; Kotake, T.; Matsuura, K.; Inui, M.; Kamimura, A. Concise synthesis of 2-benzazepine derivatives and their biological activity. *J. Org. Chem.* **2012**, *77*, 4017-4028.
198. Kleywegt, G. J.; Jones, T. A. Phi/Psi-chology: Ramachandran revisited. *Structure* **1996**, *4*, 1395-1400.
199. Kellogg, G. E.; Abraham, D. J. Hydrophobicity: Is LogP_{o/w} more than the sum of its parts? *Eur. J. Med. Chem.* **2000**, *35*, 651-661.
200. Changeux, J.-P.; Taly, A. Nicotinic receptors, allosteric proteins and medicine. *Trends Mol. Med.* **2008**, *14*, 93-102.
201. Hansen, S. B.; Taylor, P. Galanthamine and non-competitive inhibitor binding to ACh-binding protein: Evidence for a binding site on non- α -subunit interfaces of heteromeric neuronal nicotinic receptors. *J. Mol. Biol.* **2007**, *369*, 895-901.
202. Glennon, R. A.; Salley, J. J. Jr; Steinsland, O. S.; Nelson, S. Synthesis and evaluation of novel alkylpiperazines as potential dopamine antagonists. *J. Med. Chem.* **1981**, *24*, 678-683.
203. Barniol-Xicota, M.; Turcu, A. L.; Codony, S.; Escolano, C.; Vázquez, S. Direct reductive alkylation of amine hydrochlorides with aldehyde bisulfite adducts. *Tetrahedron Lett.* **2014**, *55*, 2548-2550.

204. Arnold, Z.; Hejno, K. Synthetische stoffe mit uterotonischer wirkung ii. vom 3,4-dimethoxybenzylamin abgeleitete tertiäre amine. *Collect. Czech. Chem. C.* **1955**, *20*, 567-570.
205. Stedman, E. CCXLV.- The isomeric hydroxybenzyl dimethylamines. *J. Chem. Soc.* **1927**, *0*, 1902-1906.
206. Venkatesan, A. M.; Santos, O. D.; Asselin, M.; Grosu, G. T.; Evrard, D. A.; Mewshaw, R. E.; Meagher, K. Benzofuranyl- and benzothienyl-piperazinyl quinolones and methods of their use. US2009/54454 A1, February 26, 2009.
207. Burns, P. A.; Taylor, N. J.; Rodrigo, R. The synthesis and some chemical reactions of a 5a-methyl 2H-naphtho[1,8-bc]furan. *Can. J. Chem.* **1994**, *72*, 42-50.
208. Blatt, L. M.; Seiwert, S.; Beigelman, L.; Kercher, T.; Kennedy, A. L.; Andrews, S. W. Novel inhibitors of Hepatitis C viral replication. WO2008005511 (A2), January 10, 2008.
209. Xichen, L.; Feng, R.; Yugui, S. 1,2,4-oxadiazol derivatives, their pharmaceutical compositions and their use as Sphingosine 1-phosphate 1 receptor agonists. WO2010145203 (A1), December, 23, 2010
210. Wang, Y.; Chen, F.; Di, H.; Xu, Y.; Xiao, Q.; Wang, X.; Wei, H.; Lu, Y.; Zhang, L.; Zhu, J.; Sheng, C.; Lan, L.; Li, J. Discovery of potent benzofuran-derived diapophytoene desaturase (CrtN) inhibitors with enhanced oral bioavailability for the treatment of methicillin-resistant *Staphylococcus aureus* (MRSA) Infections. *J. Med. Chem.* **2016**, *59*, 3215-3230.
211. Yao, W.; Ma, X.; Guo, L.; Jia, X.; Hu, A.; Huang, Z. A highly efficient catalytic α -alkylation of unactivated amides using primary alcohols. *Tetrahedron Lett.* **2016**, *57*, 2919-2921.
212. Pandit, C. R.; Mani, N. S. Expedient reductive amination of aldehyde bisulfite adducts. *Synthesis (Stuttg)* **2009**, *23*, 4032-4036.
213. Kim, J-S.; Pandya, A.; Weltzin, M.; Edmonds, B. W.; Schulte, M. K.; Glennon R. A. Synthesis of desformylflustrabromine and its evaluation as an $\alpha 4\beta 2$ and $\alpha 7$ nACh receptor modulator. *Bioorg. Med. Chem. Lett.* **2007**, *17*, 4855-4860.
214. Weltzin, M. M.; Schulte, M. K. Desformylflustrabromine modulates $\alpha 4\beta 2$ neuronal nicotinic acetylcholine receptor high- and low-sensitivity isoforms at allosteric clefts containing the $\beta 2$ subunit. *J. Pharmacol. Exp. Ther.* **2015**, *354*, 184-194.
215. German, N.; Kim, J-S.; Jain, A.; Dukat, M.; Pandya, A.; Ma, Y.; Weltzin, M.; Schulte, M. K.; Glennon, R. A. Deconstruction of the $\alpha 4\beta 2$ nicotinic acetylcholine receptor positive allosteric modulator desformylflustrabromine. *J. Med. Chem.* **2011**, *54*, 7259-7267.
216. Peng, X.; Katz, M.; Gerzanich, V.; Anand, R.; Lindstrom, J. Human $\alpha 7$ acetylcholine receptor: Cloning of the $\alpha 7$ subunit from the SH-SY5Y cell line and determination of pharmacological properties of native receptors and functional $\alpha 7$ homomers expressed in *Xenopus* oocytes. *Mol. Pharmacol.* **1993**, *45*, 546-554.
217. Sievers, F.; Wilm, A.; Dineen, D.; Gibson, T. J.; Karplus, K.; Li, W.; Lopez, R.; McWilliam, H.; Remmert, M.; Söding, J.; Thompson, J. D.; Higgins, D. G. Fast,

- scalable generation of high-quality protein multiple sequence alignments using Clustal Omega. *Mol. Syst. Biol.* **2011**, 7, 1-6.
218. Eswar, N.; Webb, B.; Marti-Renom, M. A.; Madhusudhan, M. S.; Eramian, D.; Shen, M.-Y.; Pieper, U.; Sali, A. Comparative protein structure modeling using modeller. *Curr. Protoc. Bioinformatics* **2007**, 5.6.1-5.6.30.
219. Jones, G.; Willett, P.; Glen, R. C.; Leach, A. R.; Taylor, R. Development and validation of a genetic algorithm for flexible docking. *J. Mol. Biol.* **2011**, 267, 727-748.
220. Kowal, N. M.; Ahring, P. K.; Liao, V. W. Y.; Indurti, D. C.; Harvey, B. S.; O'Connor, S. M.; Chebib, M.; Olafsdottir, E. S.; Balle, T. Galantamine is not a positive allosteric modulator of human $\alpha 4\beta 2$ or $\alpha 7$ nicotinic acetylcholine receptors. *Brit. J. Pharmacol.* **2018**, April 18. DOI: 10.1111/bph.14329. [Epub ahead of print]

APPENDIX

Note added in proof: Additional biological data from electrophysiological studies became available after submission of the dissertation to the research committee. This appendix was provided to the committee members and was available at the time of the oral defense. Additionally, the HINT scores for the deconstructed analogs were also calculated and provided at the time of the defense.

TEVC assay

Electrophysiological data for three molecules, galantamine (**3**; HBr), lycoramine (**6**; free base), and compound **34** were provided by Dr. Marvin K. Schulte's laboratory as conducted by his graduate student, Laura DeCristofano.

The compounds did not elicit agonist-like responses in the assay and neither did they potentiate ACh responses. This is in contrast to the preliminary screening assay conducted and reported in this dissertation.

Dose-response curves of compounds **3**, **6**, and **34** with concentrations ranging from 0.01 to 300 μM in the presence of ACh (100 μM). The assays were run in triplicate for **3** and **6**

and in duplicate for **34**. The responses were normalized to the response elicited by 100 μM of ACh. From Figure A1, galantamine (**3**) seems to behave like an antagonist by inhibiting the ACh-evoked currents with an IC_{50} of 107 μM . This antagonist (inhibitory) behavior of galantamine at nAChRs at higher concentrations (above 10 μM) has been reported previously in the literature.^{23,102} The potentiating effect of galantamine (100 nM) for ACh-evoked currents (250 μM) in human $\alpha 7$ nAChRs was 22%.²³ In our studies, it is possible that a potentiating of ACh (100 μM)-evoked currents might occur at 100 and 300 nM concentrations of galantamine (Figure A1) but seemed insignificant after averaging the data. Further optimization of the TEVC method is required in order to have an assay sensitive enough to detect small potentiating effects.

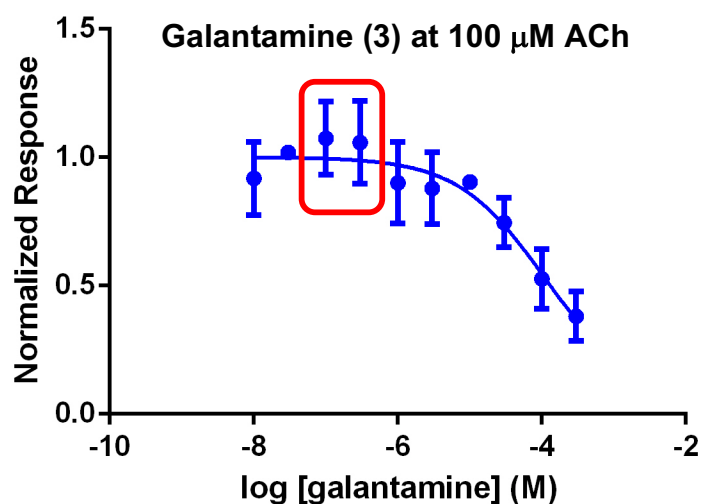


Figure A1. Dose-response curve for galantamine (**3**) in the presence of ACh (100 μM). The assay was run in triplicate.

Lycoramine (**6**) (Figure A2), obtained upon reduction of the cyclohexenol double bond of galantamine retains the antagonist-like effect of galantamine. Further deconstruction of the complete cyclohexenol ring of galantamine results in **34**, which also retains the antagonist-like effect of its parent, galantamine. Although a complete IC₅₀ curve was not generated for **34**, the results (Figure A3) indicate inhibition of ACh-evoked currents at high concentrations. This suggests that the cyclohexenol ring of galantamine (**3**) is not required for antagonizing the ACh-evoked currents.

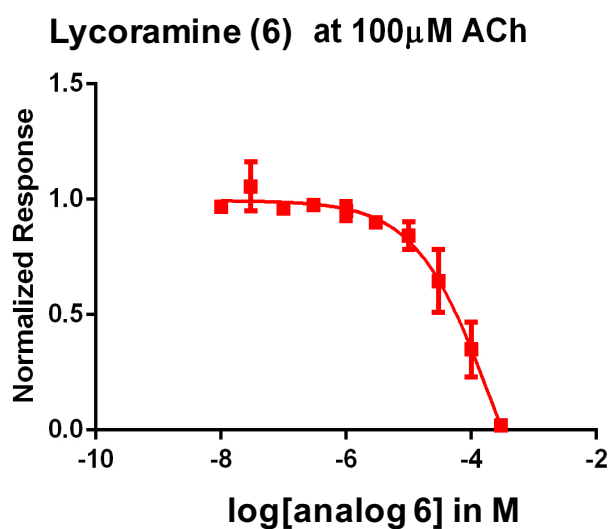


Figure A2. Dose-response curve for lycoramine (**6**) in the presence of ACh (100 μ M). The assay was run in triplicate.

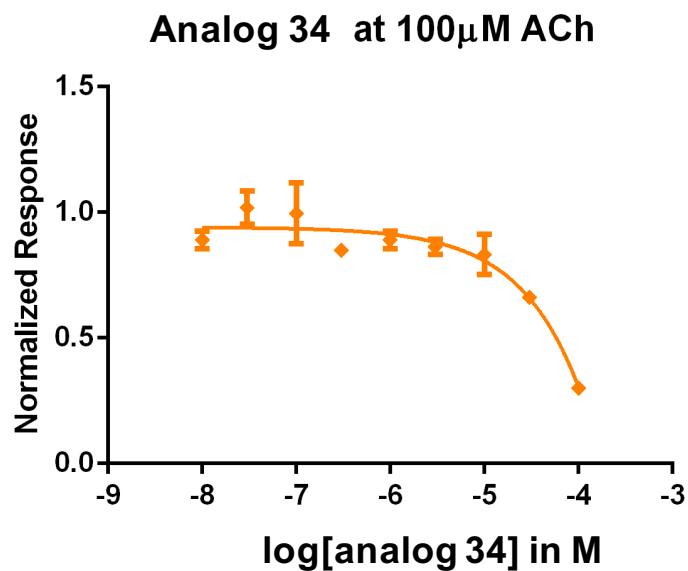


Figure A3. Dose-response curve for compound **34** in the presence of ACh (100 μ M). The assay was run in duplicate.

The IC_{50} values are indicated in Table A1.

Table A1. IC_{50} values for compounds **3**, **6**, and **34** for ACh (100 μ M) from the TEVC assay.

COMPOUND	IC_{50} (μ M)
Galantamine (3)	107 μ M
Lycoramine (6 ; Free Base)	209 μ M
34	Could not be determined

Thus, it could be concluded that an intact structure of galantamine is not necessary for its inhibitory action at human $\alpha 7$ nAChRs.

At around the time that this dissertation was submitted to my research committee, an article was published online,²²⁰ which reported that galantamine was not a PAM at the human $\alpha 7$ nAChRs expressed in *X. laevis* oocytes. Galantamine (10 nM-1 μ M) could neither evoke agonist-like responses, nor potentiate ACh-evoked currents in the human $\alpha 7$ nAChRs.²²⁰ Concentrations of galantamine above 10 μ M, resulted in an inhibition of ACh-evoked currents with an IC_{50} of 55 μ M.²²⁰ The observation that galantamine does not potentiate ACh-evoked currents in the human $\alpha 7$ nAChRs is consistent with our findings.

Molecular Modeling

The HINT scores for each deconstructed analog was determined and is highlighted in Table A2.

Table A2. HINT scores for the deconstructed analogs are expressed in terms of favorable polar and hydrophobic interactions. The total HINT score for each analog is also indicated along with observed hydrogen bond interactions with protein residues.

ANALOG	POLAR	HYDROPHOBIC	TOTAL HINT SCORE	H-BOND/IONIC INTERACTIONS
Galantamine: Mode-I	718	411	393	O-Thr223, O-Thr221; O-Thr221, Ser206 and Asp219
Mode-II	129	367	106	No key interactions
Modified galantamine; 6	723	334	184	O-Thr221, O-Asp219
44	122	299	-17	Furan O, Thr221
Furobenzazepine; 34	74	298	17	O-Thr223, Lys165
Benzofurans; 50	613	298	206	O-Thr223; N-Asp219
51	1395	273	981	N-Asp219
35_R	728	346	213	N-Asp219
35_S	856	384	380	O-Thr223, N-Asp219
52_R	1529	346	1305	N-Asp219
52_S	879	383	694	N-Asp219
36	805	258	1547	Furan O, Thr223
Benzazepines; 37	158	311	14	O-Ser206; O-Thr221
38	188	346	15	O-Ser206
Phenylpropylamines; 39	1156	495	660	O-Thr221;O-Thr223; N-Asp219
40	853	357	289	N-Asp219
Benzylamines; 41	572	344	131	Methoxy O Thr 223; N-Asp219
42	666	386	244	methoxy O Thr223; N –Asp 219

In the docking studies performed with galantamine (**3**) in our human $\alpha 7$ nAChR homology models, none of the docking modes exhibited a plausible ionically-reinforced hydrogen bond between the protonated amine of galantamine and the oxygen atom of Asp219. To ascertain why this strong interaction was not observed, we conducted additional docking studies with galantamine and Asp219 in the human $\alpha 7$ nAChR homology model. Figure A4 displays a result of docking galantamine 6 Å around Asp219. Although the nitrogen atom of galantamine is oriented towards the docking site, it does not form an interaction with Asp219. Instead, the nitrogen atom forms a hydrogen bond with the hydroxyl oxygen atom of Ser206.

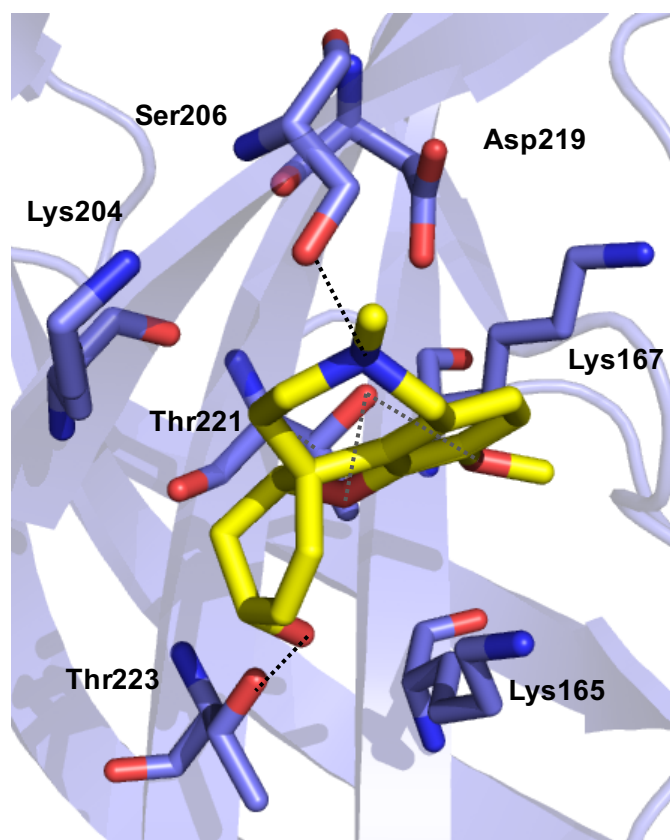


Figure A4. Docking result of galantamine 6 Å within Asp219. The amine did not interact with the Asp219 residue, instead forming hydrogen bonds with Ser206, while the oxygen atoms of galantamine participated in hydrogen bonds with Thr221 and Thr223.

To explore this further, we forced an interaction between the amine nitrogen atom and the Asp219 oxygen atom by constraining the distance of 1.5-3.5 Å between these two atoms. The constrained interaction as displayed in Figure A5 displayed an ionically-reinforced hydrogen bond interaction between the nitrogen atom of galantamine and oxygen atom of Asp219, resulting in a high total HINT score. However, the space-filling

representation of the ligand and protein revealed potential steric clashes between these two entities.

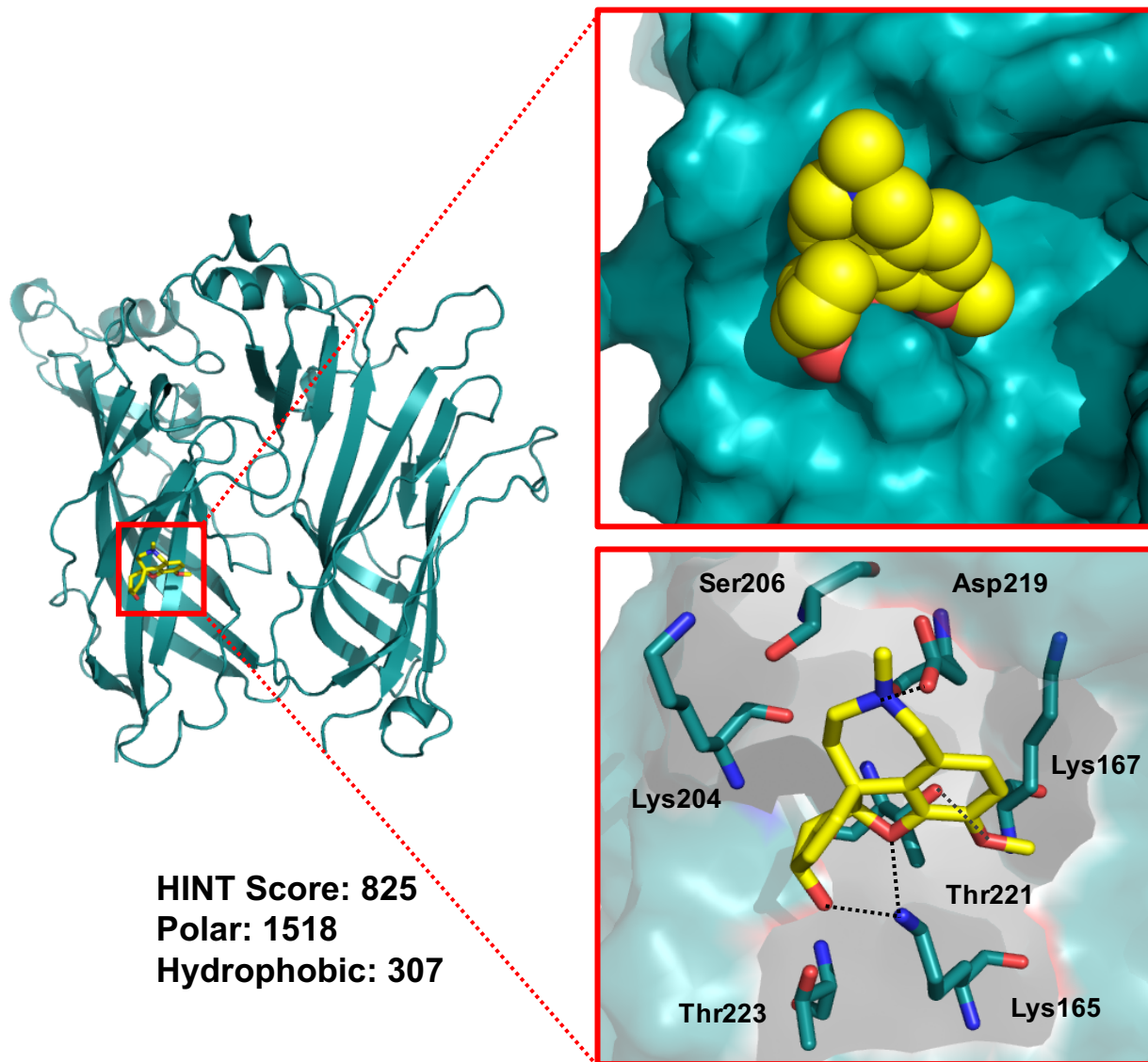


Figure A5. Forced interaction of galantamine with Asp219. The constraint applied was that the nitrogen atom of galantamine would form a hydrogen bond with the oxygen atom of Asp219. The forced interaction resulted in galantamine's nitrogen atom being located 2.5 Å away from the oxygen atom of Asp219. The furan and hydroxyl oxygen atoms participate in hydrogen bonds with Lys165, while the methoxy oxygen atom formed a hydrogen bond with Thr221.

Another way to analyze this interaction was to dock galantamine 10 Å around Asp219 by specifying a hydrogen-bond interaction between the nitrogen atom of galantamine and the Asp219 oxygen atoms. This docking, as displayed in Figure A6, resulted in an interaction between the nitrogen atom of galantamine and the Asp219 oxygen atom, however, once again, surface and space-filling representations indicated possible clashes.

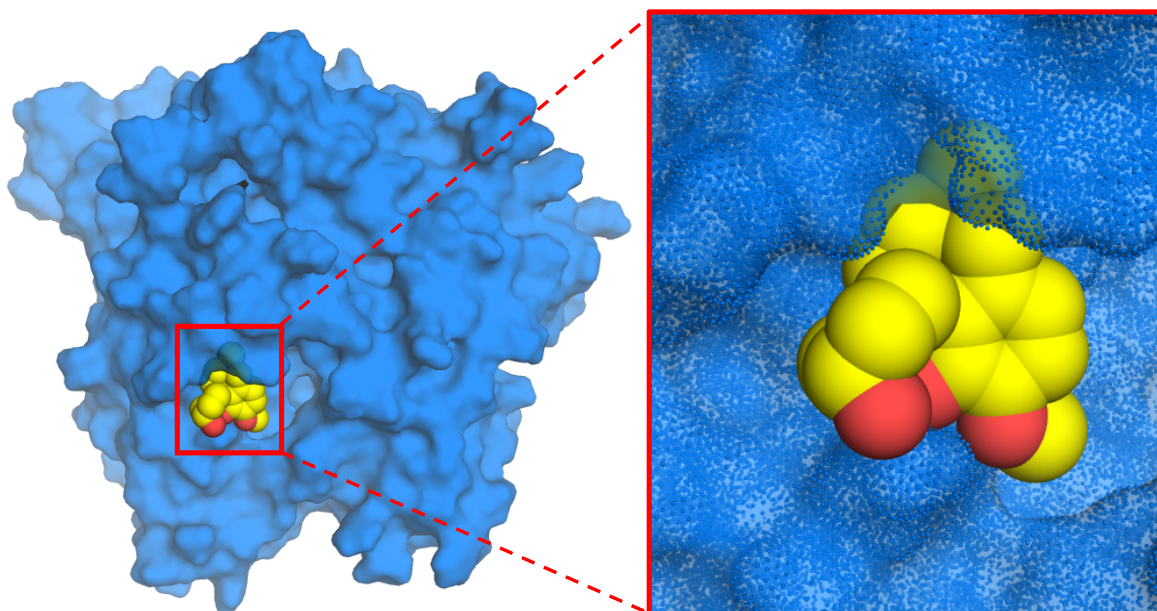


Figure A6. Forced docking of galantamine 10 Å around Asp219. Galantamine is indicated by yellow space-filling spheres.

From these studies, it can be concluded that a lack of ionically-reinforced hydrogen bond between the nitrogen atom and Asp219 might be because Asp219 is located in an unreachable pocket.

VITA

Malaika Dilip Argade was born on October 19, 1988 to Dilip Vilas Argade and Manjiri Argade in Pune, India. She received her Bachelor's degree in Pharmaceutical Sciences from the University of Mumbai in June 2010, following which she enrolled in the Master's program in the Department of Medicinal Chemistry, School of Pharmacy at Virginia Commonwealth University (VCU). After graduating with a Master's degree in Medicinal Chemistry in August, 2012, Malaika was employed in the Department of Biology, VCU between August 2012-May 2014. Following this, she enrolled in the PhD program in Integrative Life Sciences, Virginia Commonwealth University in August 2014.